Fall 2016

Fluid dynamic factors as a cause and effect of biofilm formation of Staphylococcus aureus biofilms

Erica Sherman
University of Nebraska - Lincoln, sherman.erica@gmail.com

FLUID DYNAMIC FACTORS AS A CAUSE AND EFFECT OF BIOFILM FORMATION OF *STAPHYLOCOCCUS AUREUS* BIOFILMS

by

Erica Sherman

A DISSERTATION

Presented to the Faculty of

The Graduate College at the University of Nebraska

In Partial Fulfillment of Requirements

For the Degree of Doctor of Philosophy

Major: Mechanical Engineering & Applied Mechanics

(Fluid Mechanics)

Under the Supervision of Professor Timothy Wei

Lincoln, Nebraska.

November, 2016.

FLUID DYNAMIC FACTORS AS A CAUSE AND EFFECT OF BIOFILM FORMATION OF STAPHYLOCCUS AUREUS BIOFILMS

Erica Sherman, Ph.D.

University of Nebraska, 2016

Adviser: Timothy Wei

Staphylococcus aureus bacteria are able to form biofilms and distinctive tower structures that facilitate their ability to tolerate treatment and to spread within the human body. The formation of towers, which break off, get carried downstream and serve to initiate biofilms in other parts of the body are of particular interest here. It is known that flow conditions play a role in the development, dispersion and propagation of biofilms in general. The influence of flow on tower formation and ultimately what factors lead to tower formation, however, is not at all understood. This work is focused on the effect of applied shear stress on tower development. The hypothesis being examined is that tower structures form within a specific range of shear stresses and that there is an as yet ill-defined fluid dynamic phenomenon that occurs hours before a tower forms. In this study, a range of shear stresses is examined that brackets 0.6 dynes/cm^2, the nominal shear stress where towers seem most likely to form. The biofilm structure is known to be a temporally and spatially heterogeneous structure, which must be taken into account when considering the tower formation frequency and the local flow environment. How this structure differs as a function of applied shear, the experimental stage of biofilm development, and the likelihood of tower formation is analyzed. This work includes μPTV measurements and cell density data indicating variations in flow and biofilm evolution as a function of the applied shear. Causal relations between flow and biofilm

development will be discussed as well as the presentation of specific biofilm development terms as predictive measures of tower formation.

DEDICATION

This work is dedicated to my grandfather, Enzio Macor. His passion for learning was evident in everything he did and shone through no matter what life sent his way. His example leaves me humbled and sparks a fire in my heart.

ACKNOWLEDGEMENTS

My work is a cumulative result of the support, inspiration, and effort of those around me who have helped me to become who I am today. Each person has played a role, no matter how big or small, which has fostered my growth and for that I am thankful.

First and foremost, my parents have provided tremendous support and encouragement to try and keep trying no matter what, and to work hard at whatever I choose to do. By their example I've learned to keep my mind open to new experiences and to always be learning.

My brothers, Christopher and Andrew, have pushed me from the start, whether on the playground or playing video games, and despite any teasing, they've shown me that they've always got my back. Thanks for making me stronger.

Dr. Wei, the guiding and disruptive force who encouraged me to pursue a PhD and to move to Nebraska, has had a profound effect on my life as a researcher and a person. Whether it has been teaching me the fundamentals of experiments, reminding me to look at the bigger picture, or showing me firsthand what a kind and caring person is, Dr. Wei has always been there with a smile, a corny joke, and a way forward.

I also wouldn't be here without the help and humor of my labmates over the years. Chia, Ben, and Lori have been such a wonderful and critical part of surviving and being able to laugh about graduate school and thoughts of them will always make me smile.

Thanks to my committee members, Dr. Sangjin Ryu, Dr. Sidy Ndao, and Dr. Kenneth Bayles, who have all contributed valuable feedback and resources to shape and develop my research.

A huge thank you to Dr. Derek Moormeier and Jennifer Endres, whose generosity of spirit and time was critical in helping me set up and run experiments.

And incredibly, my husband Adam has been there when I needed him most, whether it was to provide encouragement, support, or a glass of something to take the edge off. Life would be much harder without him.

CONTENTS

LIST OF TABLES

LIST OF FIGURES

CHAPTER 1

INTRODUCTION

1.1. Introducing *Staphylococcus aureus*

Staphylococcal bacteria are recognized as the most frequent cause of biofilm-associated infections, primarily for lower respiratory tract infections and surgical site infections, and secondarily for nosocomial bacteremia, pneumonia, and cardiovascular infections [1]. Roughly 40% of the general population are colonized with *S. aureus* in particular, and therefore carry an increased risk for infections associated with surgery, dialysis, or intravascular devices [2]. *S. aureus* also acts opportunistically in patients with chronic diseases, such as Cystic Fibrosis [3]. The lethal reputation of *S. aureus* can be due to the combination of its high presence in the population and its ability to form a biofilm.

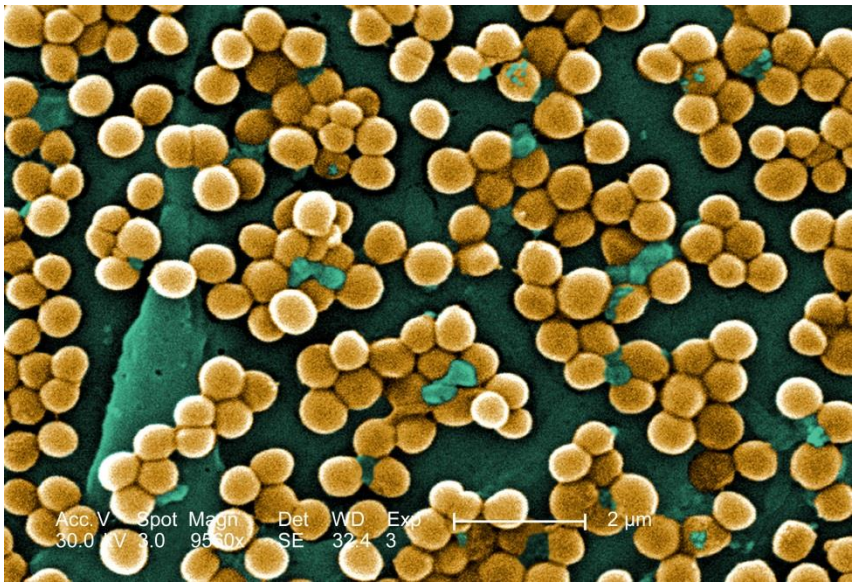

Figure 1.1 A Scanning Electron Micrograph (SEM) depicting numerous clumps of methicillin-resistant *Staphylococcus aureus*, commonly referred to as MRSA. Magnified 9560x [4].

The *S. aureus* bacterium is non-motile, meaning it lacks external mechanisms with which to propel or pull itself along surfaces or within a flow. Biofilm formation of the wild-type UAMS-1 strain of *S. aureus* is characterized by the deposition of cells on a surface, film growth, cell exodus, maturation, and dispersal [5]. Staphylococci bacteria are approximately 1 um in diameter and have a spherical shape [6]. *S. aureus* have been observed to form large towers in the later part of biofilm development that break off into the flow, likely to colonize a downstream location. Demonstrating the effect of flow on biofilm development, these tower structures only form in flow cell studies and not under static conditions [7]. Generally, *S. aureus* take 24-72 hours to develop a biofilm, but the particular species under study would reach the tower stage between 10-16 hours in flow assays [8, 5]. This complex process involves a dynamic film structure that has heterogeneous spatial, biological, and material properties. Relevant studies and literature will be presented below.

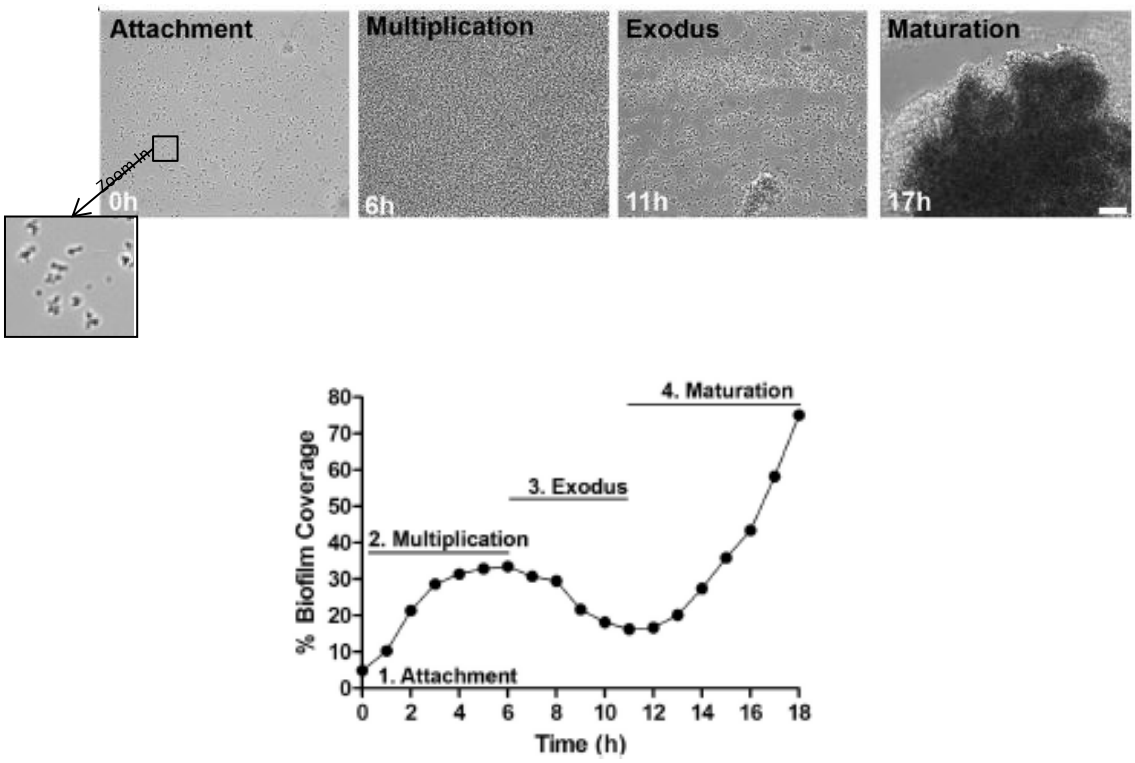

Figure 1.2 Snapshots during S. aureus Biofilm development depicting changes in cell coverage across the field of view. The zoomed-in box highlights the cells, shown as darker circles clumped together. Below is a graph that quantifies the percent biofilm coverage as a function of time during a normal experiment [5].

1.2 Biofilm Background and Function

Biofilm formation has been observed in several strains of bacteria, and general observations regarding chemical signaling and structure have been performed. Different bacteria grow different types of biofilms as determined by their respective environments and physical characteristics [9]. The presence of biofilms in aquatic, industrial, and medical settings further complicates the modeling and understanding of biofilm behavior. In comparison to planktonic cultures, bacterial biofilms appear to be structurally organized in a way to take advantage of nutrients, protect against attack, and assist in

biofilm propagation. Biofilm populations exist in virtually all nutrient-sufficient aquatic systems independent of system geometry and the type of ecosystem involved [10].

A biofilm is a community of cells that are irreversibly attached to a surface or each other, embedded in a matrix of extracellular polymeric substances that they have produced, and exhibit altered behavior, as opposed to bacteria floating freely in a planktonic state [3]. Cells that may be resistant to antimicrobial strategies within a biofilm may regain their susceptibility once the biofilm matures and disperses cells back into the environment [11]. Research has shown that the formation of a biofilm provides key advantages relating to mechanical stability, growth rate and susceptibility to antimicrobial agents as compared to the free-floating planktonic state [12].

1.2.1 Biological

While it is generally assumed that bacteria cells in a planktonic culture have uniform physiological activities, the environmental conditions and physiological responses of the bacteria in a biofilm are not homogeneous. Biofilms have concentration gradients in nutrients and signaling compounds, along with cells at different levels of metabolic activity [13]. These differences can lead to spatial heterogeneities within a biofilm and throughout its lifecycle. Thus the biological activity of individual and groups of bacteria within a biofilm play an important role in understanding the bigger picture of the biofilm life cycle.

The formation of a biofilm has been shown to involve the chemical signaling of individual bacterium cells for the benefit of the colony. Quorum sensing is interpreted as a communication system for bacteria that regulates gene expression in response to

changes in cell-population density [14]. This system is especially effective in biofilms because of the high local cell density, even in the presence of other species of bacteria [15]. In fact, studies have shown that activation of the agr-quorum sensing system within *S. aureus* biofilms is necessary for cell detachment and dispersal and can be influenced by environmental or cell density cues [16]. Quorum sensing involves gene transcription, and biofilm-associated cells have been shown to grow significantly more slowly than planktonic cells, allowing them to become more resistant to antimicrobial agents [3]. Additionally, biofilm associated cells of *Pseudomonas aeruginosa* use cell-to-cell communication to coordinate differentiation in biofilm architecture [17].

Quorum sensing activity has also been shown to be directly affected by flow conditions. Research has shown that heterogeneous quorum sensing activation in biofilms depends on biofilm thickness as well as proximity to flow due to the advection of extracellular signaling molecules [18]. In fact, the presence or rate of flow can increase the minimum amount of biomass required to initiate quorum sensing In the case of very high flow rates, the biofilm community in a study never fully induced quorum sensing [19]. Quorum sensing can be used to directly control biofilm architecture, metabolic activity, and motion, and facilitates a biofilm's interaction with its environment.

Coordinated behavior among bacteria in biofilms has been observed, specifically concerning autolysis and cell death. Autolysis refers to self-destructive cell or tissue degradation, usually facilitated by specific enzymes, which releases the contents of the cell [20]. While autolysis and programmed cell death can often be the result of antibiotic interference, pH, temperature, and other factors, cell death is a highly regulated and complex process which may also be directly induced or repressed by molecular

regulation [21, 22]. The role of cell death in population differentiation and dispersal has been studied specifically for the *Pseudomonas aeruginosa* biofilm [23]. Autolysis has also been observed in the development of *S. aureus* biofilms, where a fraction of the biofilm cells will self-digest. Autolysis of a small percentage of biofilms cells enhances biofilm adhesion and formation due to the release of proteins and extracellular DNA (eDNA) [24]. Importantly, studies have shown that early release of eDNA through cell lysis facilitates biofilm adherence and eDNA itself is an important structural component in mature *S. aureus* biofilms [7, 25, 26]. While autolysis is an important function in biofilm development, research has shown that less than 1% of the wild-type population of *S. aureus* biofilm undergoes cell lysis within the first 24 hours of biofilm development [25].

As a biofilm is comprised of embedded bacteria cells, cell surface properties and interactions have been shown to play an integral part in formation. Genetic manipulation of bacteria has begun to identify specific genes involved in biofilm formation [27]. Such differentiation has been credited in the development of a biofilm's heterogeneous structure. Particularly, adhesion proteins on the surface or cell wall of *S. aureus* are produced at different rates depending on the part of the biofilm growth cycle, improving its ability to adhere to biomaterials and other bacteria [28].

Often these experiments involve molecular tagging or bulk chemical analysis of a biofilm, which can provide time sensitive information but often may not provide the spatial sensitivity desired for such a heterogeneous structure.

1.2.2 Structural

Bacteria within a biofilm secrete extracellular polymeric substances that hold them together. These substances may include polysaccharides, proteins, or even nucleic acids and may also function as protection against antimicrobial action [13].

Researchers have created conceptual models to differentiate between biofilm structures. Biofilms in medical and marine environments have been observed to form cell clusters in matrix-enclosed ‘towers’ and ‘mushrooms’ separated by interstitial channels [3, 29]. Diversification in structure and cell density may provide better access to flow, and therefore nutrients, as it’s been suggested that a cluster of cells without an internal nutrient pathway are limited in size to between 100 um and 1mm [30].

Research studies have investigated the relationship between access to nutrients and biofilm formation. A computational study suggested a link between high nutrient concentration in a substrate and film structure. However, while it considers molecular diffusion, the results are uncoupled from the flow environment [31]. An experimental study that demonstrated the relationship between nutrient supply and bacteria growth within a biofilm provides details on individual cell metabolic activity as a function of position and time [32]. In fact, a review of experimental studies has shown that biofilms have heterogeneous structures, access to nutrients, genetic expression, and metabolic activity, all of which factor into unique environmental niches within the biofilm [13]. Such differences in activity as well as the production of extracellular signaling molecules can generate forces that directly affect the biofilm itself [30].

Experimental observations provide confirmation that the biofilm structures of *S. aureus* are temporally and spatially heterogeneous, consisted of discrete cell clusters

separated by interstitial channels and voids [12]. In fact, tower structures that developed in more mature *S. aureus* biofilms appear to have internal cavities lined with a layer of eDNA and dead cells [7]. The eDNA serves to provide structural support and may play a role in surface and cell-to-cell adhesion [11]. More recent work revealed genetic differences regarding cell death between two different types of tower structures, expanding the understanding of biofilm structure, development, and dispersion in *S. aureus* [33].

Challenges exist in quantifying biofilm populations. Several techniques employed for cell counting in biofilms require the harvesting of biofilms from their substrate, and therefore cannot completely recover the cells and are not time sensitive [3]. These studies are largely qualitative or low resolution models that provide insight into the diverse biofilm community but may not provide enough physical insight to connect the biochemical environment to the fluid stress environment that the biofilm experiences. A noninvasive method to calculate cell coverage over time in within a channel using brightfield images was presented by Moormeier, and can be performed simultaneously with velocity measurements or other such data acquisitions [5].

Researchers have estimated properties of film structure from bulk observations or experimental images on specific structures. Studies have evaluated the morphology of biofilm structures using image analysis, providing microscale detail, but are often limited to 2-dimensional data [34].

Experiments have been conducted to better characterize the material properties of individual bacteria, with an eye towards the evolution of improved material models that consider the non-homogeneous structure of biofilms. Studies such as Chen’s have

furthered the concept that the viscoelastic deformation of the bacterium cell during contact with a surface plays a role in adhesion and detachment [35]. In addition to the better understanding viscoelastic nature of the biofilm itself, study of dispersion of rolling *S. aureus* emboli highlighted the behavior of viscoelastic tethers [36]. The viscoelastic nature of the biofilm polymer may help reduce drag on the biofilm itself [29]. Biofilms can also be considered as composites of colloids embedded in a cross-linked polymer gel, with a common feature being that the viscoelastic properties of the biofilms are dependent on the fraction of liquid in the material [30]. These properties can be significantly affected by the availability of water in the biofilms environment. Additional computational studies have incorporated this understanding to improve their models [37].

1.2.3 Fluid Interaction

Biofilms can grow under fluid conditions ordinarily dangerous to individual bacteria, and in fact may use these conditions to facilitate their growth and spread. A force diagram presented by Persat clearly presents the balance between hydrodynamic shear force, adhesive forces, and friction due to surface motility [38]. Biofilms formed at high shear environments have been shown to be stronger and more resistant to failure than those formed in low-shear environments [3]. Additionally, biofilms formed in environments with higher shear or higher fluctuations in shear may also have a higher tolerance to antibiotics [39].

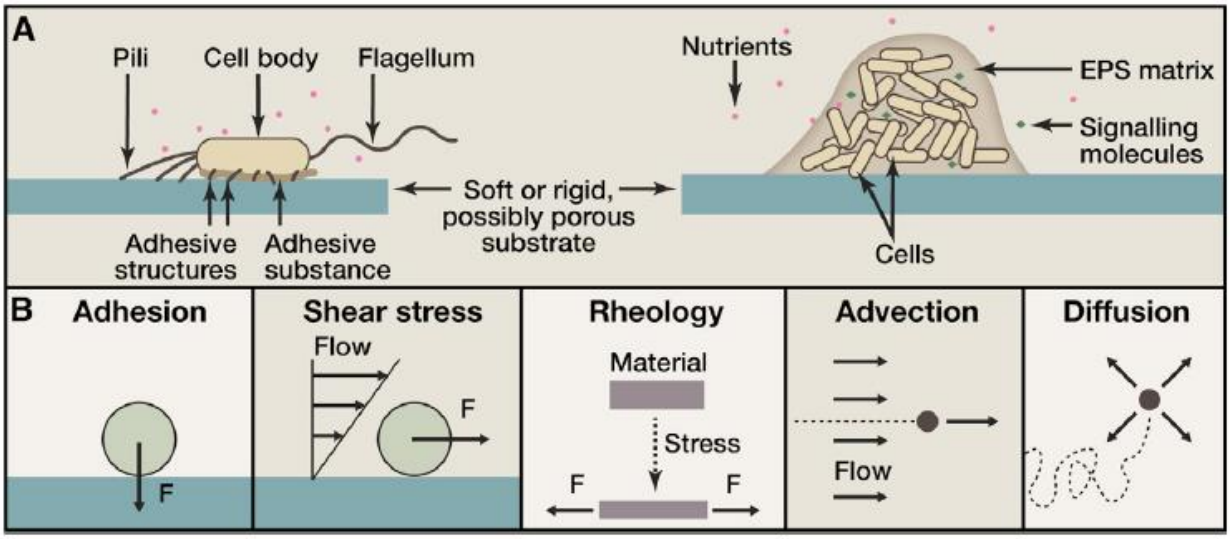

Figure 1.3 A) shows representations of common components in bacteria for mobility, adhesion, and structural integrity. B) shows the distinct role different forces have on a specific cell [38].

Varying and steady fluid shear are conditions that *S. aureus* biofilms encounter in physiological settings such as catheter and vascular infections, and are important considerations in experimental study [9]. Such studies have observed creeping behavior as well as the formation and spread of rolling emboli of biofilm-associated cells as biofilm responses to fluid shear [36]. Interestingly, studies have been performed that varied the applied shear and measure biofilm deformation to estimate its viscoelastic properties [29].

Additional research in mixed-species biofilm formation indicated that the breakoff of biofilm clusters and streamers had a direct relationship with the value of the wall shear stress, presented as a result of the dominance of drag force over the streamer material strength [29]. While such experiments allowed for the calculation of variables of interest such as pressure drop and velocity, experimental measurement limitations such as using a pressure transducer and speed limited imaging systems ultimately prevented a higher temporal and spatial resolution understanding of biofilm structure breakoff.

In fact, flow conditions may directly influence the formation and spread of biofilms as well as its resistance to antibiotics and the immune system. The increased resistance of biofilms, combined with their ability to detach, may allow them to more easily overcome the immune system. One such study states that sessile cell and emboli detachment from a biofilm when its tensile strength is exceeded is the structural characteristic that has the greatest impact on bacterial infections [3]. This may occur during changes in direction or in rate of flow. Antibiotic resistance of biofilm emboli has been shown to be dependent on the size of the detached emboli and also due to the slower growth of biofilm-associated cells as opposed to planktonic cells [12].

Since *S. aureus* does not employ swimming mechanisms such as flagella its sensitivity to the flow environment may be essential to its dispersion strategy. In fact, studies in curved geometries where S. aureus has been shown to form biofilm streamers at corners seems to indicate that by forming streamers, S. aureus benefits from the mass transport of new cells to the streamer location, fortifying its porous structure and facilitating its growth to block channels [9]. Generally, motility may enable a cell to acquire nutrients or move towards more favorable conditions [15]. In fact, high shear flows may prove challenging for swimming or motile bacteria to travel towards new areas or nutrients, as it tends to promote surface attachment [40].

1.3 Research Goals

It has been shown that biofilm behavior is highly complex and that it is a temporally and spatially dynamic system which appears to interact with and respond to its environment. While there have been biochemical and physical structural studies, there is

a lack of knowledge of the instantaneous behavior of distinct structures within a biofilm as part of a fluid environment. Questions surrounding the details of fluid-structure interaction during tower development and failure remain, in addition to the interaction between cellular processes and these mechanical forces.

A significant contribution would be to use a non-invasive imaging technique that can allow for fluid and structural observations of biofilm growth in a temporally and spatially detailed manner. The ability to experimentally resolve growth and detachment of individual cell and cell towers combined with a similar level of knowledge of the fluid environment would not only describe the force distribution during tower evolution but also may provide indicators of what leads to tower growth. The use of micro-Particle Tracking Velocimetry provides the temporal and spatial resolution that is ideal for this pursuit.

Specifically, data collection for the purpose of generating planes of 2-dimensional velocity fields will yield the instantaneous wall shear stress experienced by the biofilm during development. Cell coverage data provides a more detailed description of the heterogeneous biofilm boundary conditions during development to pair with flow information. These two measures enable direct comparison of biofilm growth between biofilms that do and do not develop towers. Additionally, quantification of biofilm growth and changes in the flow field across different applied flow rates will better describe the link between bulk flow and biofilm response.

Hypothesis and specific aims:

The working hypothesis is that there are fluid dynamic indicators that precede tower formation and that tower formation is indeed stress dependent. The study of

formation and breakup of towers requires the ability to predict and control their formation, and this study is the first to incorporate a mechanics based approach to this problem. The specific aims of this dissertation are:

- Identify wall shear stress during biofilm formation that precedes tower development by generating a time series of two-dimensional velocity fields
- Determine the frequency of tower formation as a function of applied shear
- Determine cell density behavior as a function of applied shear

1.4 Coordinate System

Experiments were conducted within a microchannel with a rectangular cross section. Figure 1.4 illustrates the Cartesian coordinate system that is used for all calculations. The x-axis is parallel to the flow and is also referred to as streamwise direction. The y-axis is perpendicular to channel side and is referred to as the transverse direction. The z-axis is perpendicular to the channel bottom and the direction of flow and is referred to as the wall-normal direction.

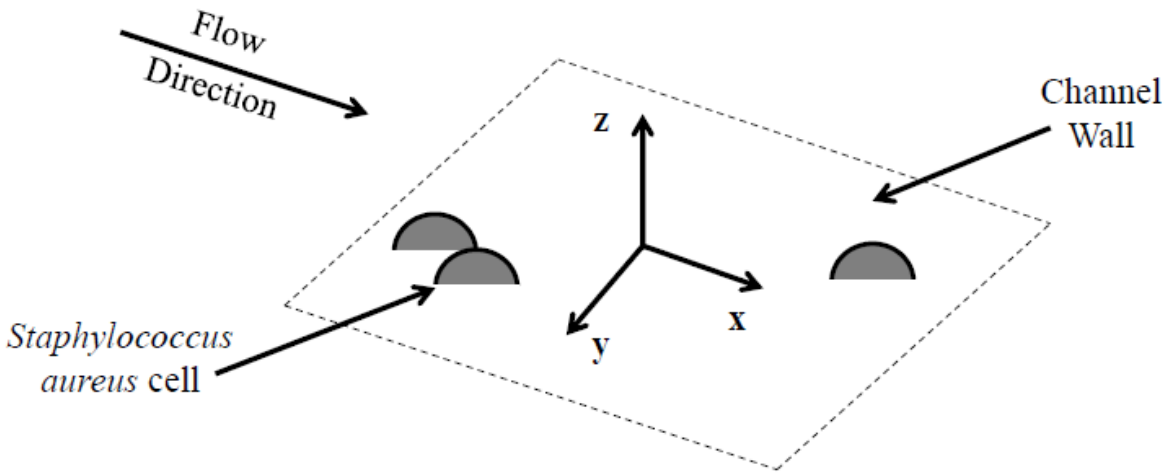

Figure 1.4 Coordinate Axis for experimental measurements within Fluxion Bioflux™ 1000 microchannel.

CHAPTER 2

EXPERIMENTAL MATERIALS AND APPARATUS

This *S. aureus* flow study required examination of the development of tower structures over extended periods of time (i.e. 10-16 hours). A microscope, flow channel, and pump system was used to create a proper flow and growth environment for observation. A standard micro particle tracking velocimetry (μPTV) technique was employed in order to collect flow data in a time and scale sensitive manner requiring a high speed camera for recording data. A separate automatic imaging procedure using the same equipment was used for collecting cell density data in order to have a higher sampling frequency. Information regarding these systems and the preparation of S. aureus cells are described below.

2.1 Information on *S. aureus* isolates

The S. aureus strains used in this study were derived from osteomyelitis isolate UAMS-1. All experiments were initiated with fresh overnight cultures grown at 37C in tryptic soy broth (TSB; EMD Biosciences, Gibbstown, NJ).

2.2 Information on Flow Control System

The Bioflux^{TM} 1000 microfluidic system (Fluxion Biosciences Inc., San Francisco, CA) was used for all experiments to observe the development of biofilms over time at a specified flow rate. The Bioflux^{TM} system includes a Nikon Ti-S inverted microscope, with hardware controllers for pump and microscope stage manipulation, a vapor trap to

reduce condensation, a pressure interface to connect the pump to the plates, and a heating plate to maintain desired temperatures. Figure 2.1 displays these components.

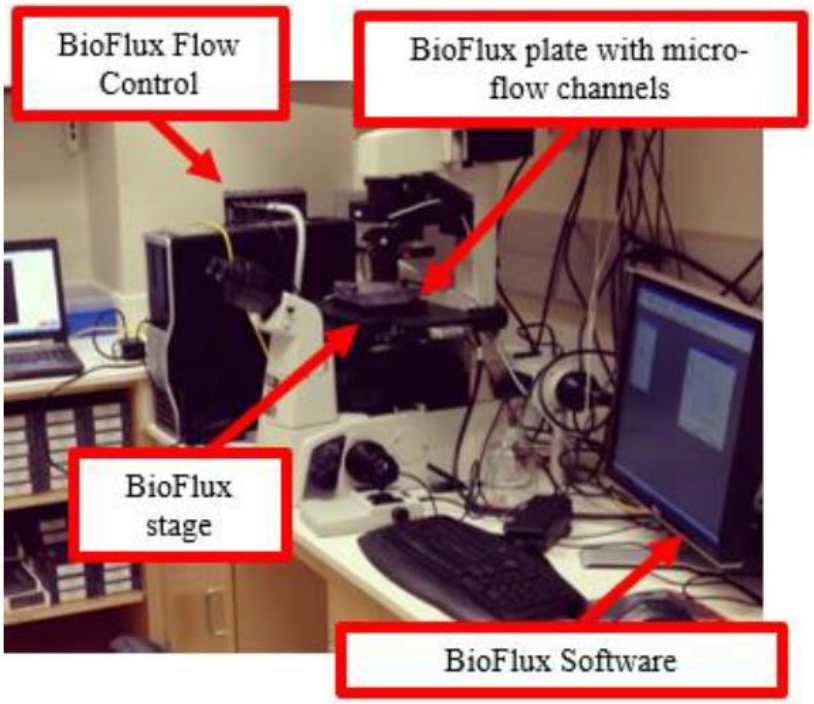

Figure 2.1 The basic components of The Bioflux™ system [41].

Either a 24-well or a 48-well plate with embedded micro channels was used to study *in vitro* flow condition, depending on the desired flow rate. Both the 24- and 48-well plates could be run using applied shear stresses ranging from 0 – 20 dyne/cm^2. The 24-well plate included eight embedded flow channels while the 48-well plate includes twenty four embedded flow channels. Every channel in a 24-well plate had two input wells and one output well, while the channels in the 48-well plate had one input well and one output well. Figure 2.2 shows both the 24-well and 48-well Bioflux™ Plate layout. The input and output well volumes are 3 mL for the 24-well plates and 1 mL for the 48-well plates.

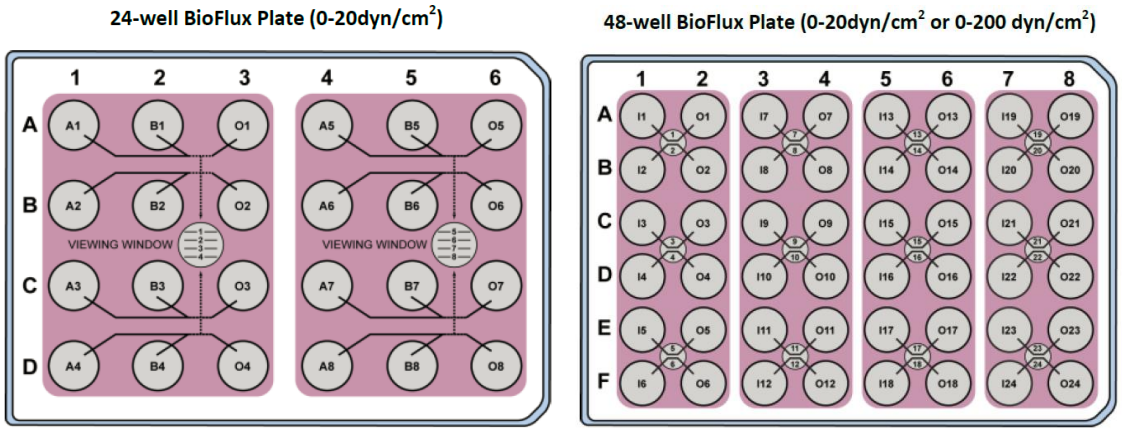

Figure 2.2 Representation of the 24- and 48-well Bioflux™ plates [42].

The Bioflux™ plate microfluidic structures were cast from PDMS and secured on top of a 180 µm cover slip glass; this also served as the channel bottom. The channels had a rectangular cross section, with a 350 µm width and a 70 µm height. Bioflux™ PC software was used to select the desired shear rate and channel in order to direct the pump to apply a pressure difference across the desired channel, creating flow. The same software was used to control the automated microscope stage, which could be moved vertically in increments of 0.1 um.

The x-y position of the stage could also be controlled through the PC software and this feature was used during separate automated experiments for cell density. It was not used for µPTV experiments. Additionally, the Bioflux™ plate fit into a heating plate that allowed for precise control of the working temperature during experiments. The Bioflux™ PC software was set to maintain a 37 C temperature for all experiments.

A Phantom Miro M310 (Vision Research, Wayne, NJ) high speed color camera was used to record all images for PTV. It used a thermoelectrically-cooled CMOS sensor with a 1024 x 768 pixel resolution, a12-bit pixel depth, and 20 um pixel size. The camera was attached to a Nikon Ti-S inverted microscope and controlled by Phantom Camera Control

(PCC) software (Vision Research, Wayne, NJ). The Retiga EXi camera from QIMAGING was used for all cell density data. It is a CCD camera which has a 1392 x 1040 pixel resolution and a 6.45 μm pixel size. A Nikon Plan Fluor ELWD 40x/0.60na Ph2 DM objective was used. The light source, a LED microscopic lamp, was capable of 100W but was operated at 40 percent maximum intensity to avoid disrupting normal biological activity of the bacteria.

2.3 Micro-Particle Tracking Velocimetry

Flow velocity data were obtained from micro-Particle Tracking Velocimetry (μPTV). This technique involves recording video sequences of a flow seeded with small neutrally buoyant particles. A particle tracking algorithm then calculated individual velocities for every particle in the field of view. The experimental materials and technique is discussed further below.

The aim of the μPTV technique is to measure flow velocity in a noninvasive way. The μPTV technique requires seeding particles, an imaging system, and a light source. Figure 2.3 provides an example of how PTV works. Two images are taken in quick succession, separated by a short, known time period of Δt. The velocity is calculated using the known particle displacement of each particle, Δx, and the time between images. The particle tracking algorithm records the velocity for each moving particle from multiple image pairs and then averages the velocity across distinct 45x45 pixel sections of the channel field of view to create a composite velocity field. The experiment is set up in such a way to reduce the influence of out-of-plane particles and image processing

techniques are employed in order to remove background particles to better isolate the moving, in-plane particles.

The experimental flow setup includes a flow channel and a pump. This experiment investigated flow on the microscale, meaning that the camera was attached to a microscope and used a microscope objective to focus on a particular z-plane inside the microchannel. The light source illuminated the seeding particles which are carried along in the flow. The high speed camera records sequences of images with a short time period between images. The particle tracking algorithm uses the small particle displacement between image pairs to calculate individual particle velocities within the field of view.

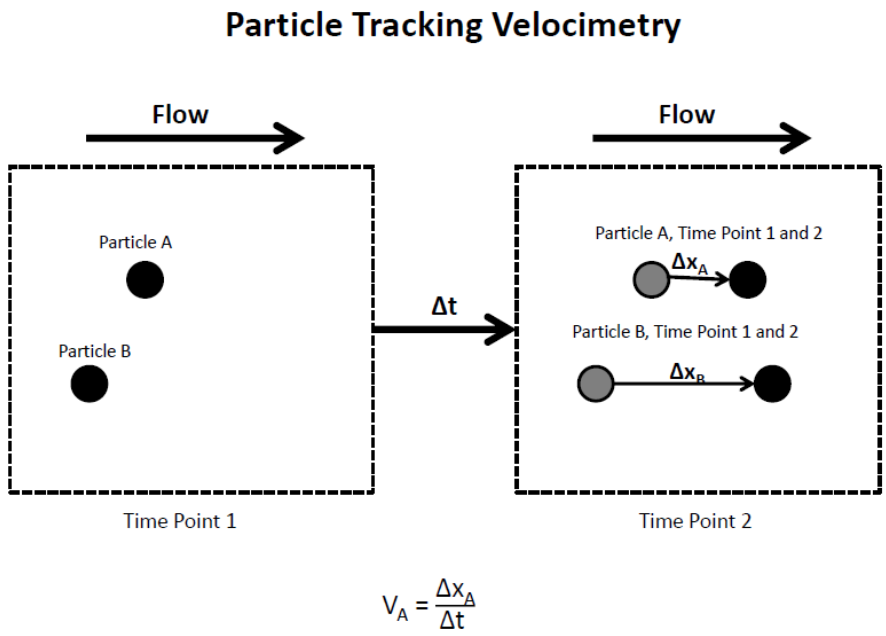

Figure 2.3 An example of how velocity is calculated using particle displacement. Particles A and B move a short distance, Δx, over a short time period, Δt. The velocity is calculated using the known displacement of each individual particle over time.

The *S. aureus* cells themselves served as the necessary seeding particles. They are approximately 1 um in diameter and thus are larger than the wavelength of the

illuminating light. These cells are not neutrally buoyant and will settle on the channel bottom after flow has been stopped. However, cells did not fall out of focus between image pairs because the time interval was brief. *S. aureus* cells had a cell doubling time of 30 minutes and the seeding density of unattached cells in the flow increased with time during the experiment. Trial experiments using neutrally buoyant 1 μm seeding particles exhibited abnormal biofilm behavior. While smaller particles may avoid this issue and provide a more consistent seeding density, smaller particle sizes would potentially reduce the effectiveness of the particle tracking algorithm. This necessitated the use of the bacteria itself as a seeding particle in order to avoid altering normal *S. aureus* biofilm development.

Data were recorded in the lower 20 um of the channel, where cell density was highest, to best observe biofilm formation. Trypsin Soy Broth (TSB) was the working fluid because it was suitable for S. aureus biofilm growth and was maintained at the ideal temperature of 37C.

A challenge of μPTV is that more of the volume of the flow microchannel is illuminated as opposed to a thin, two-dimensional slice of the field of view. The camera records a two dimensional image that may include out-of-plane particles, potentially contributing to error in vertical identification of the measurement plane. This issue requires determining the thickness of the measurement plane, or the depth of field, as well as the appropriate image thresholding parameters to use to isolate out-of-plane particles when processing images.

The depth of field of a microscope objective is a described as the distance from the nearest object plane in focus to that of the farthest plane also in focus [43]. The equation is

$$D_f = \frac{\lambda \cdot n}{NA^2} + \frac{n}{M \cdot NA} e \qquad \text{Eq. 2.1}$$

Where λ is the wavelength of the illumination source, n is the index of refraction of the medium, and NA and M are the numerical aperture and magnification of the microscope objective. The variable e is the lateral resolution or the minimal detectable distance between two closely spaced points in a specimen, and is defined as

$$e = \frac{0.61 \cdot \lambda}{NA} \qquad \text{Eq. 2.2}$$

The microscope objective used was the CFI Super Plan Fluor ELWD 40x, which had a magnification, M, of 40x and a numerical aperture, NA, of 0.6. The illumination wavelength was 550 nm and the index of refraction of water is 1.33. These values yielded a depth of field of 2.1 µm and a lateral resolution of 0.55 µm. A pixel to unit length scale in the data as determined by the camera sensor was found to be 2.06 pixel/µm based on the known pixel resolution and the width of the microchannel. It is also important to note that the microscope objective had a working distance of 2.8-3.6 mm, which suited the distance between the microscope objective and the top of the automated stage upon which the Bioflux^{TM} plate was placed. The correction ring was set to 0.18 to account for the thickness of the glass bottom of the microchannel.

The next step in identifying the vertical plane position more accurately requires image processing techniques to minimize the amount of planes across which a cell was visible. Grayscale images that had light intensity values of 0-256 were converted to a

binary image using a specific threshold value. Different threshold values were tested on a series of images at multiple planes over stationary cells to identify the value that best reduced the amount of planes across which those cells were visible. An image was taken at vertical increments of 0.1 μm over a distance of 4 μm and the threshold value of 71 yielded 7 images, or 0.6 μm, across which the particles were visible. This means the experimental plane thickness was 0.6 μm and that there is a $\pm$ 0.30 μm uncertainty in vertical position. Figure 2.4 shows a series of 25 pixel x 25 pixel cropped areas from the 40 images described, with a 0.1 μm separation between each image. The grayscale images in the 'A' group were converted to a binary image using the threshold value as described above, the result of which is shown in the 'B' group.

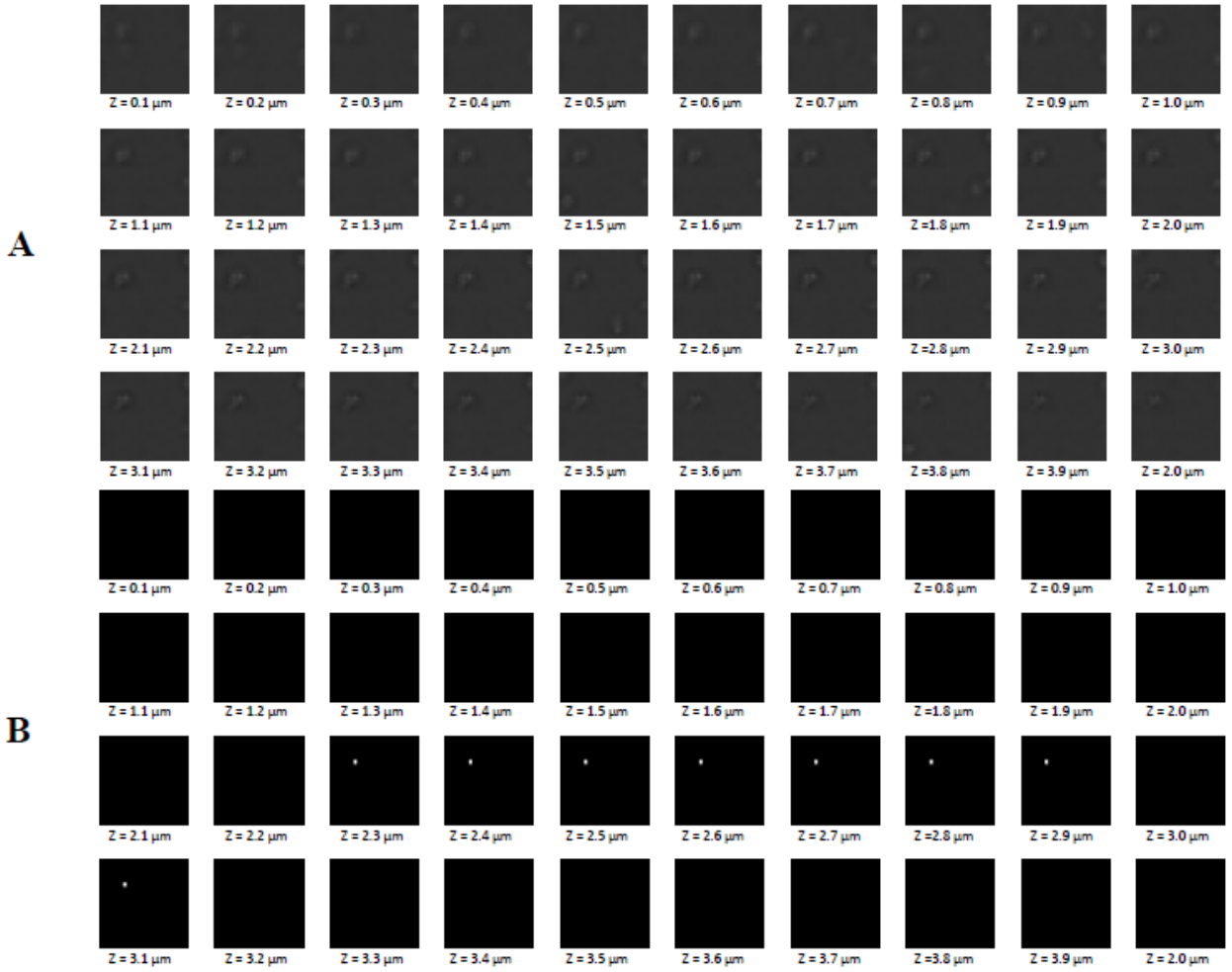

Figure 2.4 Images were recorded at 40 vertical planes spaced 0.1 um apart. A) Shows the grayscale images, cropped to frame a cell. B) Shows the same images which have been converted to a binary image using a threshold value of 71, yielding 7 consecutive planes over which the particle is still visible.

CHAPTER 3

EXPERIMENTAL METHODS

3.1 Preparing *S. aureus* for experiments

The Bioflux^{TM} 1000 microfluidic system was used for all experiments to observe the development of biofilms over time under different flow rates. In order to grow biofilms in the Bioflux^{TM} system, the channels were first primed for 5 minutes with 200 µL of TSB at 5.0 dynes/cm^2. After priming, the tryptic soy broth (TSB) was aspirated from the output wells and replaced with 200 µL of fresh overnight cultures diluted to an optical density (OD) of 0.8. The channels were seeded by pumping from the output wells to the input wells at 2.0 dynes/cm^2 for 5-10 seconds. Cells were allowed to attach to the surface of the channels for 1 hour at 37C. Excess inoculums were carefully aspirated off, and either 1 or 3 mL of 50% TSB, depending on the plate used, were added to the input well(s) and pumped at a constant, specified shear for 16 hours.

3.2 µPTV and the Flow System

The *S. aureus* cells served as the seeding particles for all experiments. Total seeding particle density changed over the course of the experiment due to cell reproduction, which occurs approximately every 30 minutes. Local seeding particle density within the field of view also changed with time due to cell exodus, a cell clearing event that occurs approximately halfway through biofilm development in these experiments, as well as due to cell adhesion and cell clump formation, during the later stages of biofilm development. The optimum seeding density for recording data occurred within the first few micrometers of the channel bottom as S. aureus cells tend to settle

along the channel bottom over time. Therefore data were recorded within 10-15 µm of the channel bottom. Cell settling did not occur quickly enough to cause cell dropout within image pairs or across images recorded at a given time point.

The working fluid was trypsin soy broth (TSB; EMD Biosciences, Gibbstown, NJ), which has a dynamic viscosity of 0.88 cP at the working temperature of 37C [44].

The BiofluxTM micro-flow control system used an electropneumatic pump with the 24-well and 48-well Bioflux^{TM} plates to conduct experiments at 0.15, 0.3, 0.6, 0.9, and 1.5 dynes/cm2. These shear stresses correspond to flow rates of 16, 32, 64, 95, and 159 µL/hr and the applied shear stress of 0.6 dynes/cm^2 yields a Reynolds numbers of 0.001.

3.3 Imaging System

Brightfield images for µPTV were recorded at 45 or 90 minute intervals, with image pairs recorded at a specific frequency with a burst period that maintained a particle displacement of approximately 10 pixels within image pairs. Table 3.1 provides more information on the exposure, frequency, and burst period settings for the different applied shears that were tested. 2000 to 4000 images were recorded at each plane and it took approximately about 2 minutes to record and save at each plane. Planes are separated by either 1 or 2 um, depending on the data set. Brightfield images recorded for purely cell density data were recorded at 5 minute intervals for approximately 16 hours. One image was recorded per channel at each time point. For µPTV and cell density data, the light source, a LED microscopic lamp which was capable of 100W, was operated at 40 percent

maximum intensity to avoid disrupting normal biological activity of the S. aureus bacteria.

Table 3.1 Applied Shear, exposure, burst period, and frequency settings for experiments.

Applied Shear	Plate Size	Exposure [μs]	Frequency [Hz]	Burst Period [μs]
0.15	48-well	500	75	1200
0.6	48-well	500	50	1200
1.5	24-well	500	100	5000

3.4 Position Identification

The channel bottom was located using both the Bioflux controller and visual confirmation prior to recording data at each position in order to reduce error in plane relocation. The controller allowed for vertical movement of the stage in 0.1 um increments. μPTV experiments required the recording data at several planes separated about 1 or 2 um in the same channel position. After identification of the channel bottom, the microscope stage was moved only in one direction in order to reduce error from hysteresis. First the microscope was focused on the space just below the channel bottom then the stage was moved down so that higher planes above the channel bottom were brought into focus.

3.5 Data Processing

Identification and categorization of cells both in flow and settled on the channel bottom were necessary for both calculating the cell number density and using the PTV technique. The identification process required recognizing and using the difference in grayscale intensity values and the channel bottom for the purposes of isolating moving

cells from stationary cells. The field of view was broken into distinct 25 x 25 pixel regions to better compare the flow and biofilm properties of tower and non-tower areas.

Images used for calculating cell density were inverted so that the cells showed as brighter than the background then converted to binary using a specific threshold value for each data set in order to isolate cells. The experimental data used for this purpose was recorded at 5 minute intervals and three images were averaged together to create a background image of non-moving cells, yielding a new time interval of 15 minutes. The number of bright pixels, representing cells, in a given 25 x 25 pixel region were summed and divided by the pixel area, yielding a cell density value of bright pixels per pixel area. The cell density was calculated in a given channel at all time points starting at the beginning of the experiment.

Images used for PTV were converted to grayscale and then converted to a binary image using an intensity threshold value. A background image was generated every 100 image pairs in order to adapt to any changes in the biofilm. Lastly, a filtering process was used to remove any noise remaining from image processing prior to using the PTV algorithm. These steps are shown in Figure 3.1. Generated velocities were averaged over a 45 x 45 pixel window to smooth the velocity field. More information on the algorithm can be found in Lambert [41].

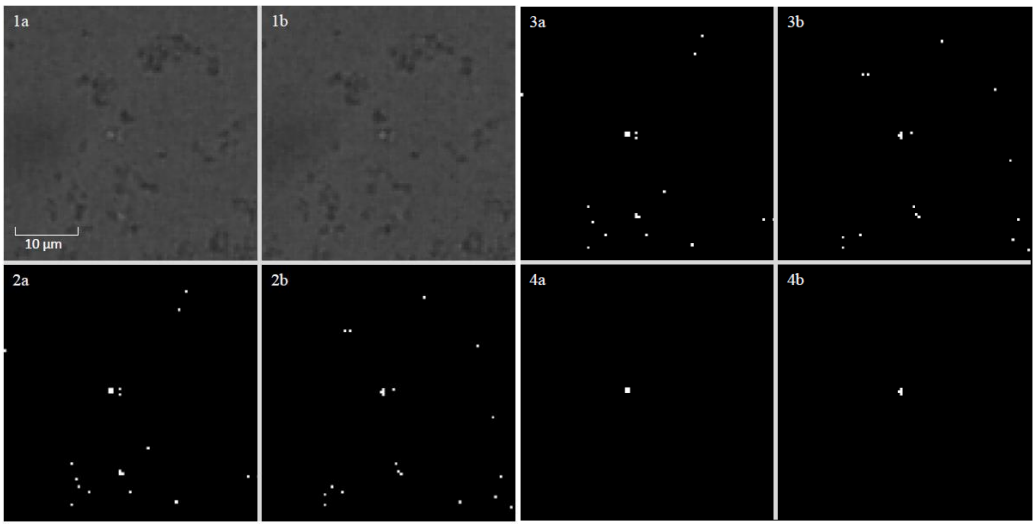

Figure 3.1 A series of image pairs showing the image processing steps to prepare a raw image pair for the Particle Tracking Velocimetry algorithm. Images 1a and 1b show a raw image pair, which have been converted to grayscale from a RGB format. Images 2a and 2b show the image pair after the threshold process. Images 3a and 3b show the image pair after background removal. Images 4a and 4b show the image pair after a filtering process has removed any remaining noise.

3.6 Analysis

The data collected for the purposes of calculating cell density as a function of time served to measure structural characteristics during biofilm formation and leading up to tower development. It also facilitated the observation of the frequency with which towers may form in the *S. aureus* biofilm for different applied shear stresses.

The first term analyzed using the cell density data is the average cell density, whereby the cell density that was calculated in each 25 x 25 pixel region as described in section 3.5 was averaged across the entire channel. As there were multiple channels of data which did and did not form towers, the average cell density in a single channel was averaged with other channels, separated into tower and non-tower forming categories.

The Spatial Root Mean Square of these average cell densities was calculated using the equation 3.1 and non-dimensionalized by the average cell density in the channel at each time point. The Spatial RMS of cell density describes the range of cell densities across the channel.

$$spatial\ RMS(t) = \left[\frac{1}{yz}\sum_{ij}^{yz}\left(CD_{ij}(t) - \overline{CD_t}\right)^2\right]^{\frac{1}{2}} \qquad \text{Equation 3.1}$$

Where,

y =number of 25x25 pixel boxes in a row (height)

z = number of 25x25 pixel boxes in a column (width)

t = represents the given time point at which the spatial RMS is calculated

$\overline{CD_t}$ = the average cell density of all of the 25x25 pixel regions used in the spatial RMS calculation, for the given time point of calculation

$CD_{ij}(t)$ = the cell density of the 25x25 pixel region at the specific y-row and z-column for the given time point of calculation

Presenting the cell density distribution across the channel at each time provides more information than the bulk cell density average and can be used to examine whether and how cell density shows any differences between tower and non-tower forming channels.

While viewing the cell density distribution at each time provides a qualitative comparison between tower and non-tower forming channels, calculating the skewness of the cell density distribution creates a metric to make more direct comparisons across data sets. The Skewness is calculated using equation 3.2.

$$Skewness(t) = \frac{1}{RMS}\left[\frac{1}{yz}\sum_{ij}^{yz}\left(CD_{ij}(t) - \overline{CD_t}\right)^3\right]^{\frac{1}{3}} \qquad \text{Equation 3.2}$$

Where,

y =number of 25x25 pixel regions in a row (height)

z = number of 25x25 pixel regions in a column (width)

t = represents the given time point at which the spatial RMS is calculated

$\overline{CD_t}$ = the average cell density of all of the 25x25 pixel boxes used in the spatial RMS calculation, for the given time point of calculation

RMS = the average dimensional spatial RMS value at this time point for the pixel area used.

Evaluating the flow results requires considering that there is only data for one channel each for a tower and non-tower forming biofilm. The complexity of the experiment and the low frequency of tower formation prevented the availability of multiple data sets for comparison. The study of these results as they are can provide meaningful information as this method and process has not been attempted previously.

Specifically, qualitative observations of the velocity field where the tower forms in one channel and where it does not in the other channel can answer the question of how the flow field changes prior to tower formation in the area where a tower forms. Further calculating the average velocity in the specific region of tower formation prior to its formation could quantify any local flow phenomena that are present in comparison to the flow field in the non-tower forming channel. This is accomplished by simply averaging all velocity within the designated region of tower formation at each time point. Furthermore, calculating the spatial RMS of the velocity within the specific region of tower formation prior to formation describes the distribution of velocity values as a function of time, which may serve as an indicator for tower formation. The spatial RMS of the velocity is calculated using equation 3.1, except using the instantaneous velocity at a given coordinate and the average velocity within the region instead of cell density. The

spatial RMS of velocity as presented in the results section has been non-dimensionalized by the average cell density in the region from the first time point after cell exodus.

CHAPTER 4

RESULTS

The experimental results for the *S. aureus* flow and cell studies are presented below. The study of *S. aureus* biofilm tower formation frequency as a function of applied shear stress serves to establish whether there is indeed a relationship between the applied shear stress and tower formation, and if there is, to quantify it. A deeper look into the change in average cell density in the channel over the course of biofilm formation at different applied shear stresses, for both tower and non-tower forming channels, further serves to distinguish differences in biofilm formation across the applied shear stresses studied that may play a role in the different tower forming frequencies. While calculating the average cell density in a channel provides a quantitative description of the biofilm, it is important to further calculate the Spatial Root Mean Square (RMS) of the average cell density on the channel bottom in order to describe how uniform the distribution of cell density is.

Additional information on the spatial profile of the cell density at a given time point in the development of the biofilm is found by considering the cell density distribution within the channel as a function of time and applied shear stress, which may also contribute to differences in tower forming frequencies. Often, a raw image showing cells adhered to the channel bottom in early stages of biofilm development for channels where a tower will form and where a tower will not form are indistinguishable from one another prior to tower formation. Studying the cell density distribution at these time points may provide insight into cell density differences that are not visible to the naked eye. Calculating the skewness of the cell density distributions provides a metric by which

to compare the cell density distributions of channels for the different applied shear stresses studied.

The study of the velocity fields of tower and non-tower forming channels may help to determine whether there are localized flow phenomena which contribute to the formation of a tower within a biofilm. The case of the applied shear stress of 0.6 dynes/cm^2 was chosen due to its high tower forming frequency. Visual comparisons of the velocity fields are presented and complemented by the calculation of average velocity and the Spatial Root Mean Square which serve to distinguish any statistical differences in the velocity field between the tower and non-tower forming cases.

4.1 Tower Forming Frequency and Fluid Shear Relationship

Informal observations indicated that there may be a relationship between the applied shear stress and the frequency of tower formation within the *S. aureus* biofilm, but this relationship has not yet been verified. This first section serves to quantify the frequency of tower formation as a function of applied shear stress to determine what, if any, relationship exists, by testing applied shear stresses that cover an order of magnitude.

Experiments were run for the applied shear stresses of 0.15, 0.3, 0.6, 0.9, and 1.5 dynes/cm^2, and images were recorded at fifteen minute intervals over the duration of biofilm formation. A minimum of 18 channels that underwent exodus and did not clog were used for each applied shear stress in order to determine the fraction of channels that developed towers.

Table 4.1 shows the tower forming frequency for the applied shear stresses of 0.15, 0.3, 0.6, 0.9, and 1.5 dynes/cm^2. The results show that the applied shear stress of 0.6 dynes/cm^2 had the highest tower forming frequency of 0.33. The tower forming frequency decreased as the applied shear stress increased or decreased from 0.6 dynes/cm^2, showing that the applied shear stress has an effect on tower forming frequency and that 0.6 dynes/cm^2 is an ideal applied shear stress for creating tower forming *S. aureus* biofilms.

Table 4.1. Tower forming frequency as a function of applied shear stress for the applied shear stresses of 0.15, 0.3, 0.6, 0.9, and 1.5 dynes/cm^2.

Applied Shear Stress [dynes/cm^2]	Number of Channels	Number of Channels with Towers	Fractional Occurrence of Tower Formation
0.15	31	2	0.06
0.3	22	0	0.00
0.6	18	6	0.33
0.9	18	2	0.11
1.5	24	0	0.00

4.2 Cell Density as a function of time

As biofilms have been described as complex structures that are temporally and spatially heterogeneous, studying the average cell density in a channel at each time point during biofilm development may provide more insight into the differences between biofilms that form towers and those that do not, at any applied shear stress [12]. The cell density in the channel changes with time for each applied shear stress due to cell multiplication, attachment, and exodus.

The cell density within a channel was calculated at each time point as discussed in section 3.5. Data for each applied shear stress include multiple channels for tower and no-tower results and the data presented in this section reflect an average of those channels

for each applied shear stress. Figure 4.2.1 shows the cell density results for all of the applied shear stresses studied, broken into the average values for the tower and non-tower forming channels. Data for tower forming channels are plotted only up until a tower appears. The vertical axis shows the cell density and the horizontal axis shows the experimental time in hours.

The cell density data for 0.6 dynes/cm^2 reaches a higher value prior to exodus in comparison to the cell densities for all other applied shear stresses studied. Cell exodus follows the early stage of multiplication and occurs prior to tower development. As the applied shear stress increases from 0.15 to 0.6 dynes/cm^2 so does the average cell density. The average cell density then decreases as the applied shear stress increases from 0.6 to 1.5 dynes/cm^2. The profile of cell density as a function of time for the applied shear stress of 0.6 dynes/cm^2 follows the profile shown in Moormeier, while the other applied shear stresses show a reduced multiplication stage, exodus, and overall average cell density, indicating a connection between applied shear stress and the value and rate of change of cell density as a function of time [5].

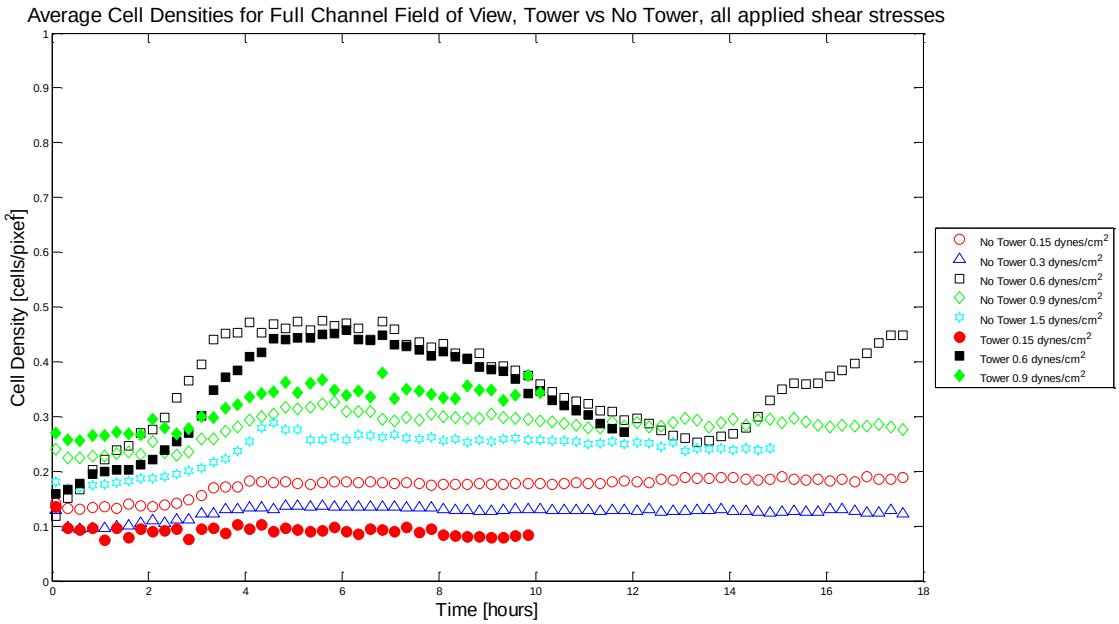

Figure 4.2.1 Averaged cell densities of all applied shears stresses as a function of time for the applied shear stresses of 0.15, 0.3, 0.6, 0.9, 1.5 dynes/cm^2. Markers representing tower data are filled in.

Investigating differences between the tower and non-tower forming channel average cell densities may provide more information at each applied shear stress regarding what biofilm conditions lead to the formation of a tower. In particular, as the applied shear stress of 0.6 dynes was found to have a higher probability of tower formation than all other tested shear stresses, the average cell density of tower forming channels at this applied shear stress may provide insight into what leads to tower formation generally.

Although the applied shear stress of 0.15 dynes/cm^2, the smallest applied shear stress studied for this work, yields a significantly lower frequency of tower formation in the *S. aureus* biofilm, the average cell density of the tower and non-tower forming channels at this applied shear stress may still provide insight into tower formation by

examining any differences that may exist when compared against eachother as well as against the data from the 0.6 dynes/cm^2 case.

The cell density for the applied shear of 0.15 dynes/cm^2 is shown in Figure 4.2.2. The vertical axis shows the cell density and the horizontal axis shows the experimental time in hours. The results are separated into the average cell density for the tower and non-tower forming channels. The tower data plotted represents the average of the cell densities from two channels which formed towers. The tower data are plotted only up until a tower appears.

There is a separation in cell density values and rate of change starting in the first four hours of the experiment. The non-tower forming channels exhibit a relatively higher average cell density in comparison to the tower forming channel and the non-tower forming channel has a small increase in cell density afte rthe first four hours of the experiment while the tower forming channels maintain a relatively constant cell density over the course of the experiment. The average tower cell density as a function of time for the applied shear stress of 0.15 dynes/cm^2 has the lowest value of all the applied shear stresses studied, and both the tower and non-tower forming cell densities do not exhibit a significant multiplication and exodus stage in comparison to the 0.6 dynes/cm^2 case.

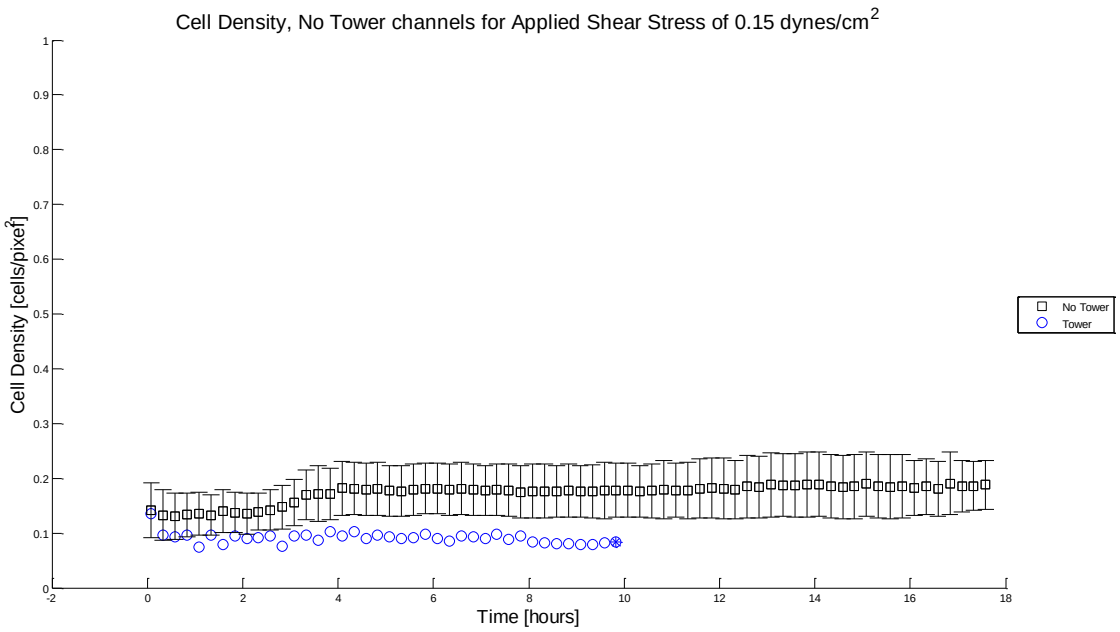

Figure 4.2.2 Cell density as a function of time for the applied shear stress of 0.15 dynes/cm^2. Average Cell density data for tower and non-tower forming channels are shown. Blue markers indicate when a tower formed.

Comparing the cell density as a function of time for the applied shear stress of 0.3 dynes/cm^2, which produced no towers, against tower forming and non-tower forming channels of other applied shear stresses may answer the question of why certain applied shear stresses are better at forming towers than others. For example, if the cell density as a function of time for the non-tower forming applied shear stresses appear similar to the cell density as a function of time for the non-tower forming channels of applied shears that do produce towers, then perhaps the behavior of cell density as a function of time is an indicator of tower formation.

The cell density for the applied shear of 0.3 dynes/cm^2 is shown in Figure 4.2.3. The vertical axis shows the cell density and the horizontal axis shows the experimental time in hours.

The average cell density for the applied shear stress of 0.3 dynes/cm^2 is higher than the average cell density for tower forming channels at the applied shear stress of 0.15 dynes/cm^2 but lower than all other averaged cell densities of the applied shear stresses studied. Similar to the average cell densities of non-tower forming channels for the applied shear stresses of 0.15, 0.9, and 1.5 dynes/cm^2, the average cell density for the applied shear stress of 0.3 dynes/cm^2 shows a small increase in cell density over the first four hours before reaching a near constant value for the remainder of the timeline of biofilm development.

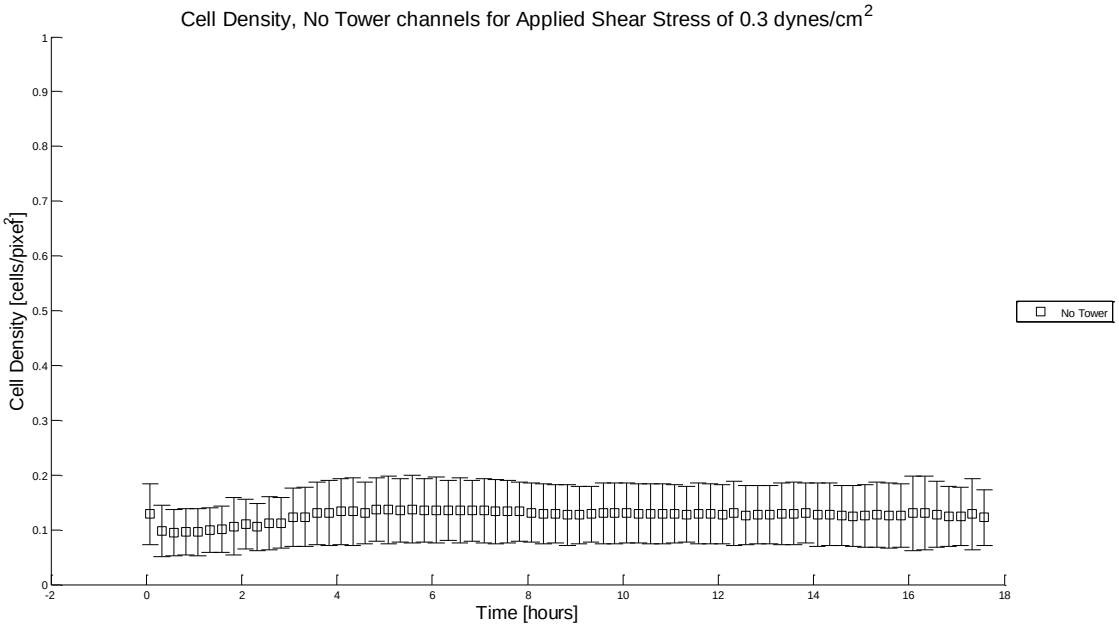

Figure 4.2.3 Cell density as a function of time for the applied shear stress of 0.3 dynes/cm^2. Average Cell density data for non-tower forming channels are shown.

The cell density for the optimal tower forming applied shear of 0.6 dynes/cm^2 is shown in Figure 4.2.4. The vertical axis shows the cell density and the horizontal axis shows the experimental time in hours. The results are separated into the average cell density for the tower and non-tower forming channels. The tower data plotted represents

the average of the cell densities of four channels which formed towers. The tower data are plotted only up until a tower appears.

The averaged non-tower forming cell density starts with a linear rate of change while the averaged tower cell density does not show a linear rate of change until two hours after the experiment starts. After exodus begins, the tower and non-tower forming cell densities follow a similar rate of change and have similar values. This shows that the difference in cell density between tower forming and non-tower forming channels occurs largely during the multiplication stage of biofilm development.

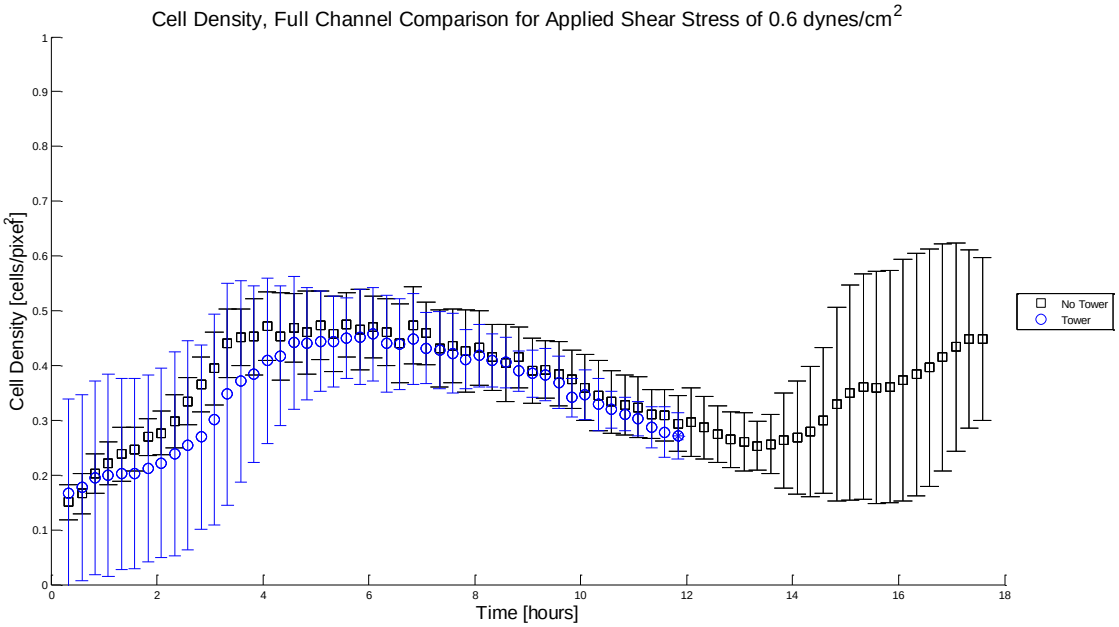

Figure 4.2.4 Cell density as a function of time for the applied shear stress of 0.6 dynes/cm^2. Average Cell density data for tower and non-tower forming channels are shown. Blue markers indicate when a tower formed.

Examining the average cell density of the tower and non-tower forming channels for the applied shear stress of 0.9 dynes/cm^2 may further quantify the difference in biofilm formation at higher applied shear stresses. The tower forming frequency for the applied shear stress of 0.9 dynes/cm^2 is nearly double that of the tower forming frequency

for the applied shear stress of 0.15 dynes/cm^2, which could be related to the average cell density as a function of time.

The cell density for applied shear of 0.9 dynes/cm^2 is shown in Figure 4.2.5. The vertical axis shows the cell density and the horizontal axis shows the experimental time in hours. The results are separated into the average cell density for the tower and non-tower forming channels. The tower data plotted represents the average cell densities of two channels which formed towers. The tower data are plotted only up until a tower appears.

The average cell densities of the tower and the no tower case have a similar rate of change of cell density across the timeline of the experiment for this applied shear stress and the average cell density of the tower forming channels is consistently larger. The type of tower that was observed may have an effect on the average channel cell density as both of the towers were observed to reach only a small size before releasing cells into the flow in comparison to other towers observed in experiments for other applied shear stresses which grow to larger sizes before detaching or blocking the channel flow entirely. The average cell density for the applied shear stress of 0.9 dynes/cm^2, for both tower and non-tower channels is higher than the average cell density of all other studied shear stresses except 0.6 dynes/cm^2. Similar to the average cell densities of non-tower forming channels for the applied shear stresses of 0.15, 0.3, and 1.5 dynes/cm^2, the average cell density for both tower and non-tower forming channels for the applied shear stress of 0.9 dynes/cm^2 shows a small increase in cell density over the first four hours before reaching a near constant value for the remainder of the timeline of biofilm development.

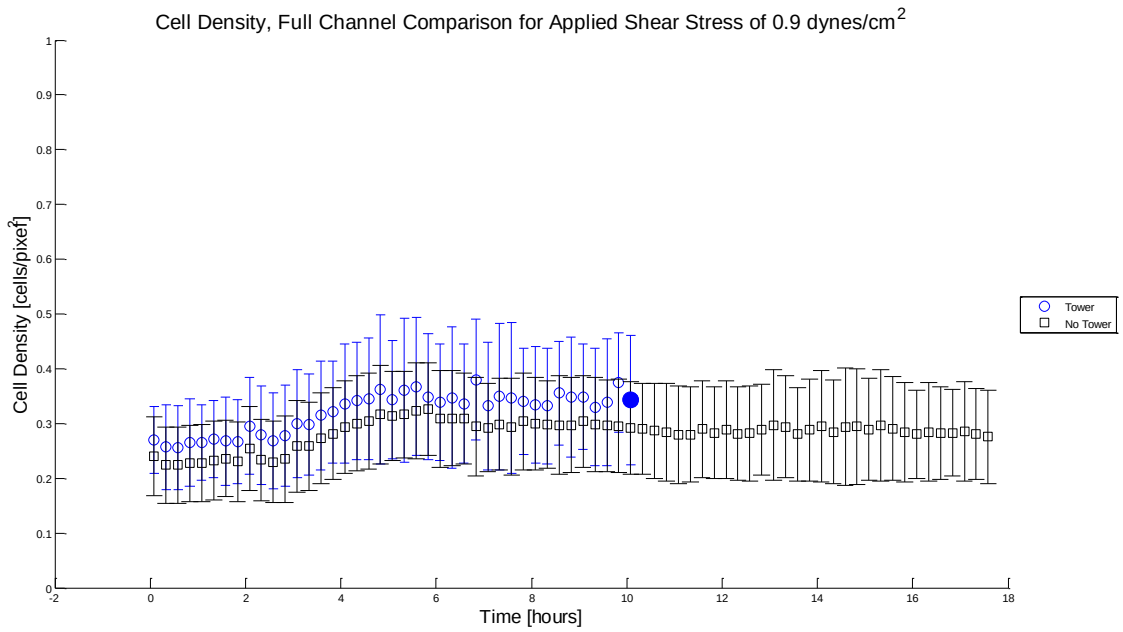

Figure 4.2.5 Cell density as a function of time for the applied shear stress of 0.9 dynes/cm^2. Average Cell density data for tower and non-tower forming channels are shown. Blue markers indicate when a tower formed.

Similar to the consideration of the average cell density of the non-tower forming channels of 0.3 dynes/cm^2, examination of the average cell density of the non-tower forming channels of 1.5 dynes/cm^2, the largest applied shear studied for this work, may provide insight into how and if average cell density is connected to tower formation.

The cell density for the applied shear of 1.5 dynes/cm^2 is shown in Figure 4.2.6. The vertical axis shows the cell density and the horizontal axis shows the experimental time in hours.

The average cell density for the applied shear stress of 1.5 dynes/cm^2 is larger than the average cell density for the applied shear stresses of 0.15 and 0.3 dynes/cm^2 but lower than the average cell density for the applied shear stresses of 0.6 and 0.9 dynes/cm^2. Similar to the average cell densities of non-tower forming channels for the applied shear stresses of 0.15, 0.3, and 0.9 dynes/cm^2, the average cell density for the

applied shear stress of 1.5 dynes/cm^2 shows a small increase in cell density over the first four hours before reaching a near constant value for the remainder of the timeline of biofilm development.

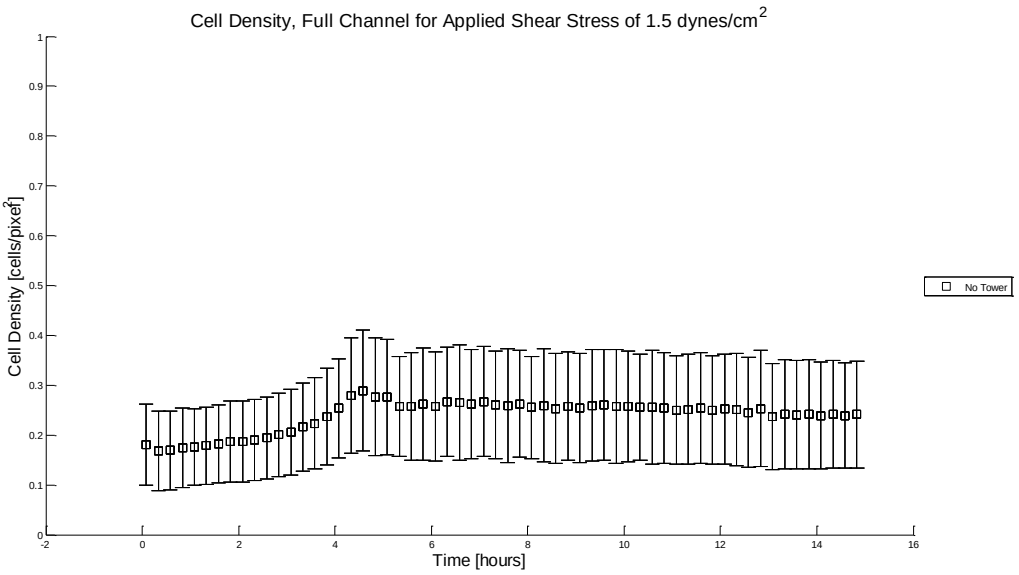

Figure 4.2.6 Cell density as a function of time for the applied shear stress of 1.5 dynes/cm^2. Average Cell density data for non-tower forming channels are shown.

4.3 Spatial RMS of Cell Density as a Function of Time

The Spatial Root Mean Square (RMS) of cell density indicates whether the cell density is uniformly distributed across the channel bottom. Since the average cell density of the channel provides a bulk value across the channel bottom it cannot provide more localized information such as how the region where the tower forms may be different from a region where the tower does not form. Comparing the Spatial RMS of cell density across applied shear stress and tower and non-tower forming channels may provide insight into the range of cell density values at a given time point, which may be different at each of the stages of biofilm development.

The Spatial RMS of the cell density within a channel was calculated at each time point as discussed in section 3.5. Figure 4.3.1 shows the spatial root mean square of cell density results for all of the applied shear stresses studied, broken into the average values for the tower and non-tower forming channels. Data for tower forming channels are plotted only up until a tower appears. The vertical axis shows the spatial root mean square of cell density, non-dimensionalized by the instantaneous average cell density and the horizontal axis shows the experimental time in hours.

Across the different applied shear stresses, the Spatial RMS of cell density for tower forming channels appears to be higher than the Spatial RMS of cell density for non-tower forming channels. After the first four hours of biofilm development the Spatial RMS of cell density appears to reach a near constant value for the non-tower forming channels. While the Spatial RMS of cell density also approaches a near constant value for tower forming channels, that value is higher than the constant value for the corresponding applied shear stress' non-tower forming channel and is more likely to display fluctuations later on in the developmental timeline. As shown in Figure 4.2.1, cell multiplication occurs during the first four hours of biofilm development for all applied shear stresses, though the cell density increases most significantly for the applied shear stress of 0.6 dynes/cm^2. Additionally the magnitude of the spatial RMS of cell density appears to to be larger or smaller depending on the applied shear stress, where a larger spatial RMS of cell density indicates a larger range of cell densities at a given time point. These findings appear to show a difference in Spatial RMS of cell density for tower and non-tower forming channels both during the cell multiplication stage and after cell exodus.

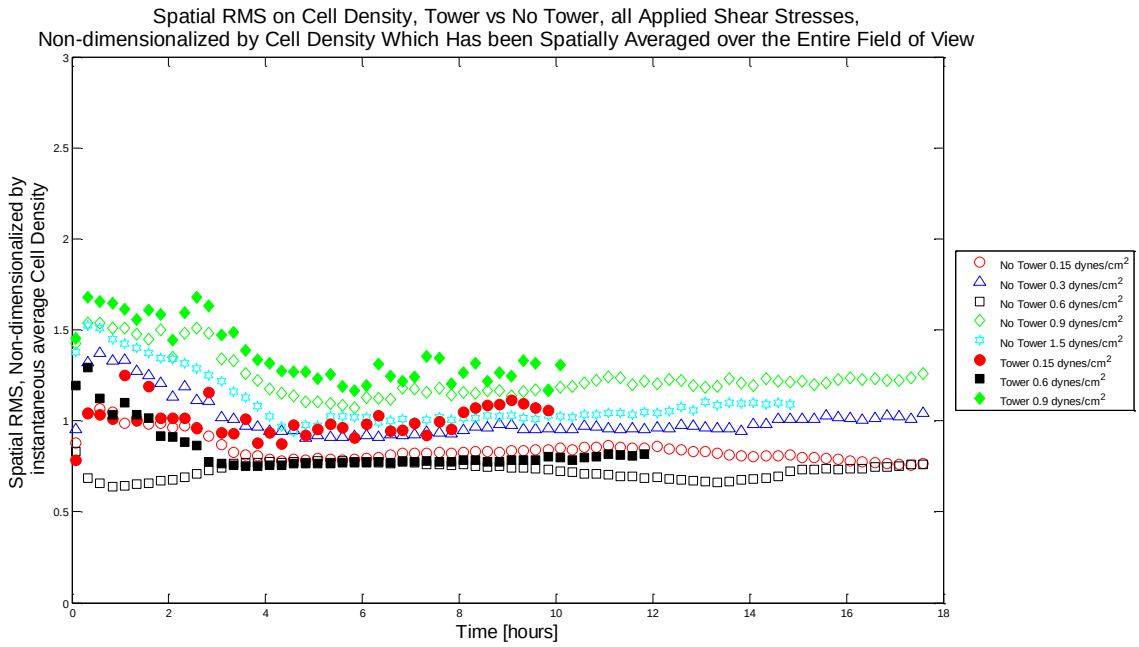

Figure 4.3.1 Spatial RMS on Cell Density of applied shear stress as a function of time for the applied shear stresses of 0.15, 0.3, 0.6, 0.9, 1.5 dynes/cm^2. Markers representing tower data are filled in.

As with studying the average cell density itself, investigating differences between the Spatial RMS of the cell density for tower and non-tower forming channel may provide more information at each applied shear stress regarding what biofilm conditions lead to the formation of a tower. The average cell density of tower forming and non-tower forming channels for the applied shear stress of 0.6 dynes/cm^2 differed from the average cell density of all other tested applied shear stresses, tower forming and non-tower forming channels alike. The Spatial RMS of the cell density for the applied shear stress of 0.6 dynes/cm^2 may further explain these differences, as well as the differences between the average cell density of the tower and non-tower forming channel for the applied shear stress of 0.6 dynes/cm^2.

While the average cell density for tower and non-tower forming channels for the applied shear stress of 0.15 dynes/cm^2 was among the lowest of all the applied shear

stresses tested, this applied shear stress still produced more towers than 0.3 and 1.5 dynes/cm^2. Comparing the spatial RMS of the cell density for tower forming and non-tower forming channels for the applied shear of 0.15 dynes/cm^2 against eachother as well as against the data from the 0.6 dynes/cm^2 case may lead to a better understanding of how and why towers might still be able to form at a lower average cell density.

The spatial RMS of cell density for the applied shear stress of 0.15 dynes/cm^2 is shown in Figure 4.3.2. The vertical axis shows the spatial root mean square of cell density, non-dimensionalized by the instantaneous cell density that has been spatially averaged across the entire field of view, and the horizontal axis shows the experimental time in hours. The results are separated into the average cell density for the tower and non-tower forming channels. The tower data plotted represents two channels which formed towers. The tower data are plotted only up until a tower appears.

After the first four hours of biofilm growth, the Spatial RMS of the cell density appears to reach a near constant value for both the tower and non-tower forming channels, with the tower forming channel having a higher Spatial RMS of cell density. As the average cell density for the non-tower forming channel is higher than the average cell density for the tower forming channel at this shear stress, the lower Spatial RMS of cell density for the non-tower forming channel indicates that it may have a more uniform cell density distribution than the tower forming channel. The Spatial RMS of the cell density for the tower channel for the applied shear stress of 0.15 dynes/cm^2 is lower during the first four hours of biofilm development than the Spatial RMS of the cell density for the tower channel for the applied shear stress of 0.6 dynes/cm^2, and fluctuates more after four

hours, meaning that the cell density distribution may start off as more uniform during the multiplication stage then become less uniform after cell exodus.

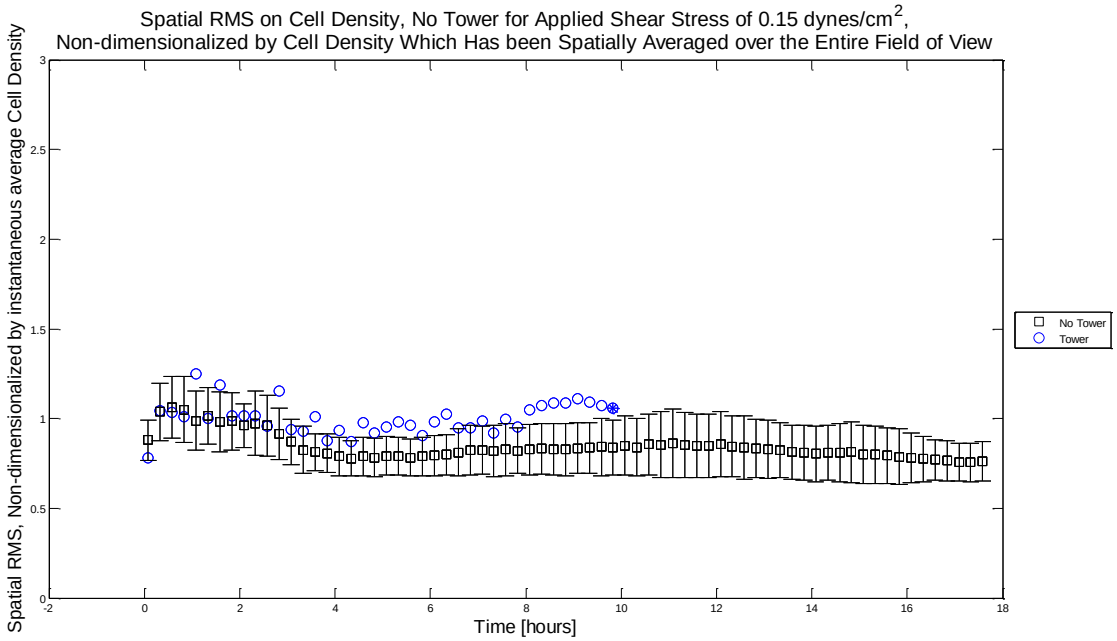

Figure 4.3.2 Spatial RMS on cell density as a function of time for the applied shear stress of 0.15 dynes/cm^2. Average Cell density data for tower and non-tower forming channels are shown.

The applied shear stress of 0.3 dynes/cm^2 yields no tower, with channels having a relatively low cell density as a function of time in comparison to the other applied shear stresses tested, except for the tower forming channels of the applied shear stress of 0.15 dynes/cm^2. However, the average cell density for the applied shear of 0.3 dynes/cm^2 increases in the first four hours in a similar fashion to the non-tower forming channels of 0.15, 0.9, and 1.5 dynes/cm^2. In evaluating and comparing the spatial RMS of the cell density for the applied shear of 0.3 dynes/cm^2 against the spatial RMS of the non-tower forming channels of 0.15, 0.9, and 1.5 dynes/cm^2 we can see if this non-tower forming applied shear has a similar range of cell densities at a given time point.

The spatial root mean square of cell density for applied shear stress of 0.3 dynes/cm^2 is shown in Figure 4.3.3. The vertical axis shows the spatial root mean square

of cell density, non-dimensionalized by the instantaneous average cell density that has been spatially averaged across the entire field of view, and the horizontal axis shows the experimental time in hours.

The Spatial RMS of cell density appears to reach a near constant value for the non-tower forming channels after the first four hours of biofilm growth, and has a similar profile to the non-tower forming channels for the applied shear stresses of 0.15, 0.9, and 1.5 dynes/cm^2. The spatial RMS of cell density for the applied shear stress of 0.3 dynes/cm^2 is larger than the spatial RMS of cell density for the applied shear stresses of 0.6 and 0.15 dynes/cm^2, but lower than the spatial RMS of cell density for the applied shear stresses of 0.9 and 1.5 dynes/cm^2.

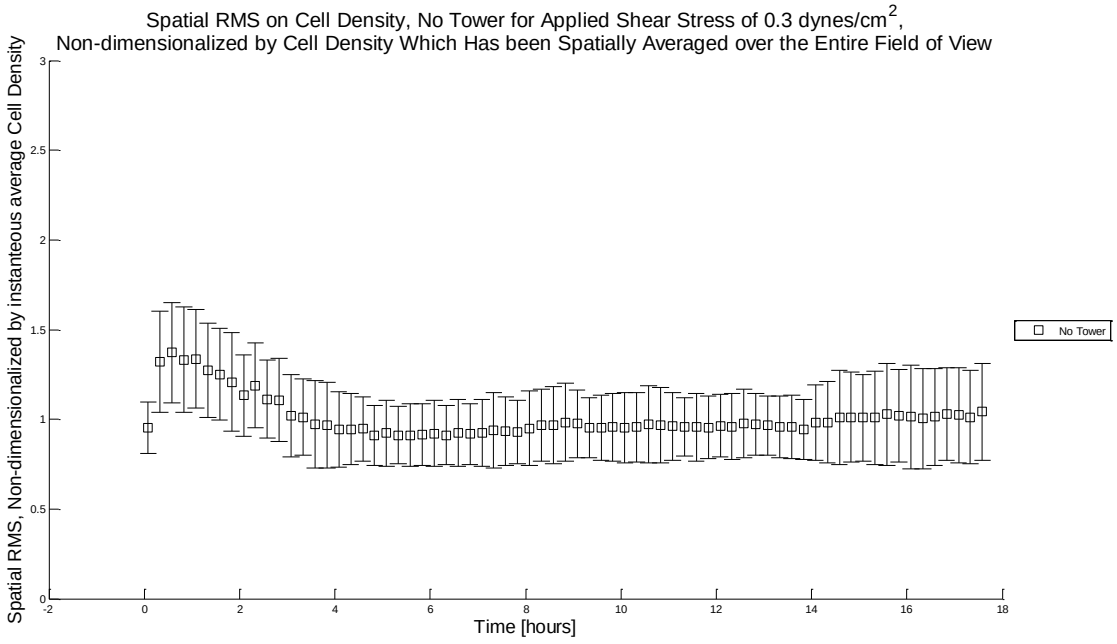

Figure 4.3.3 Spatial RMS on cell density as a function of time for the applied shear stress of 0.3 dynes/cm^2. Average Cell density data for non-tower forming channels are shown.

The spatial RMS of cell density for the optimal tower forming applied shear stress of 0.6 dynes/cm^2 is shown in Figure 4.3.4. The vertical axis shows the spatial RMS of cell density, non-dimensionalized by the instantaneous average cell density that has been

spatially averaged across the entire field of view and the horizontal axis shows the experimental time in hours. The results are separated into the average cell density for the tower and non-tower forming channels. The tower data plotted represents four channels which formed towers. The tower data are plotted only up until a tower appears.

After the first four hours of biofilm development, the Spatial RMS of cell density appears to reach a near constant value for both the tower and non-tower forming channels, with the tower forming channel having a higher Spatial RMS of cell density throughout the entire experiment. Although the the non-tower forming channel has a larger average cell density and has a more quickly increasing average cell density in the first four hours, it has a lower Spatial RMS of cell density than the tower forming channel, indicating that its cell density distribution might be more uniform during the entire experiment. The Spatial RMS of cell density for both the tower forming and non-tower forming channels for the applied shear stress of 0.6 dynes/cm^2 are lower than the Spatial RMS of average cell density for all of the other applied shear stresses tested. The Spatial RMS of cell density for the non-tower forming channel for the applied shear stress of of 0.6 dynes/cm^2 also starts off at a lower value during the cell multiplication stage and increases to reach a near constant value after cell exodus, while the Spatial RMS of cell density for the non-tower forming channels for all other applied shear stresses studied start off at a higher value during the cell multiplication stage and decrease to reach a near constant value after cell exodus.

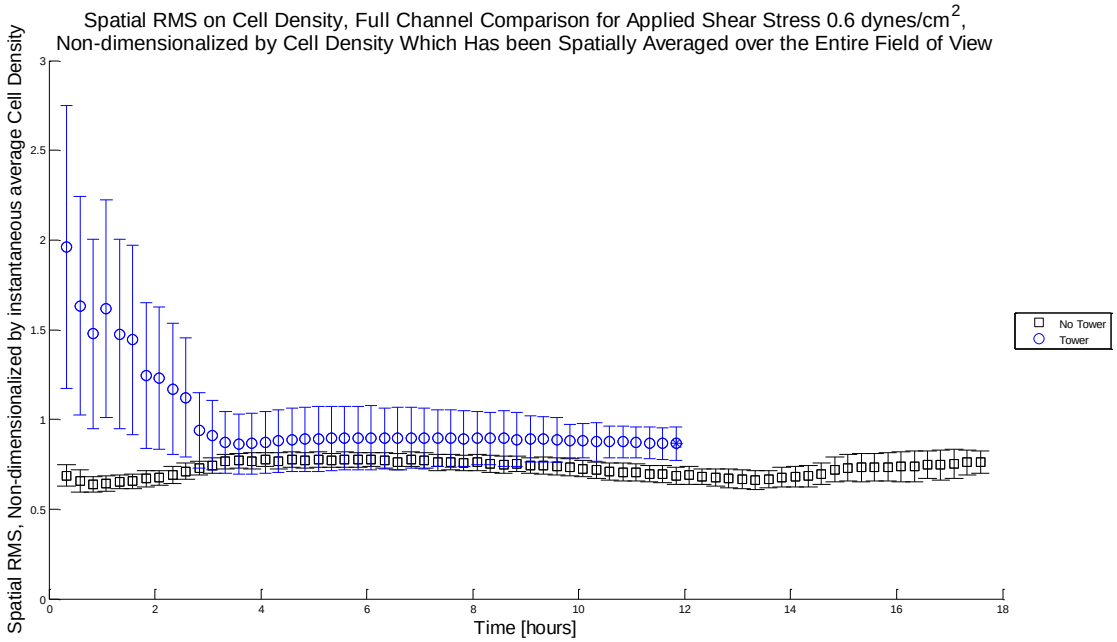

Figure 4.3.4 Spatial RMS on cell density as a function of time for the applied shear stress of 0.6 dynes/cm^2. Average Cell density data for tower and non-tower forming channels are shown. Blue markers indicate when a tower formed.

The average cell densities for the tower and non-tower forming channels for the applied shear stress of 0.9 dynes/cm^2 shown in Figure 4.2.5 was shown to be similar, possibly due to the type of tower formation that was observed. As the Spatial RMS of cell density for the tower forming channels for the applied shear stresses of 0.15 and 0.6 dynes/cm^2 had a clear difference from non-tower forming channels both during the multiplication stage and after cell exodus, comparing the Spatial RMS of cell density for the tower forming channel for the applied shear stress of 0.9 dynes/cm^2 could perhaps provide an additional means of classifying types of towers based on the Spatial RMS of cell density as a function of time.

The spatial RMS of cell density for the applied shear of 0.9 dynes/cm^2 is shown in Figure 4.3.5. The vertical axis shows the spatial root mean square of cell density, non-dimensionalized by the instantaneous average cell density that has been spatially

averaged across the entire field of view, and the horizontal axis shows the experimental time in hours. The results are separated into the average cell density for the tower and non-tower forming channels. The tower data plotted represents two channels which formed towers. The tower data are plotted only up until a tower appears.

After the first four hours of biofilm growth, the Spatial RMS of cell density appears to reach a near constant value for both the tower and non-tower forming channels. The Spatial RMS of cell density as a function of time are similar for both the tower and non-tower forming channels and are also similar to the Spatial RMS of cell density for the non-tower forming channels for the applied shear stresses of 0.15, 0.3, and 1.5 dynes/cm^2. Therefore, while two small towers are observed, their spatial RMS of cell density is more similar to the the spatial RMS of cell density for non-tower forming channels.

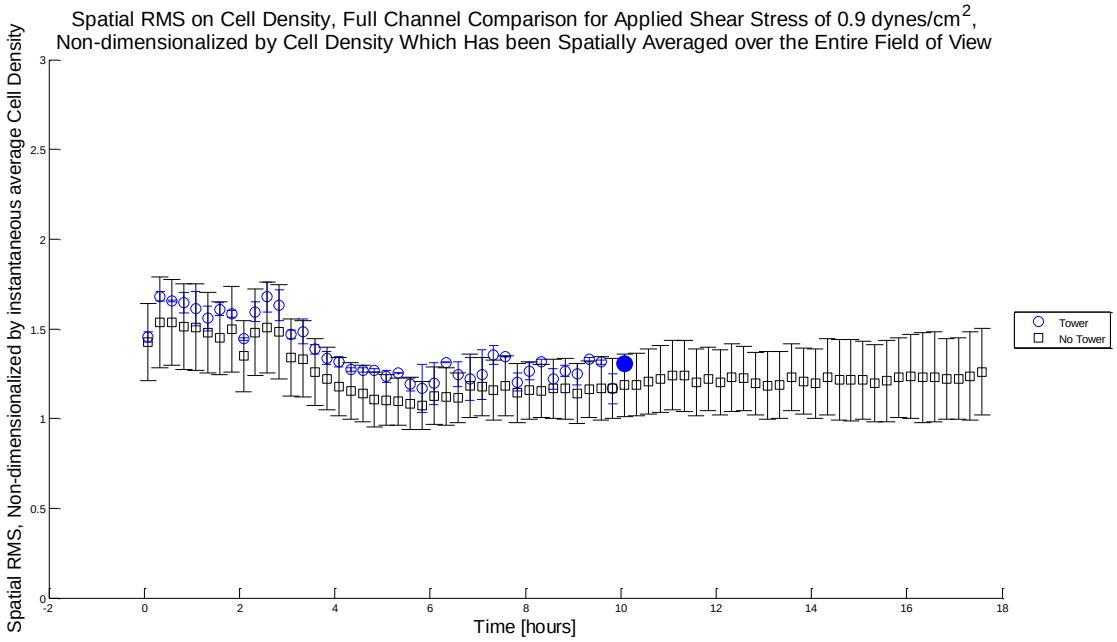

Figure 4.3.5 Spatial RMS on cell density as a function of time for the applied shear stress of 0.9 dynes/cm^2. Average Cell density data for tower and non-tower forming channels are shown. Blue markers indicate when a tower formed.

Calculating and comparing the spatial RMS of cell density for the applied shear of 1.5 dynes provides another comparison for non-tower forming channels in both applied shear stresses that did form towers and applied shear stresses that did not form towers. Examining the spatial RMS of cell density for the largest applied shear stress studied in this work may show if there is a link between the applied shear stress and the magnitude or behavior of the spatial RMS of cell density as a function of time.

The spatial RMS of cell density for the applied shear stress of 1.5 dynes/cm^2 is shown in Figure 4.3.6. The vertical axis shows the spatial root mean square of cell density, non-dimensionalized by the instantaneous average cell density and the horizontal axis shows the experimental time in hours. The results are separated into the average cell density that has been spatially averaged across the entire field of view, for the tower and non-tower forming channels.

After the first four hours of biofilm growth, the Spatial RMS of cell density appears to reach a near constant value for the non-tower forming channels. Although the Spatial RMS of cell density for the applied shear stress of 1.5 dynes/cm^2 is larger than the Spatial RMS of cell density for the applied shear stresses of 0.15, 0.3, and 0.6, it behaves in a similar way to the the non-tower forming channels of 0.15, 0.3, and 0.9 dynes/cm^2.

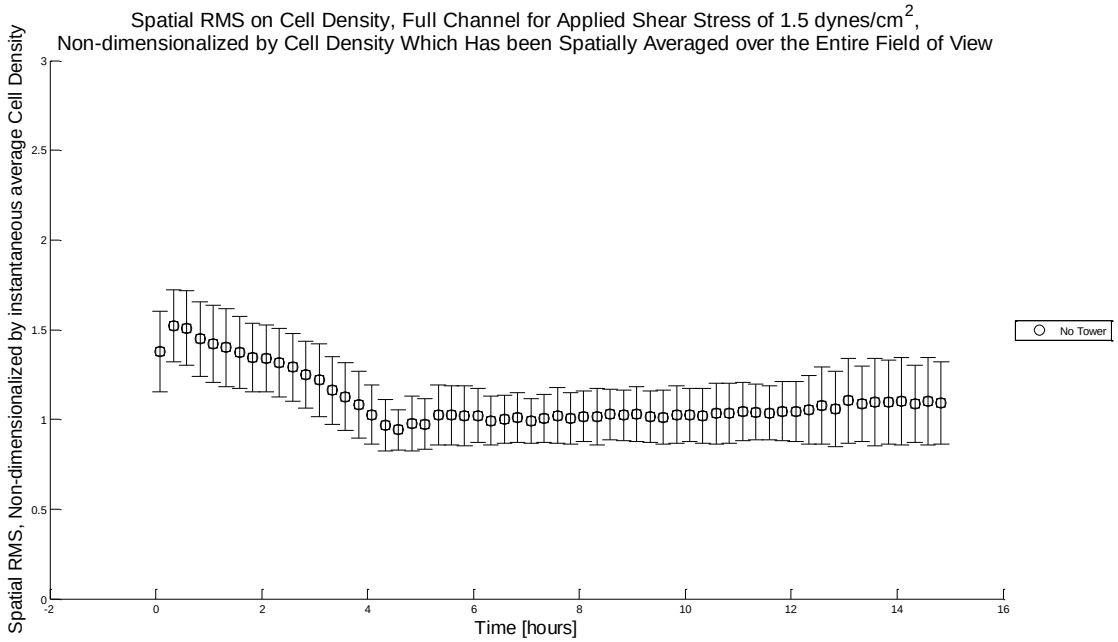

Figure 4.3.6 Spatial RMS on cell density as a function of time for the applied shear stress of 1.5 dynes/cm^2. Average Cell density data for tower and non-tower forming channels are shown.

4.4 Cell Density Distribution

The cell density distribution illustrates non-uniform behavior in cell density between tower and non-tower forming channels. The average cell density as a function of time provides a bulk value for the entire channel bottom, and while the spatial RMS provides an indication of how the cell density is distributed across the channel bottom, plotting the cell density distribution as a function of time clearly shows the frequency of specific cell density values across the channel bottom. Considering this distribution as a function of time allows for comparisons to be made prior to the development of a tower, which could potentially serve as a predictive tool.

The distribution of cell density within a channel was prepared at each time point as discussed in section 3.5. Hourly cell density distribution results are presented individually for all of the applied shear stresses studied, broken into the average values for the tower and non-tower forming channels. Non-tower forming channels are shown in

blue while tower-forming channels are shown in red. The vertical axis shows the frequency of cell density values in a 25 x 25 pixel window and the horizontal axis shows the range of cell density values from 0 to 1.

As the applied shear stress increases, the cell density distribution of both tower and non-tower forming chanels appears to cover more of the range of possible cell density values. Additionally, the cell density distribution of non-tower forming channels appear to have a more narrow and normal distribution in comparison to tower forming channels across all applied shear stresses studied. This appears to show both a relationship between distribution breadth and applied shear stress as well as between distribution shape and tower formation.

4.4.1 Cell Density Distribution as a Function of Time: 0.15 dynes/cm^2

As discussed earlier, while the applied shear stress of 0.15 dynes/cm^2 has a lower tower forming frequency, studying and comparing the cell density distribution of the tower and non-tower forming channels for this applied shear stress may provide insight as to what leads to tower formation and perhaps why 0.6 dynes/cm^2 is more likely to form towers.

These distributions are shown in Figures 4.4.1*a*-*r*, where the cell density distribution for tower forming channels is represented in red and the cell density distribution for non-tower forming channels is represented in blue. The data are presented at hourly intervals. The vertical axis shows the frequency of cell density values in a 25 x 25 pixel window and the horizontal axis shows the range of cell density values from 0 to 1.

The distribution of cell density as a function of time for the applied shear stress of 0.15 dynes/cm^2 as presented for tower forming channels show a broader range of values in comparison to the distribution of cell density as a function of time for the non-tower forming channels starting from the first experimental time point. Additionally, the cell density values that have a higher frequency for the tower forming channels are lower in value over time than those for the non-tower forming channels which is similar to the results from the applied shear stress of 0.6 dynes/cm^2. The most frequent cell densities for both tower and non-tower forming channels for the applied shear stress of 0.15 dynes/cm^2 do not reach as high of a value as those for the applied shear stress of 0.6 dynes/cm^2.

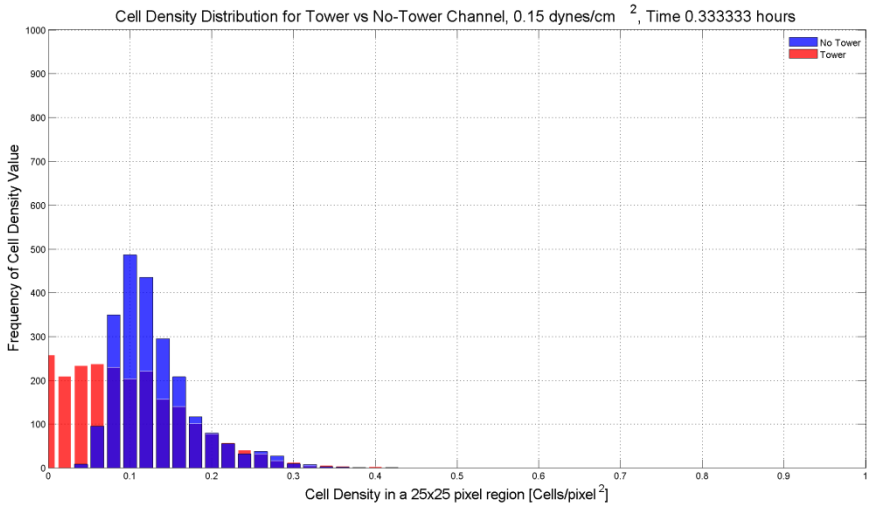

a

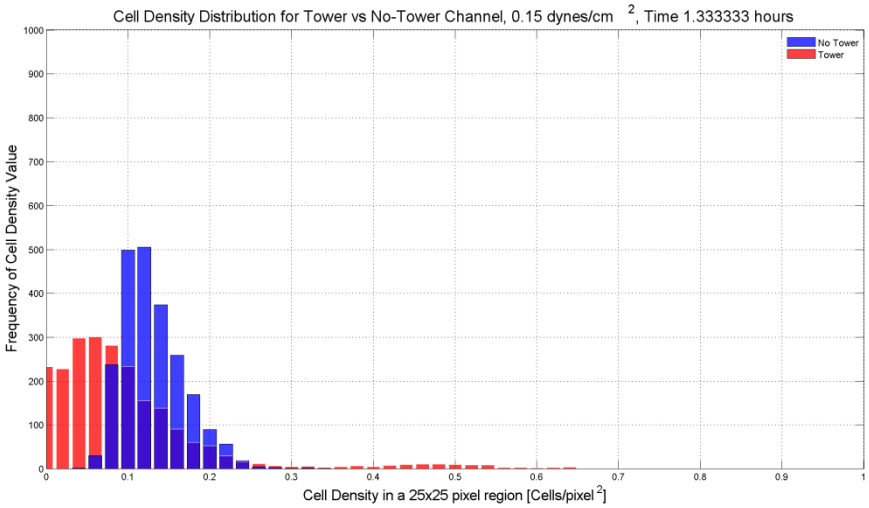
Cell Density Distribution for Tower vs No-Tower Channel, 0.15 dynes/cm 2, Time 1.333333 hours
No Tower
Tower
Frequency of Cell Density Value
Cell Density in a 25x25 pixel region [Cells/pixel 2]

b

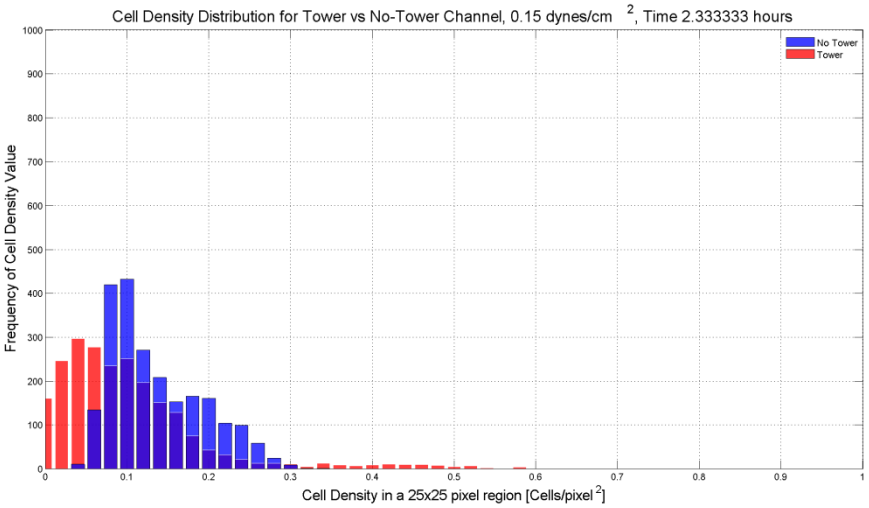
Cell Density Distribution for Tower vs No-Tower Channel, 0.15 dynes/cm 2, Time 2.333333 hours
No Tower
Tower
Frequency of Cell Density Value
Cell Density in a 25x25 pixel region [Cells/pixel 2]

c

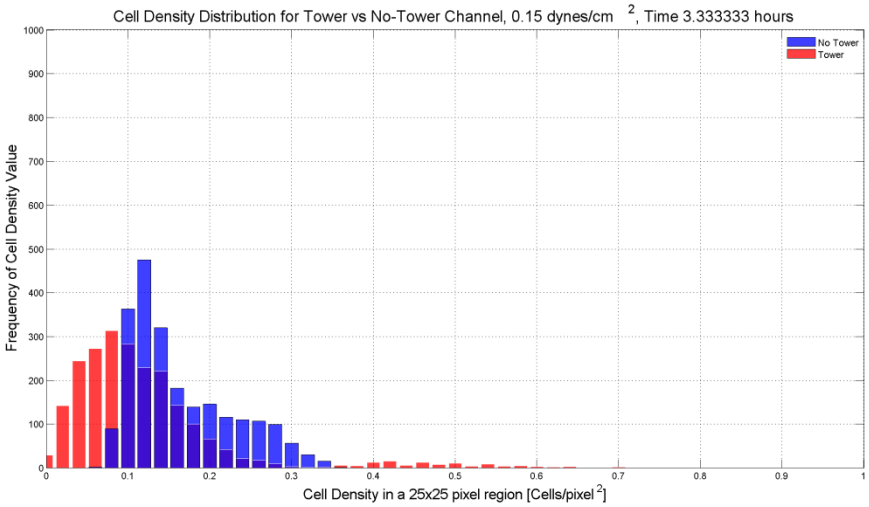
Cell Density Distribution for Tower vs No-Tower Channel, 0.15 dynes/cm 2, Time 3.333333 hours
No Tower
Tower
Frequency of Cell Density Value
Cell Density in a 25x25 pixel region [Cells/pixel 2]

d

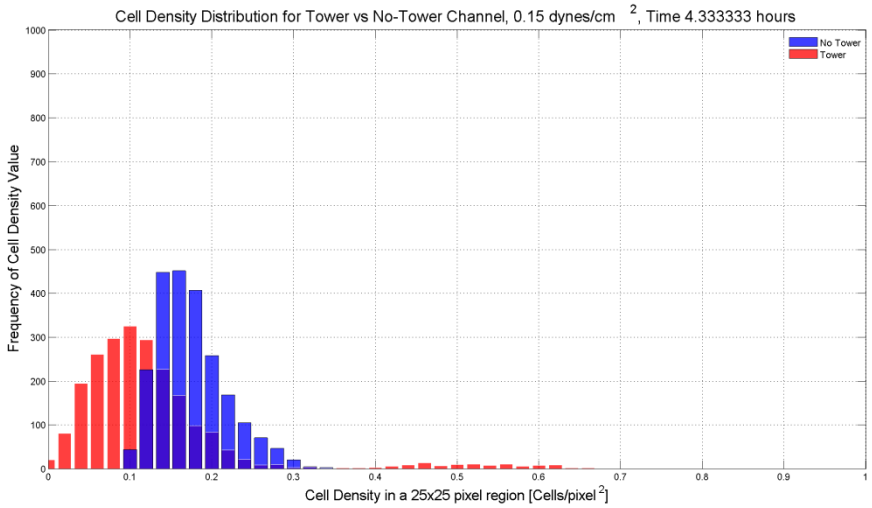
Cell Density Distribution for Tower vs No-Tower Channel, 0.15 dynes/cm 2, Time 4.333333 hours
No Tower
Tower
Frequency of Cell Density Value
Cell Density in a 25x25 pixel region [Cells/pixel 2]

e

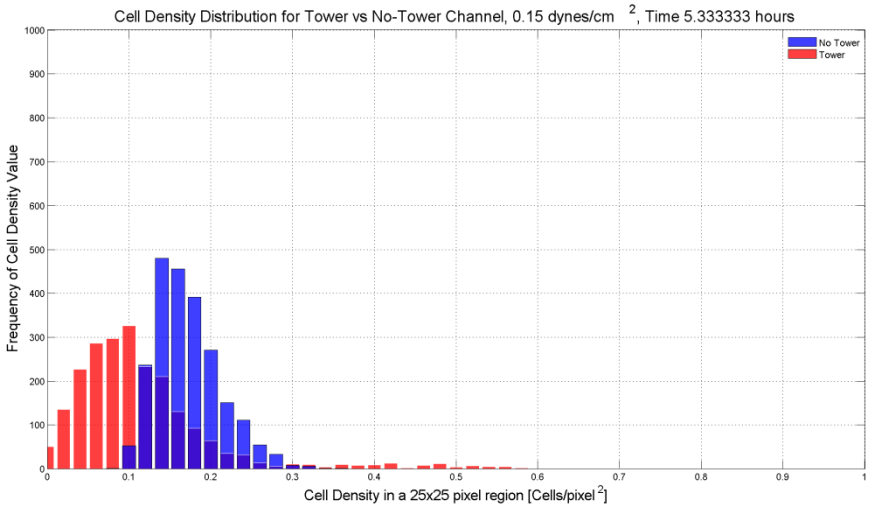
Cell Density Distribution for Tower vs No-Tower Channel, 0.15 dynes/cm 2, Time 5.333333 hours
No Tower
Tower
Frequency of Cell Density Value
Cell Density in a 25x25 pixel region [Cells/pixel 2]

f

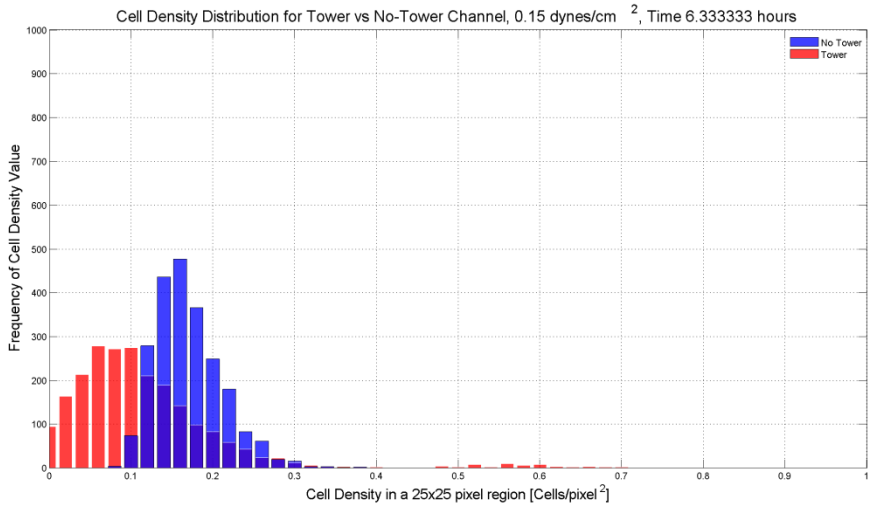
Cell Density Distribution for Tower vs No-Tower Channel, 0.15 dynes/cm 2, Time 6.333333 hours
No Tower
Tower
Frequency of Cell Density Value
Cell Density in a 25x25 pixel region [Cells/pixel 2]

g

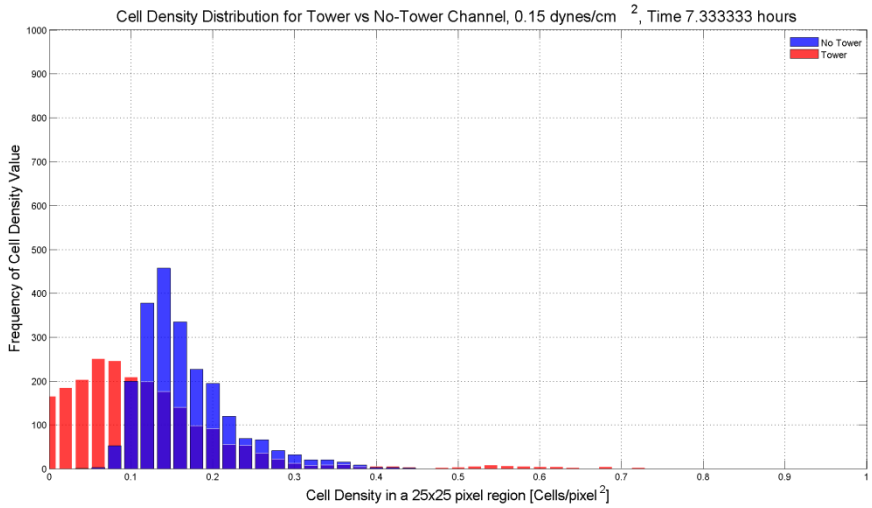
Cell Density Distribution for Tower vs No-Tower Channel, 0.15 dynes/cm 2, Time 7.333333 hours
No Tower
Tower
Frequency of Cell Density Value
Cell Density in a 25x25 pixel region [Cells/pixel 2]

h

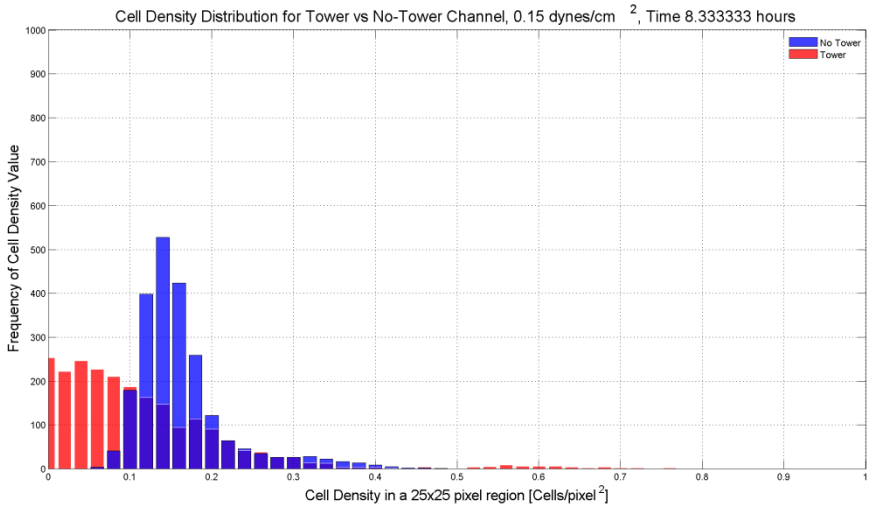
Cell Density Distribution for Tower vs No-Tower Channel, 0.15 dynes/cm 2, Time 8.333333 hours
No Tower
Tower
Frequency of Cell Density Value
Cell Density in a 25x25 pixel region [Cells/pixel 2]

i

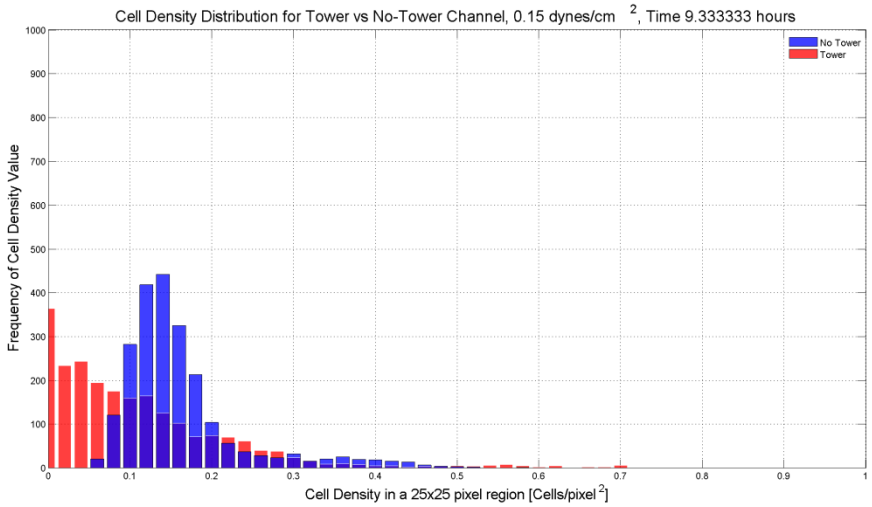
Cell Density Distribution for Tower vs No-Tower Channel, 0.15 dynes/cm 2, Time 9.333333 hours
No Tower
Tower
Frequency of Cell Density Value
Cell Density in a 25x25 pixel region [Cells/pixel 2]

j

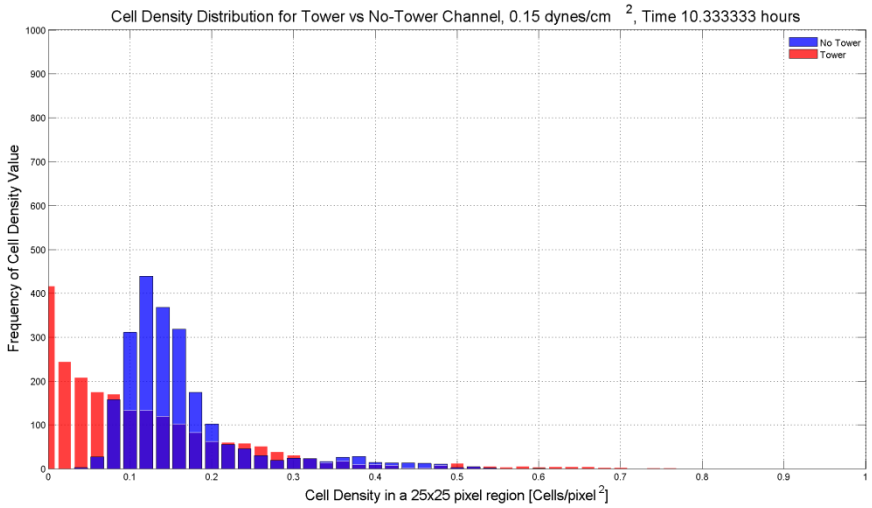
Cell Density Distribution for Tower vs No-Tower Channel, 0.15 dynes/cm 2, Time 10.333333 hours
No Tower
Tower
Frequency of Cell Density Value
Cell Density in a 25x25 pixel region [Cells/pixel 2]

k

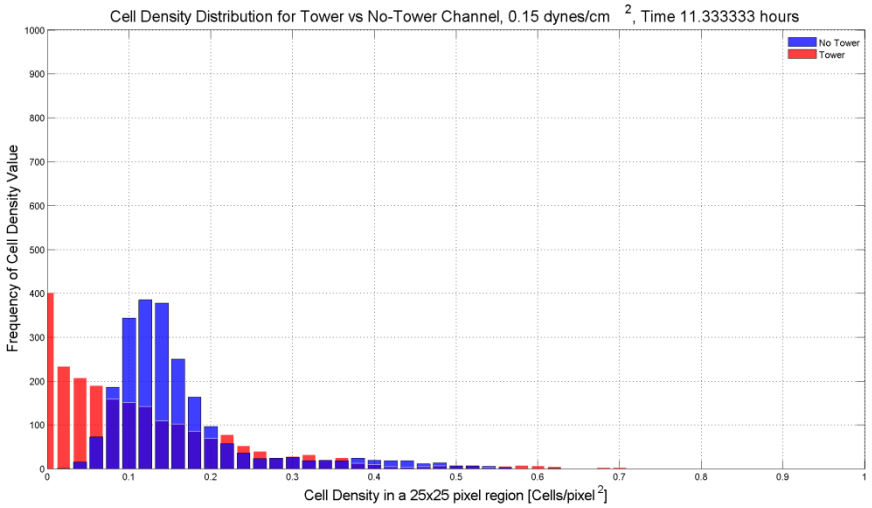
Cell Density Distribution for Tower vs No-Tower Channel, 0.15 dynes/cm 2, Time 11.333333 hours
No Tower
Tower
Frequency of Cell Density Value
Cell Density in a 25x25 pixel region [Cells/pixel 2]

l

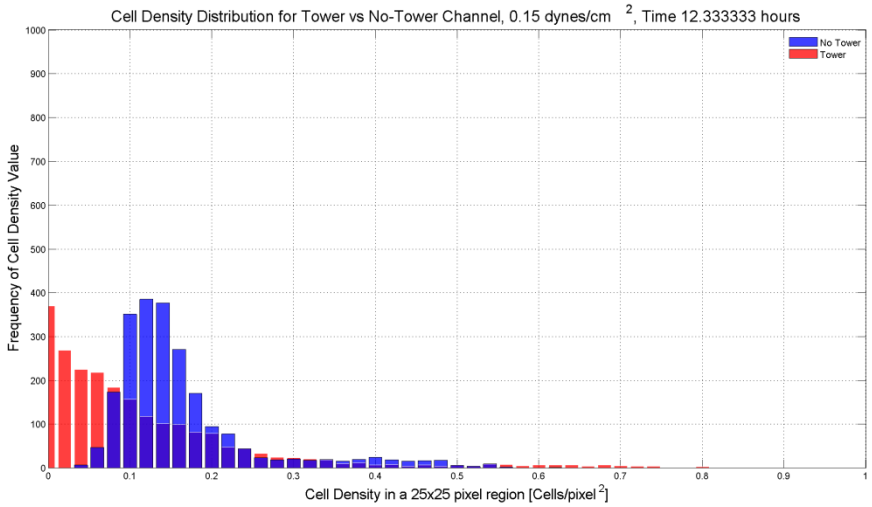
Cell Density Distribution for Tower vs No-Tower Channel, 0.15 dynes/cm 2, Time 12.333333 hours
No Tower
Tower
Frequency of Cell Density Value
Cell Density in a 25x25 pixel region [Cells/pixel 2]

m

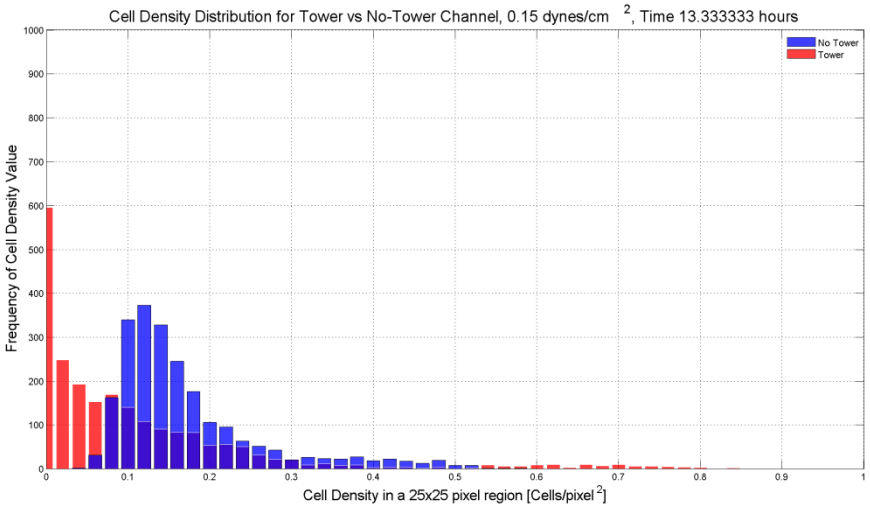
Cell Density Distribution for Tower vs No-Tower Channel, 0.15 dynes/cm 2, Time 13.333333 hours
No Tower
Tower
Frequency of Cell Density Value
Cell Density in a 25x25 pixel region [Cells/pixel 2]

n

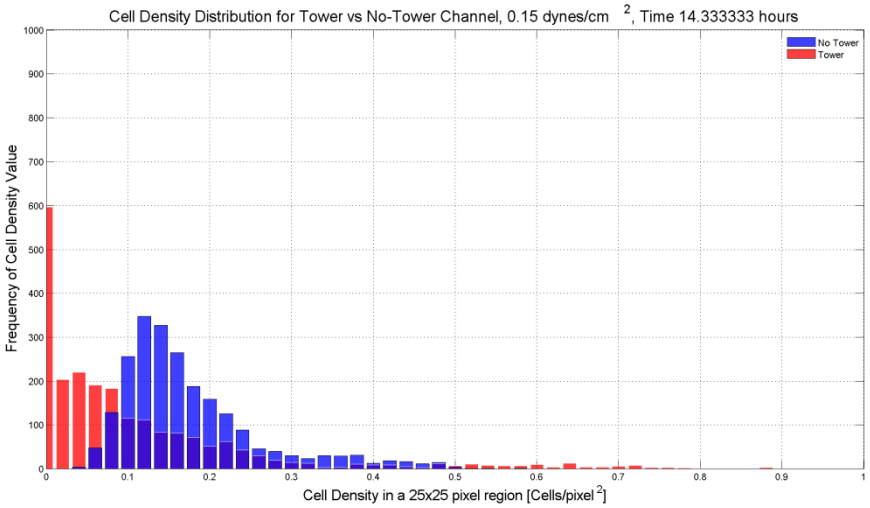
Cell Density Distribution for Tower vs No-Tower Channel, 0.15 dynes/cm 2, Time 14.333333 hours
No Tower
Tower
Frequency of Cell Density Value
Cell Density in a 25x25 pixel region [Cells/pixel 2]

o

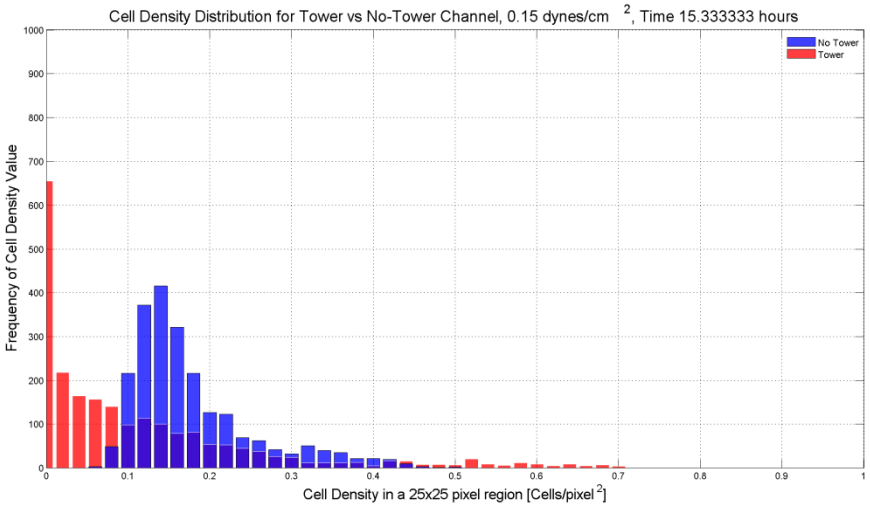
Cell Density Distribution for Tower vs No-Tower Channel, 0.15 dynes/cm 2, Time 15.333333 hours
No Tower
Tower
Frequency of Cell Density Value
Cell Density in a 25x25 pixel region [Cells/pixel 2]

p

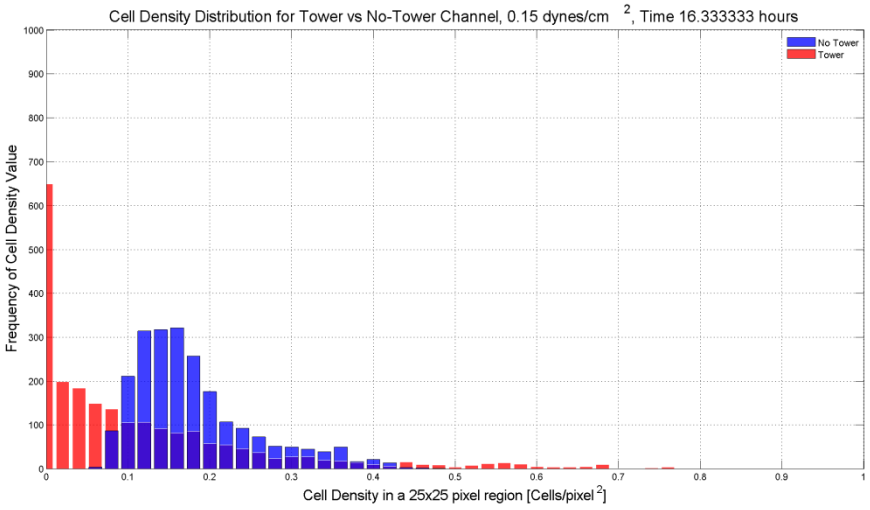

q

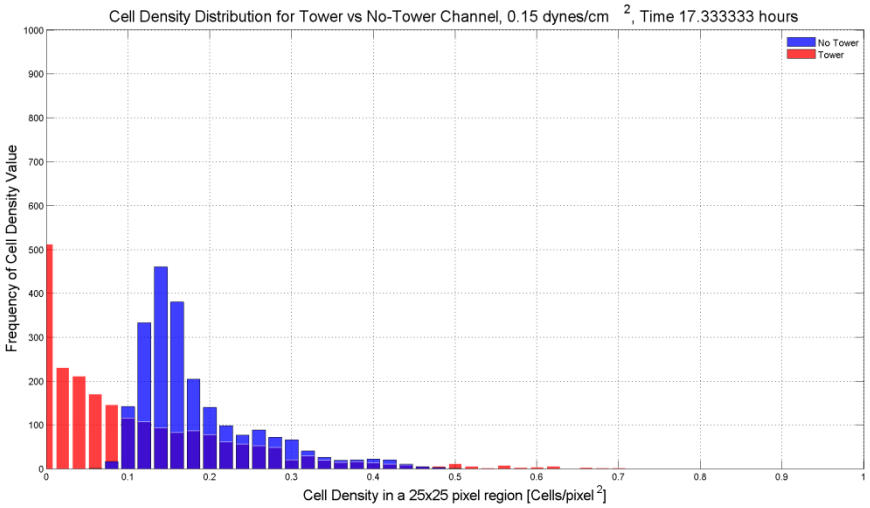

r

Figure 4.4.1 Cell Density Distributions as a function of time for the applied shear stress of 0.15 dynes/cm^2. Tower data is shown in red and non-tower data is shown in blue. Figures a-r show hourly distributions across the experimental timeline.

4.4.2 Cell Density Distribution as a Function of Time: 0.3 dynes/cm^2

Although the applied shear stress of 0.3 dynes/cm^2 does not yield any tower channels, studying the cell density distribution of its non-tower forming channels allows for a comparison of non-tower channels across the range of applied shear stresses studied

and therefore the answer of whether cell density distribution is affected by the applied shear stress as well as related to tower formation frequency.

The distributions of cell density as a function of time for the applied shear stress of 0.3 dynes/cm^2 are shown in Figures 4.4.2a-r, where the cell density distribution for non-tower forming channels is represented in blue. The data are presented at hourly intervals. The vertical axis shows the frequency of cell density values in a 25 x 25 pixel window and the horizontal axis shows the range of cell density values from 0 to 1.

The distribution of cell density as a function of time for the applied shear stress of 0.3 dynes/cm^2 as presented for non-tower forming channels has a similar breadth as the non-tower forming cell density distributions of the applied shear stresses of 0.15, and 0.6 dynes/cm^2, and a similar profile to the non-tower forming cell density distribution of the applied shear stress of 0.15 dynes/cm^2. While the cell density distribution of the applied shear stress of 0.3 dynes/cm^2 covers a similar range of cell density values as the non-tower forming cell density distribution of the applied shear stress of 0.9 dynes/cm^2, the frequency of these cell density values is different, with the higher frequency of cell density values for the applied shear stress of 0.3 dynes/cm^2 being closer to zero as opposed to the higher frequency of the cell density values for the applied shear stress of 0.9 dynes/cm^2.

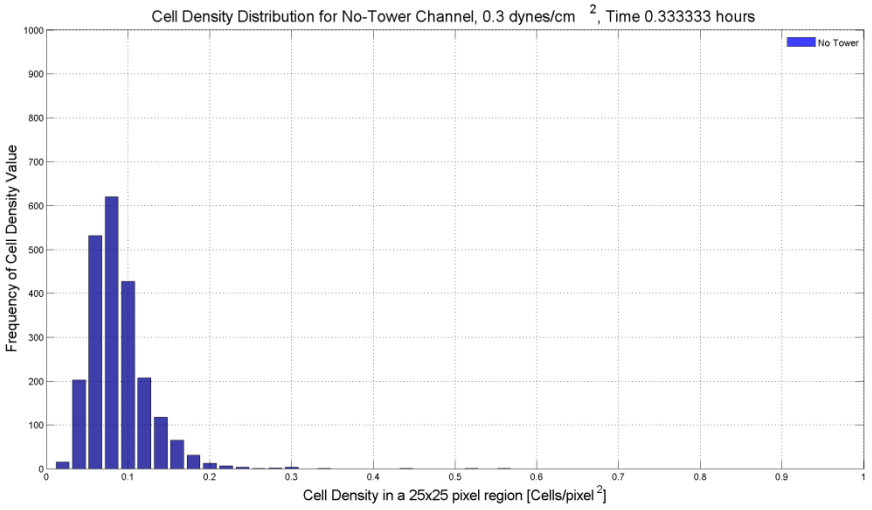
Cell Density Distribution for No-Tower Channel, 0.3 dynes/cm 2, Time 0.333333 hours
No Tower
Frequency of Cell Density Value
Cell Density in a 25x25 pixel region [Cells/pixel 2]

a

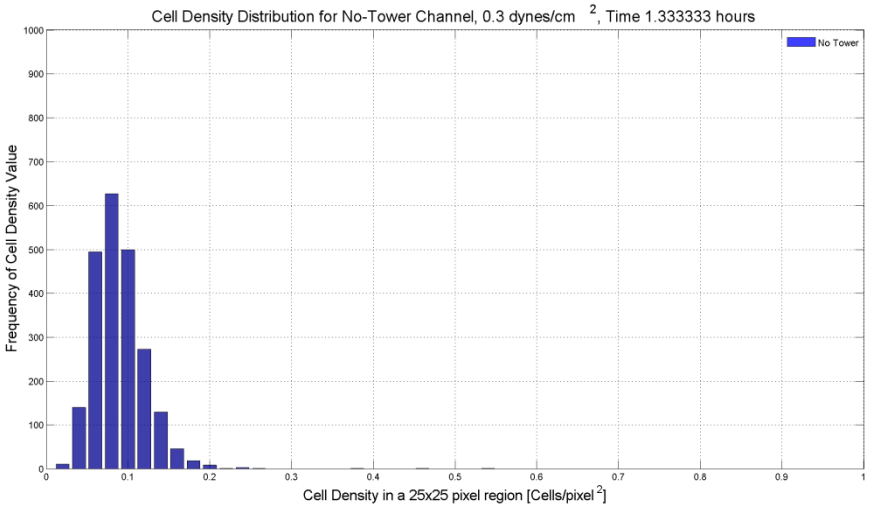
Cell Density Distribution for No-Tower Channel, 0.3 dynes/cm 2, Time 1.333333 hours
No Tower
Frequency of Cell Density Value
Cell Density in a 25x25 pixel region [Cells/pixel 2]

b

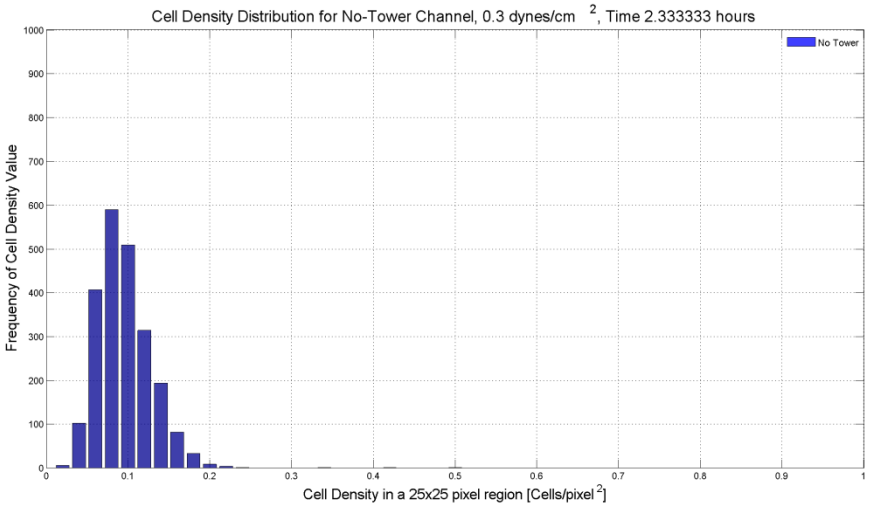
Cell Density Distribution for No-Tower Channel, 0.3 dynes/cm 2, Time 2.333333 hours
No Tower
Frequency of Cell Density Value
Cell Density in a 25x25 pixel region [Cells/pixel 2]

c

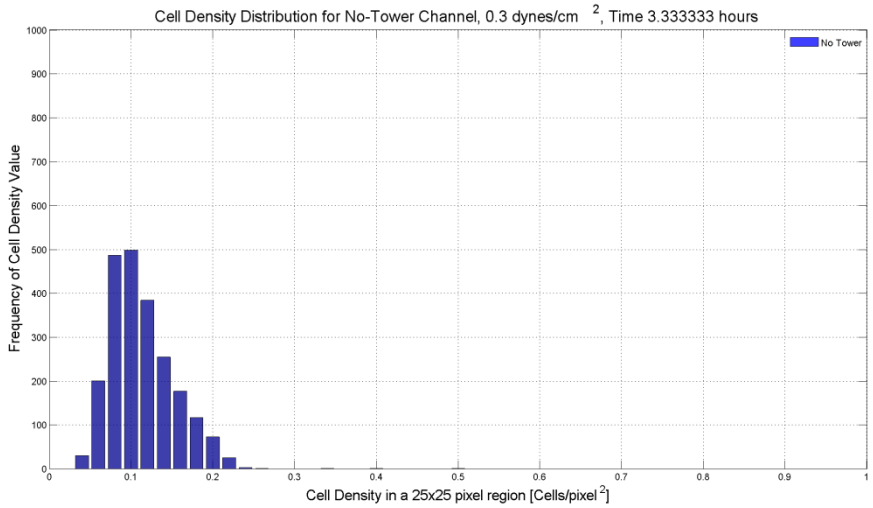
Cell Density Distribution for No-Tower Channel, 0.3 dynes/cm 2, Time 3.333333 hours
No Tower
Frequency of Cell Density Value
Cell Density in a 25x25 pixel region [Cells/pixel 2]

d

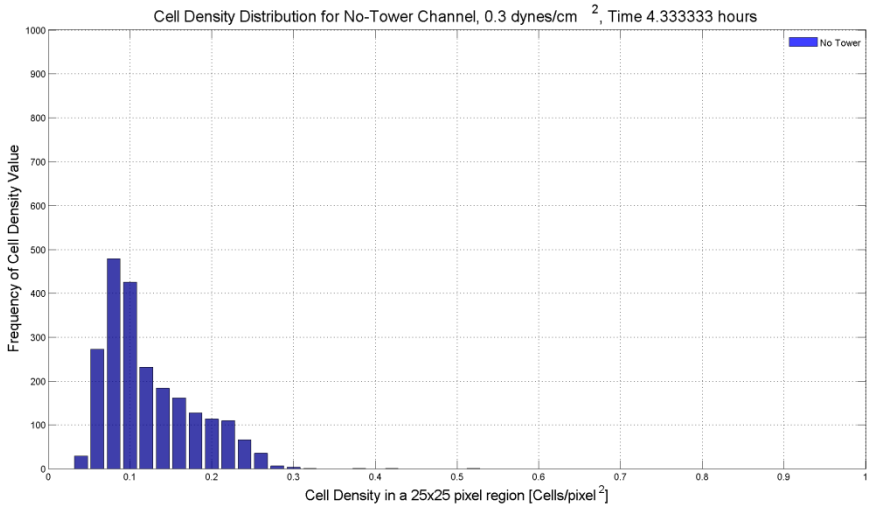
Cell Density Distribution for No-Tower Channel, 0.3 dynes/cm 2, Time 4.333333 hours
No Tower
Frequency of Cell Density Value
Cell Density in a 25x25 pixel region [Cells/pixel 2]

e

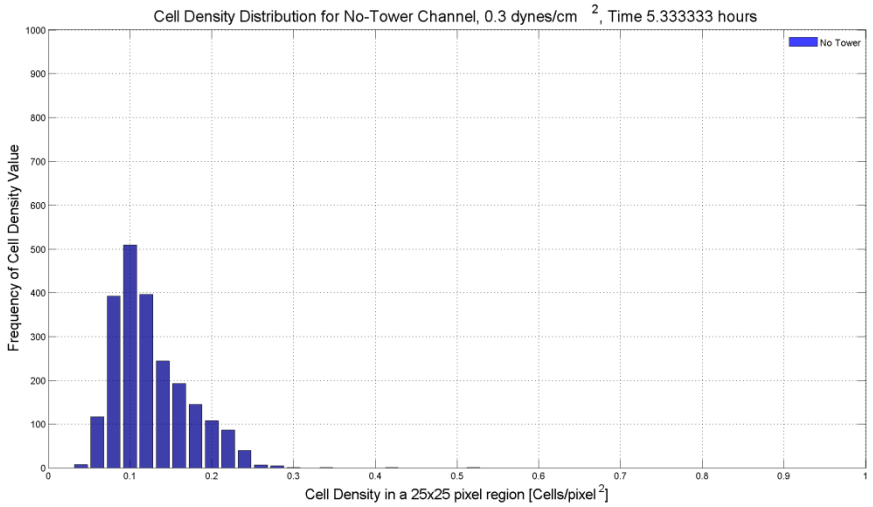
Cell Density Distribution for No-Tower Channel, 0.3 dynes/cm 2, Time 5.333333 hours
No Tower
Frequency of Cell Density Value
Cell Density in a 25x25 pixel region [Cells/pixel 2]

f

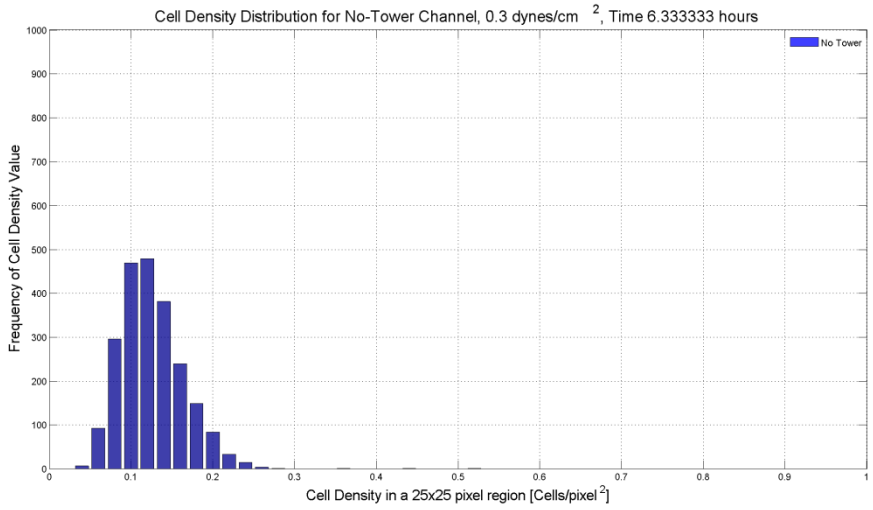
Cell Density Distribution for No-Tower Channel, 0.3 dynes/cm 2, Time 6.333333 hours
No Tower
Frequency of Cell Density Value
Cell Density in a 25x25 pixel region [Cells/pixel 2]

g

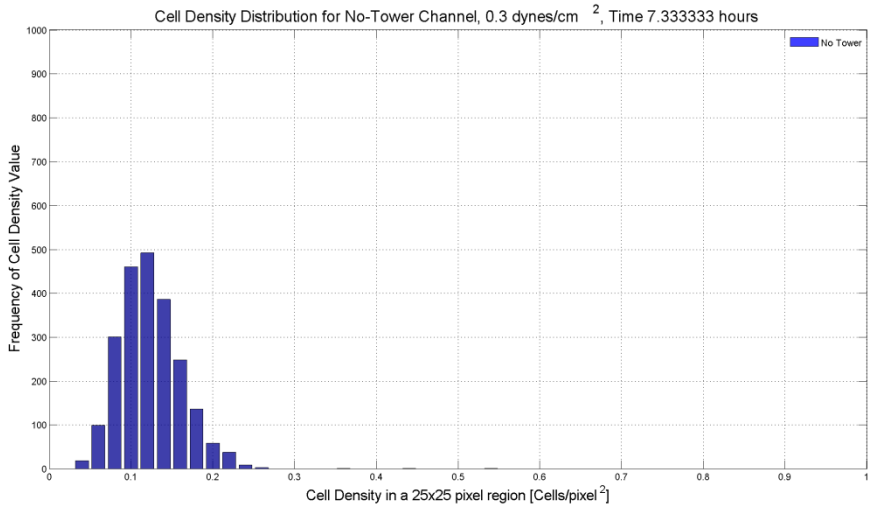
Cell Density Distribution for No-Tower Channel, 0.3 dynes/cm 2, Time 7.333333 hours
No Tower
Frequency of Cell Density Value
Cell Density in a 25x25 pixel region [Cells/pixel 2]

h

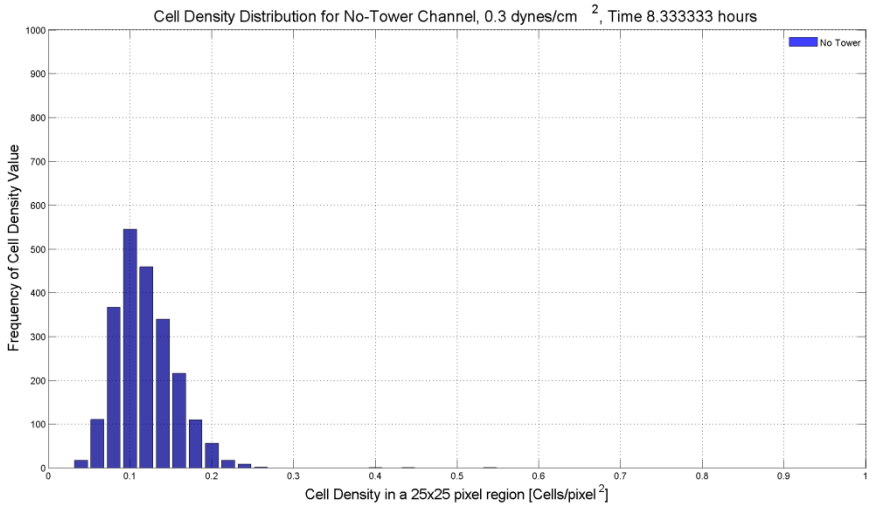
Cell Density Distribution for No-Tower Channel, 0.3 dynes/cm 2, Time 8.333333 hours
No Tower
Frequency of Cell Density Value
Cell Density in a 25x25 pixel region [Cells/pixel 2]

i

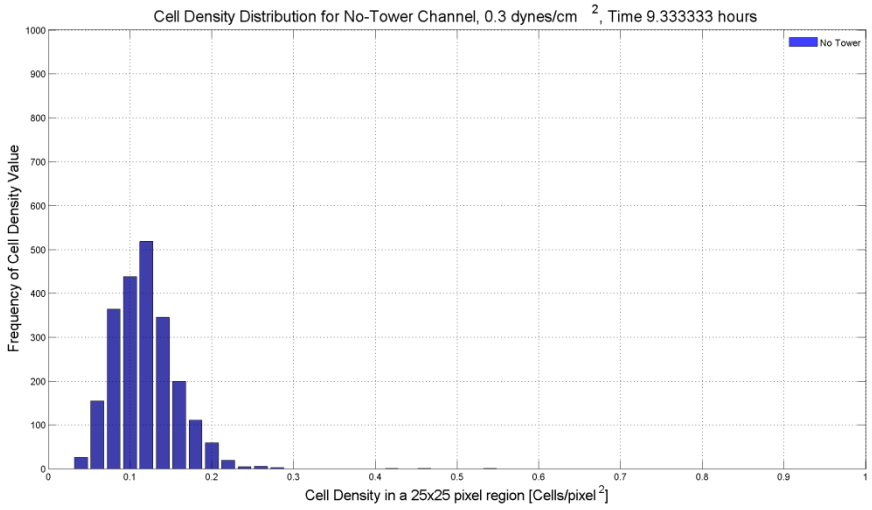
Cell Density Distribution for No-Tower Channel, 0.3 dynes/cm 2, Time 9.333333 hours
No Tower
Frequency of Cell Density Value
Cell Density in a 25x25 pixel region [Cells/pixel 2]

j

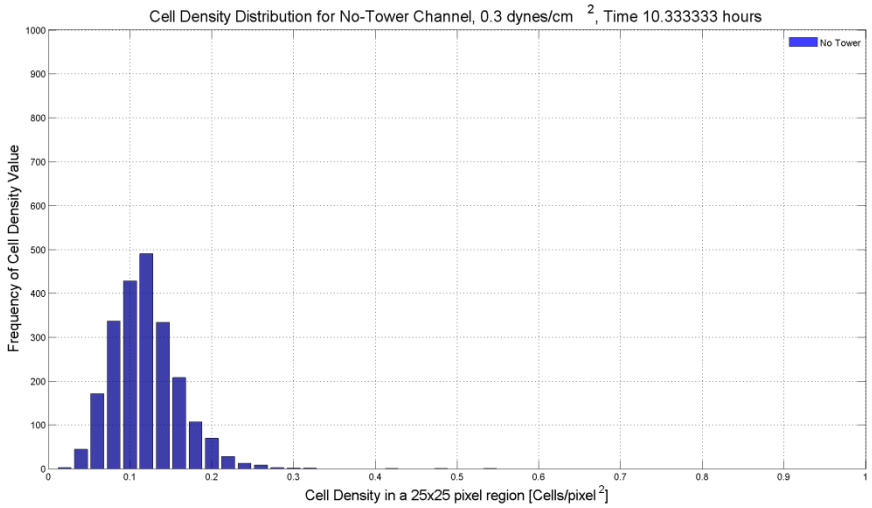
Cell Density Distribution for No-Tower Channel, 0.3 dynes/cm 2, Time 10.333333 hours
No Tower
Frequency of Cell Density Value
Cell Density in a 25x25 pixel region [Cells/pixel 2]

k

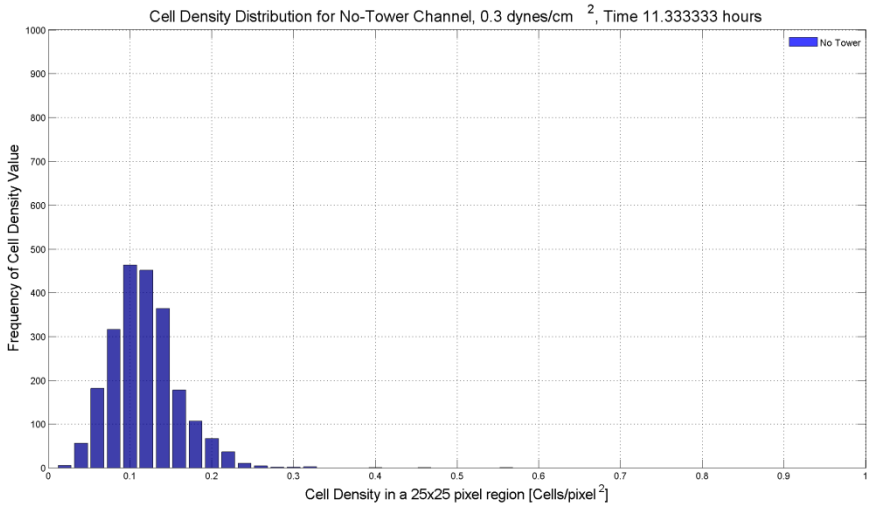
Cell Density Distribution for No-Tower Channel, 0.3 dynes/cm 2, Time 11.333333 hours
No Tower
Frequency of Cell Density Value
Cell Density in a 25x25 pixel region [Cells/pixel 2]

l

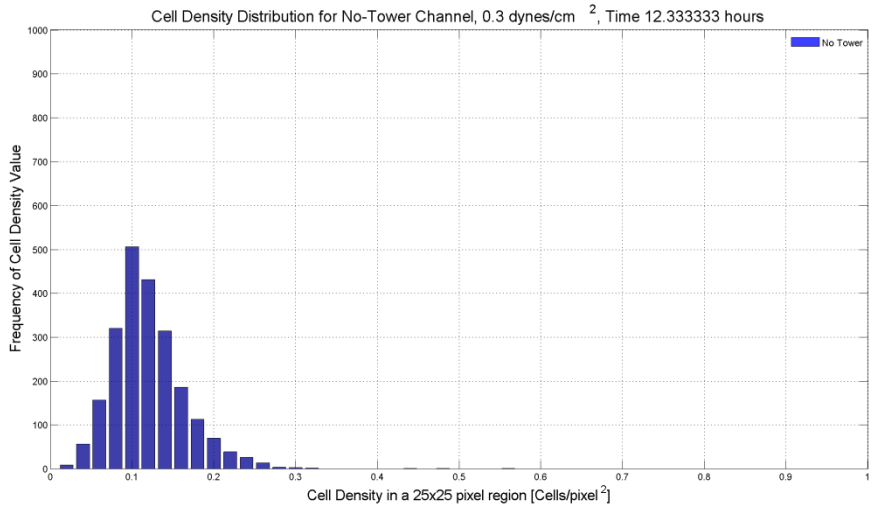
Cell Density Distribution for No-Tower Channel, 0.3 dynes/cm 2, Time 12.333333 hours
No Tower
Frequency of Cell Density Value
Cell Density in a 25x25 pixel region [Cells/pixel 2]

m

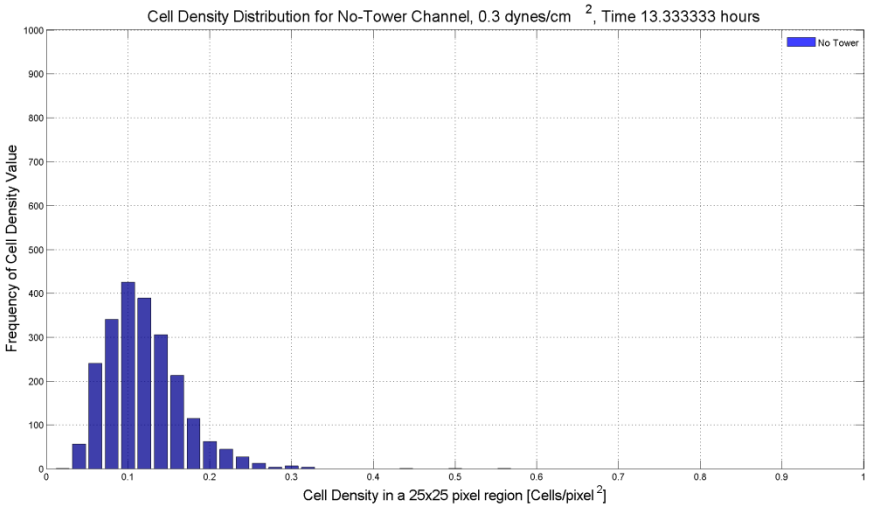
Cell Density Distribution for No-Tower Channel, 0.3 dynes/cm 2, Time 13.333333 hours
No Tower
Frequency of Cell Density Value
Cell Density in a 25x25 pixel region [Cells/pixel 2]

n

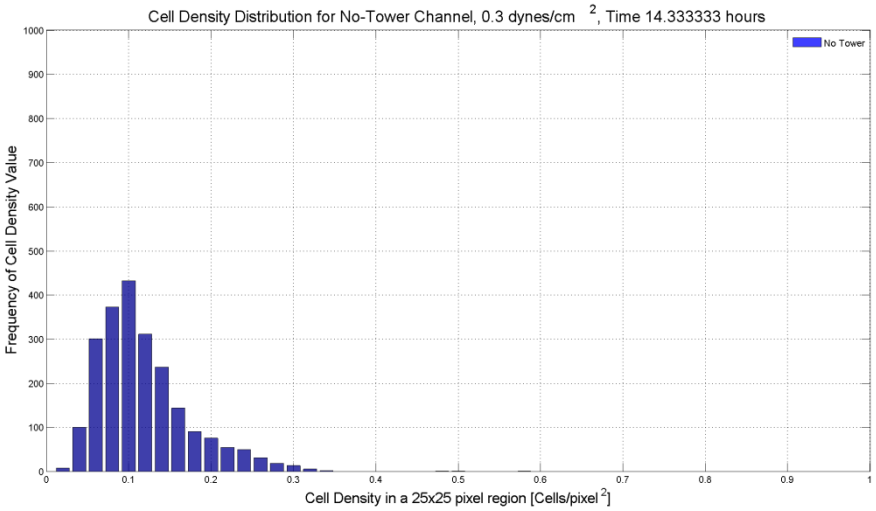
Cell Density Distribution for No-Tower Channel, 0.3 dynes/cm 2, Time 14.333333 hours
No Tower
Frequency of Cell Density Value
Cell Density in a 25x25 pixel region [Cells/pixel 2]

o

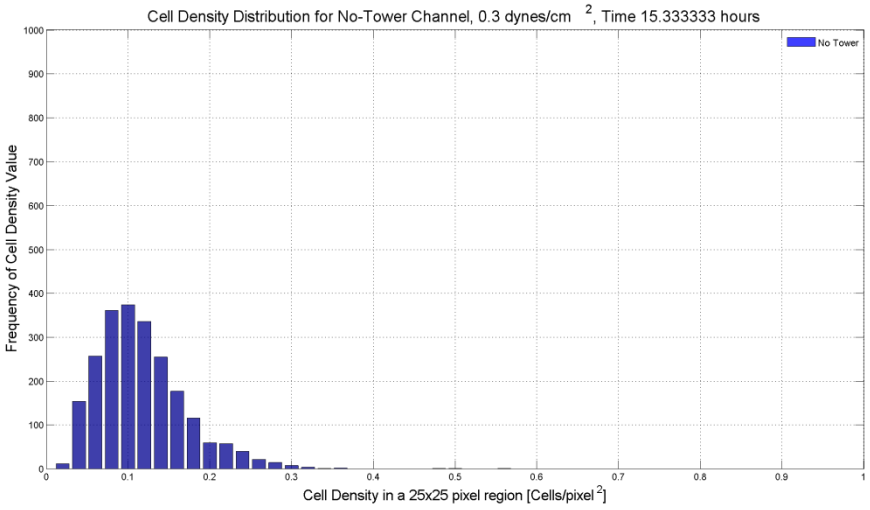
Cell Density Distribution for No-Tower Channel, 0.3 dynes/cm 2, Time 15.333333 hours
No Tower
Frequency of Cell Density Value
Cell Density in a 25x25 pixel region [Cells/pixel 2]

p

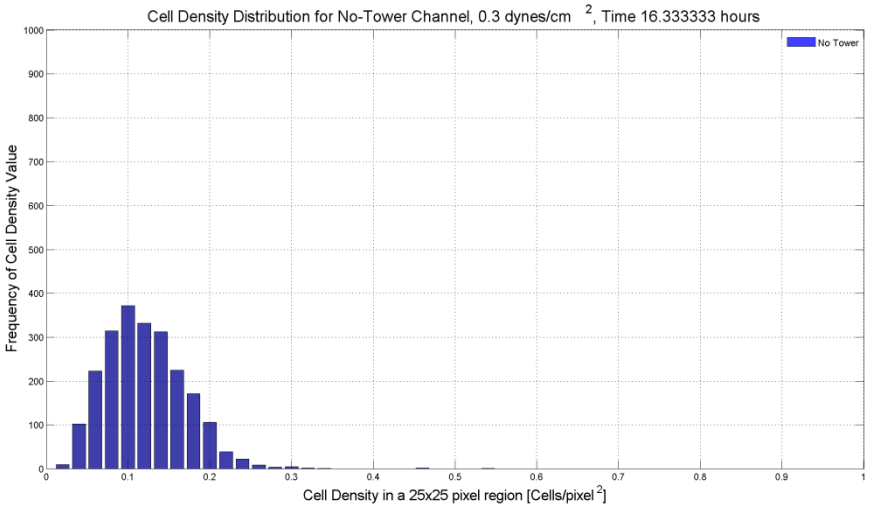
Cell Density Distribution for No-Tower Channel, 0.3 dynes/cm 2, Time 16.333333 hours
No Tower
Frequency of Cell Density Value
Cell Density in a 25x25 pixel region [Cells/pixel 2]

q

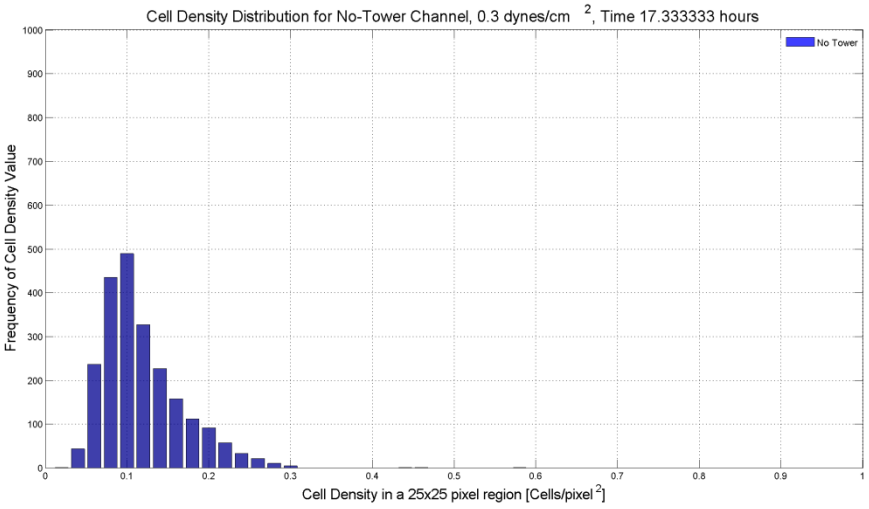
Cell Density Distribution for No-Tower Channel, 0.3 dynes/cm 2, Time 17.333333 hours
No Tower
Frequency of Cell Density Value
Cell Density in a 25x25 pixel region [Cells/pixel 2]

r

4.4.2 Cell Density Distributions as a function of time for the applied shear stress of 0.3 dynes/cm^2. Tower data is shown in red and non-tower data is shown in blue. Figures a-r show hourly distributions across the experimental timeline.

4.4.3 Cell Density Distribution as a Function of Time: 0.6 dynes/cm^2

Studying the cell density distribution as a function of time for the applied shear stress of 0.6 dynes/cm^2 allows a more clear comparison of tower and non-tower forming channels. Specifically, the cell density distribution plot shows the most frequent cell density values, the range of cell density values, and how both change as a function of time for tower and non-tower forming channels. As the applied shear stress of 0.6 dynes/cm^2 more frequently yields towers than the other applied shear stresses studied, a better understanding of how the cell density is distributed across the channel bottom may affect tower development could improve our knowledge of what affects tower formation.

The distribution of cell density as a function of time for the applied shear stress of 0.6 dynes/cm^2 is shown in Figures 4.4.3*a-r*, where the cell density distribution for tower forming channels is represented in red and the cell density distribution for non-tower forming channels is represented in blue. The data are presented at hourly intervals. The vertical axis shows the frequency of cell density values in a 25 x 25 pixel window and the horizontal axis shows the range of cell density values from 0 to 1.

The distribution of cell density as a function of time for the applied shear stress of 0.6 dynes/cm^2 as presented for tower forming channels show a broader range of values in comparison to the distribution of cell density as a function of time for the non-tower forming channels starting from the first experimental time point. As suggested in section 4.3, the lower spatial RMS of cell density for the non-tower forming channel for the

applied shear stress of 0.6 dynes may indicate a more narrow range of cell density values, which Figures 4.4.3*a-r* appear to confirm. Additionally, the cell density values that have a higher frequency for the tower forming channels are lower in value over time than those for the non-tower forming channels.

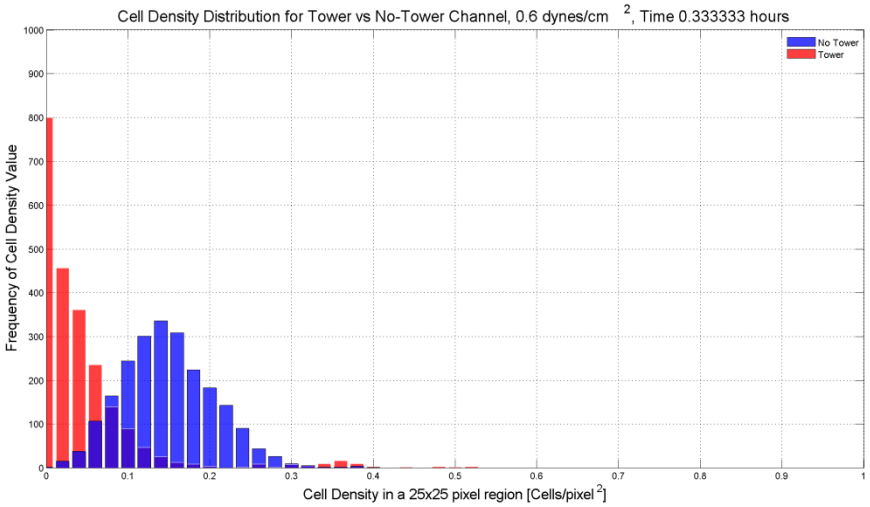

a

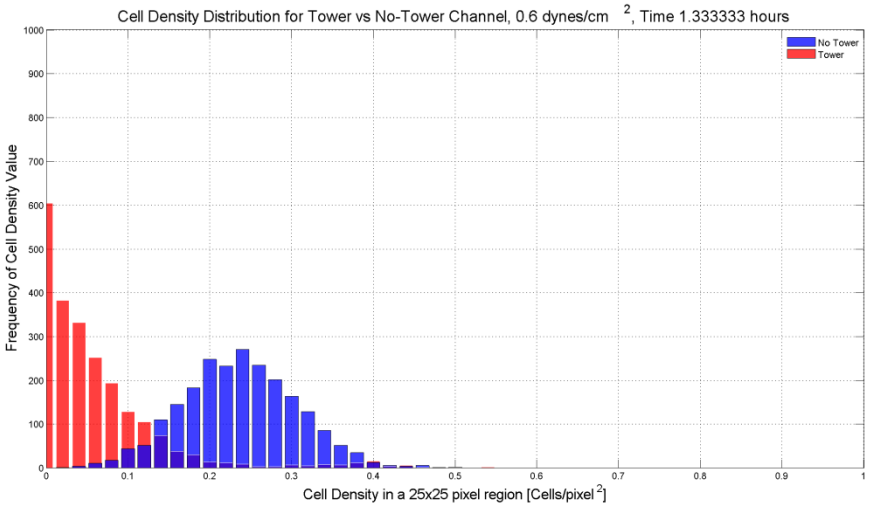

b

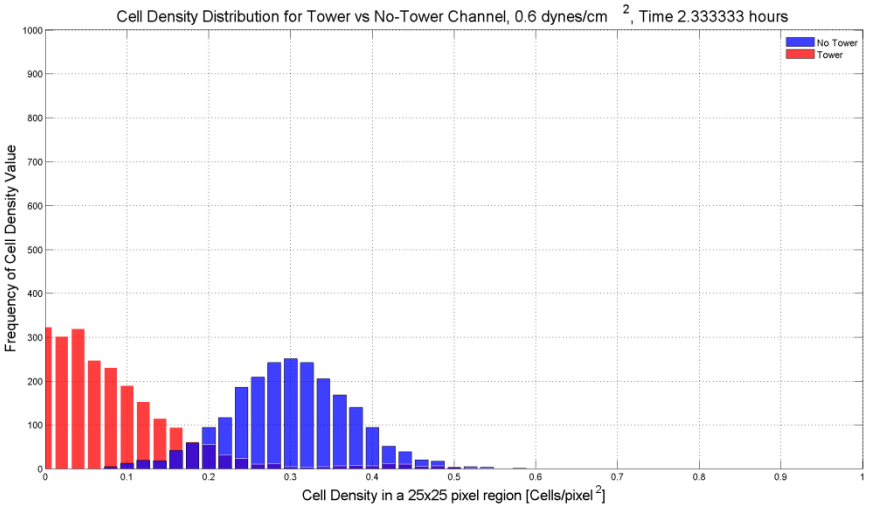
Cell Density Distribution for Tower vs No-Tower Channel, 0.6 dynes/cm 2, Time 2.333333 hours
No Tower
Tower
Frequency of Cell Density Value
Cell Density in a 25x25 pixel region [Cells/pixel 2]

c

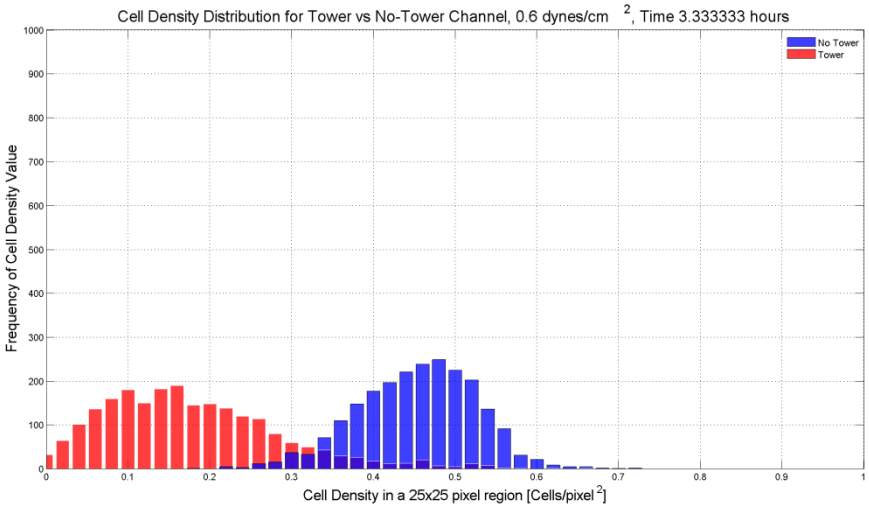
Cell Density Distribution for Tower vs No-Tower Channel, 0.6 dynes/cm 2, Time 3.333333 hours
No Tower
Tower
Frequency of Cell Density Value
Cell Density in a 25x25 pixel region [Cells/pixel 2]

d

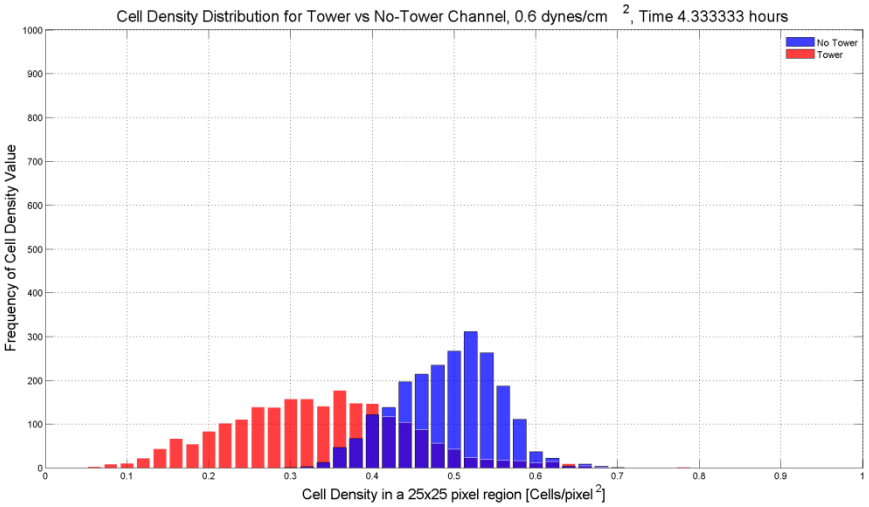
Cell Density Distribution for Tower vs No-Tower Channel, 0.6 dynes/cm 2, Time 4.333333 hours
No Tower
Tower
Frequency of Cell Density Value
Cell Density in a 25x25 pixel region [Cells/pixel 2]

e

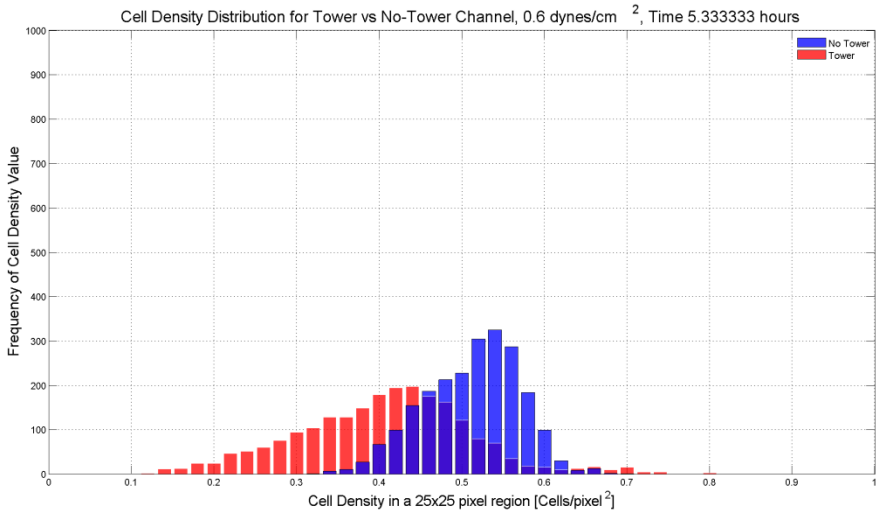
Cell Density Distribution for Tower vs No-Tower Channel, 0.6 dynes/cm 2, Time 5.333333 hours
No Tower
Tower
Frequency of Cell Density Value
Cell Density in a 25x25 pixel region [Cells/pixel 2]

f

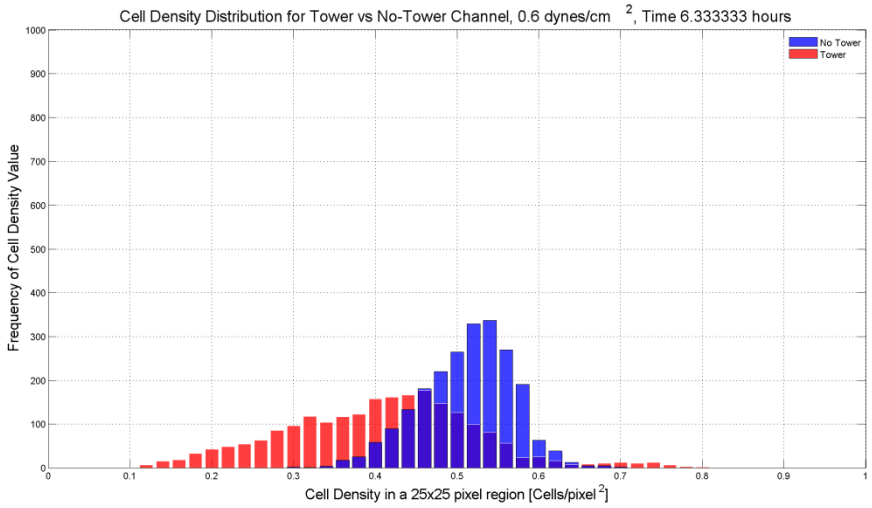
Cell Density Distribution for Tower vs No-Tower Channel, 0.6 dynes/cm 2, Time 6.333333 hours
No Tower
Tower
Frequency of Cell Density Value
Cell Density in a 25x25 pixel region [Cells/pixel 2]

g

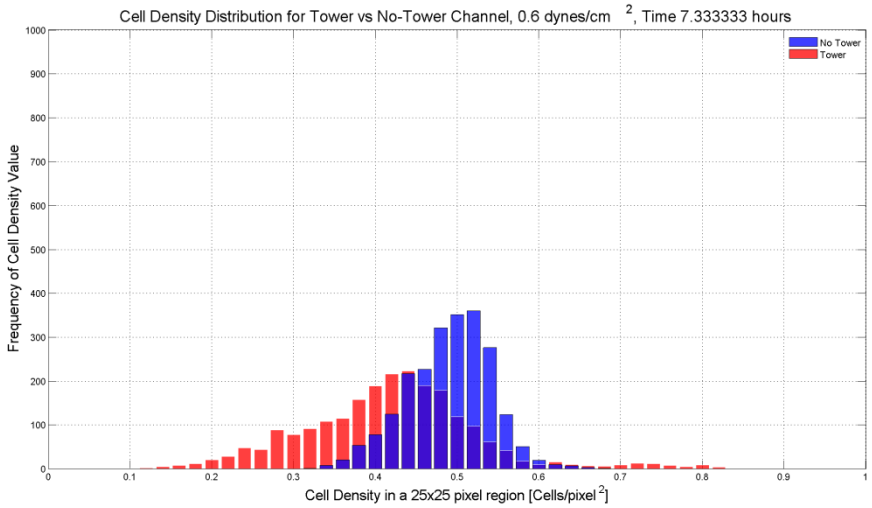
Cell Density Distribution for Tower vs No-Tower Channel, 0.6 dynes/cm 2, Time 7.333333 hours
No Tower
Tower
Frequency of Cell Density Value
Cell Density in a 25x25 pixel region [Cells/pixel 2]

h

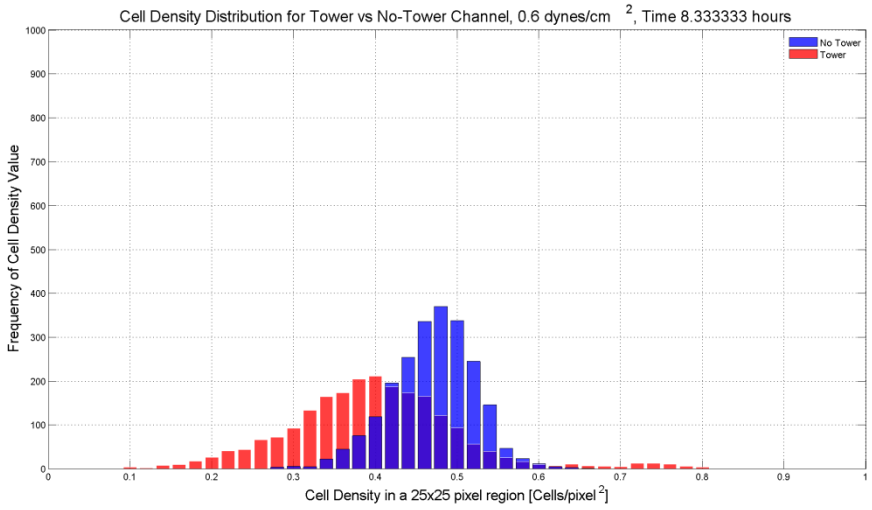
Cell Density Distribution for Tower vs No-Tower Channel, 0.6 dynes/cm 2, Time 8.333333 hours
No Tower
Tower
Frequency of Cell Density Value
Cell Density in a 25x25 pixel region [Cells/pixel 2]

i

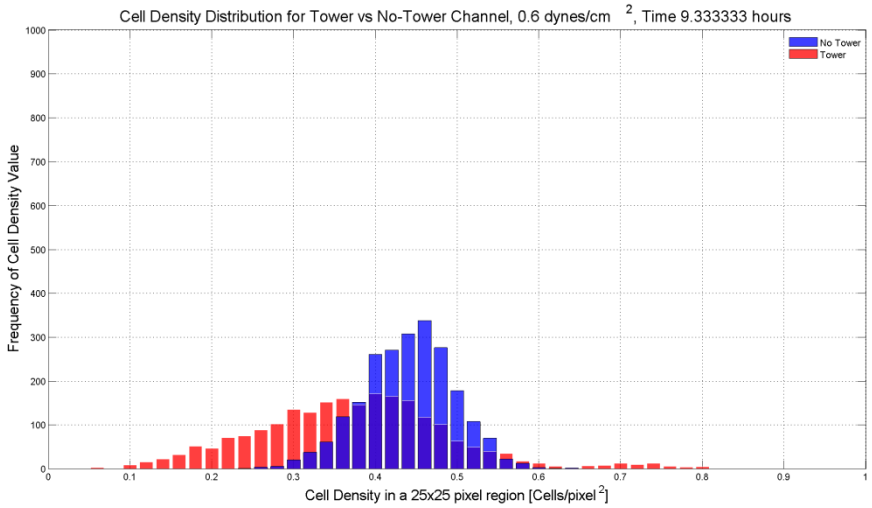
Cell Density Distribution for Tower vs No-Tower Channel, 0.6 dynes/cm 2, Time 9.333333 hours
No Tower
Tower
Frequency of Cell Density Value
Cell Density in a 25x25 pixel region [Cells/pixel 2]

j

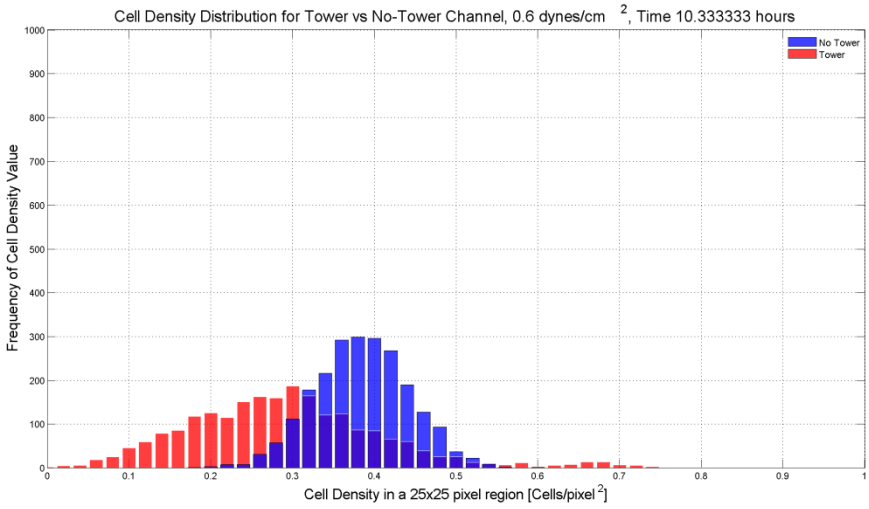
Cell Density Distribution for Tower vs No-Tower Channel, 0.6 dynes/cm 2, Time 10.333333 hours
No Tower
Tower
Frequency of Cell Density Value
Cell Density in a 25x25 pixel region [Cells/pixel 2]

k

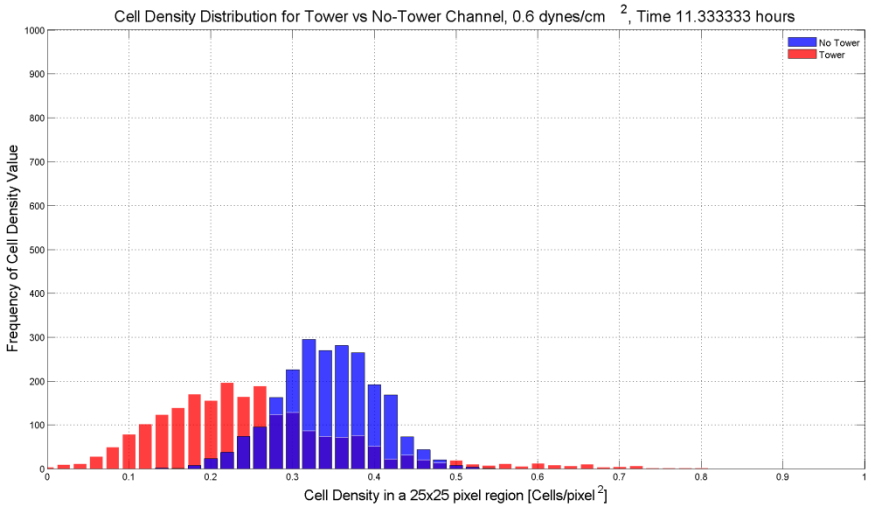
Cell Density Distribution for Tower vs No-Tower Channel, 0.6 dynes/cm 2, Time 11.333333 hours
No Tower
Tower
Frequency of Cell Density Value
Cell Density in a 25x25 pixel region [Cells/pixel 2]

l

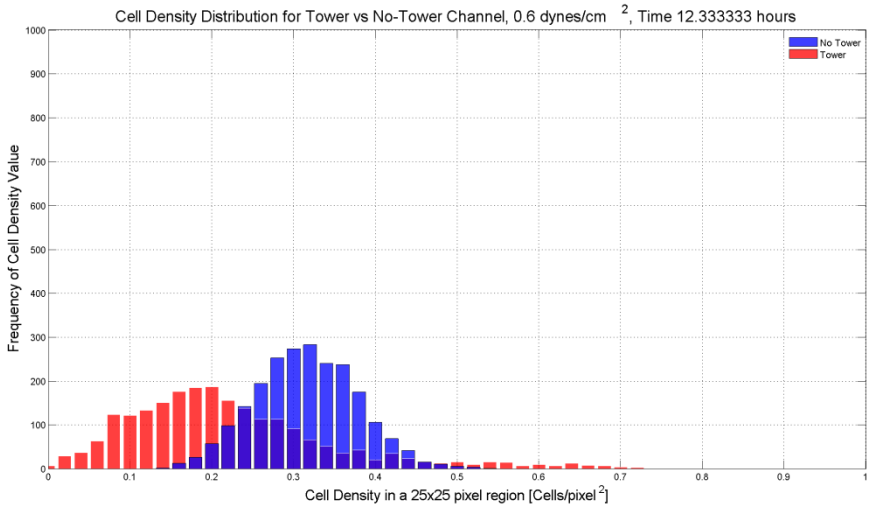
Cell Density Distribution for Tower vs No-Tower Channel, 0.6 dynes/cm 2, Time 12.333333 hours
No Tower
Tower
Frequency of Cell Density Value
Cell Density in a 25x25 pixel region [Cells/pixel 2]

m

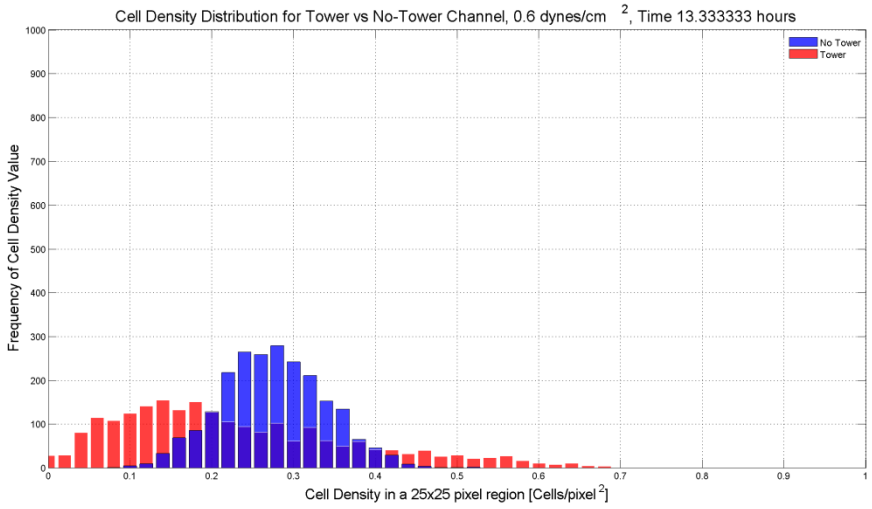
Cell Density Distribution for Tower vs No-Tower Channel, 0.6 dynes/cm 2, Time 13.333333 hours
No Tower
Tower
Frequency of Cell Density Value
Cell Density in a 25x25 pixel region [Cells/pixel 2]

n

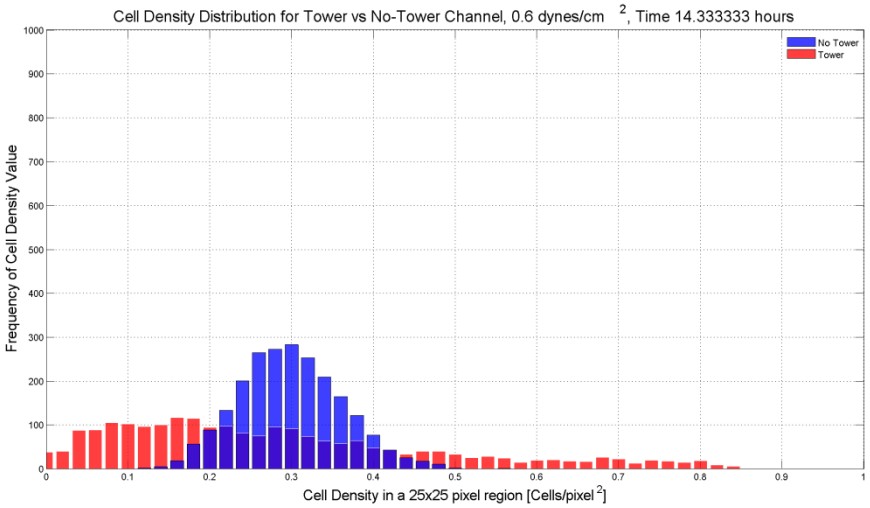
Cell Density Distribution for Tower vs No-Tower Channel, 0.6 dynes/cm 2, Time 14.333333 hours
No Tower
Tower
Frequency of Cell Density Value
Cell Density in a 25x25 pixel region [Cells/pixel 2]

o

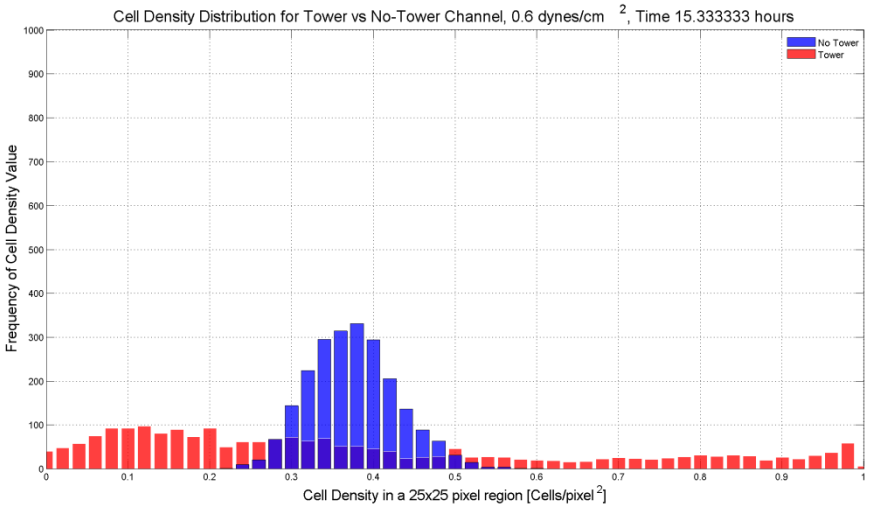
Cell Density Distribution for Tower vs No-Tower Channel, 0.6 dynes/cm 2, Time 15.333333 hours
No Tower
Tower
Frequency of Cell Density Value
Cell Density in a 25x25 pixel region [Cells/pixel 2]

p

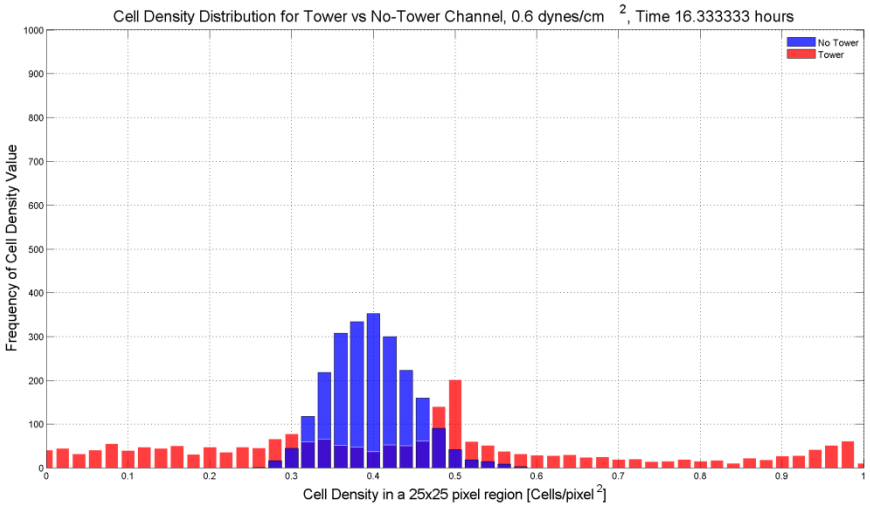
Cell Density Distribution for Tower vs No-Tower Channel, 0.6 dynes/cm 2, Time 16.333333 hours
No Tower
Tower
Frequency of Cell Density Value
Cell Density in a 25x25 pixel region [Cells/pixel 2]

q

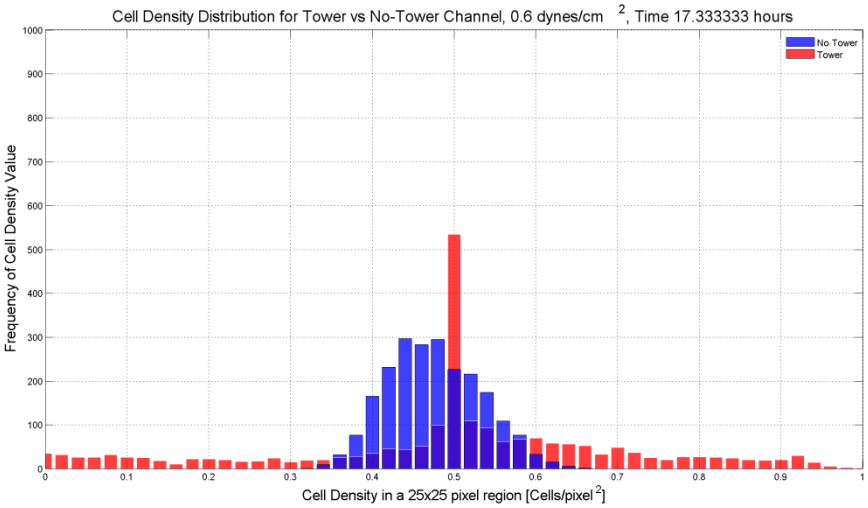

r

Figure 4.4.3 Cell Density Distributions as a function of time for the applied shear stress of 0.6 dynes/cm^2. Tower data is shown in red and non-tower data is shown in blue. Figures a-r show hourly distributions across the experimental timeline.

4.4.4 Cell Density Distribution as a Function of Time: 0.9 dynes/cm^2

Further investigation of the applied shear stress of 0.9 dynes/cm^2 by means of studying the cell density distribution helps answer the question of if there is a relationship between applied shear stress and cell density distribution and also helps to quantify the cell density distribution of the two tower forming channels to better compare the results against the tower forming channels of other applied shear stresses.

The distribution of cell density as a function of time for the applied shear stress of 0.9 dynes/cm^2 are shown in Figures 4.4.4a-r, where the cell density distribution for non-tower forming channels is represented in blue and the cell density distribution for the tower-forming channels is represented in red. The data are presented at hourly intervals. The vertical axis shows the frequency of cell density values in a 25 x 25 pixel window and the horizontal axis shows the range of cell density values from 0 to 1.

The distribution of cell density as a function of time for the applied shear stress of 0.9 dynes/cm^2 as presented for tower forming channels is similar in profile to the distribution of cell density as a function of time for the non-tower forming channels. Both distributions cover a larger range of cell density values at a given time point than the cell density distributions for other applied shear stresses studied. The similarity between the cell density distributions of the tower and non-tower forming channels for the applied shear stress of 0.9 dynes/cm^2 follows the similarities between the two observed in the cell density as a function of time and the Spatial RMS of cell density of tower and non-tower forming channels for the applied shear stress of 0.9 dynes/cm^2. The cell density distribution of the tower and non-tower forming channels for the applied shear stress of 0.9 dynes/cm^2 is similar in breadth to the cell density distribution of the non-tower forming channel of 1.5 dynes/cm^2, suggesting that perhaps the range of the cell density distribution may be related to the applied shear stress.

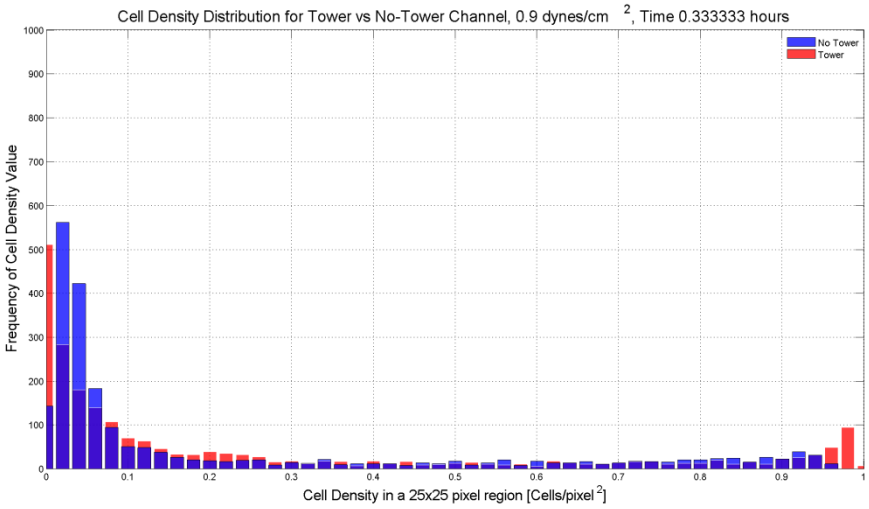

a

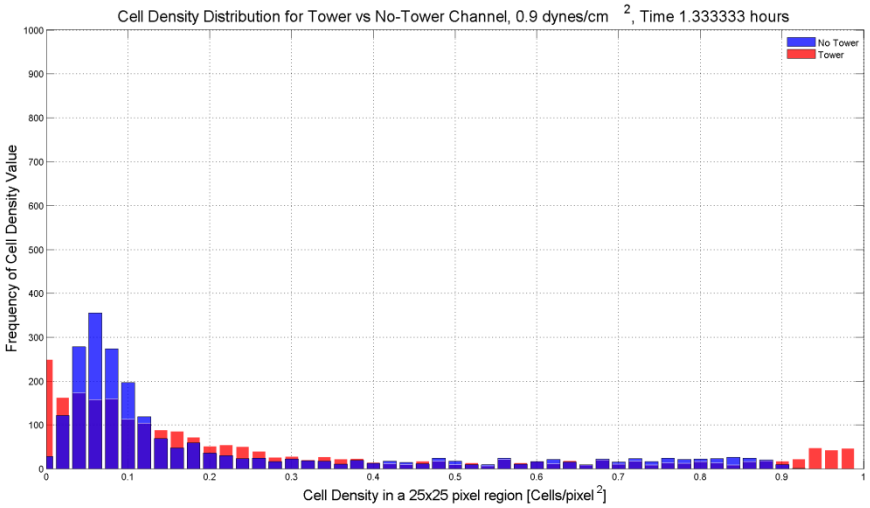
Cell Density Distribution for Tower vs No-Tower Channel, 0.9 dynes/cm 2, Time 1.333333 hours
No Tower
Tower
Frequency of Cell Density Value
Cell Density in a 25x25 pixel region [Cells/pixel 2]

b

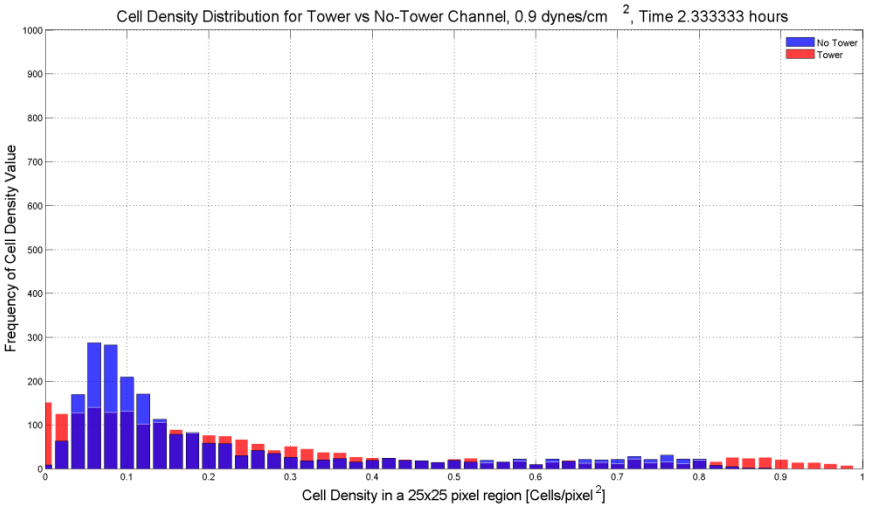
Cell Density Distribution for Tower vs No-Tower Channel, 0.9 dynes/cm 2, Time 2.333333 hours
No Tower
Tower
Frequency of Cell Density Value
Cell Density in a 25x25 pixel region [Cells/pixel 2]

c

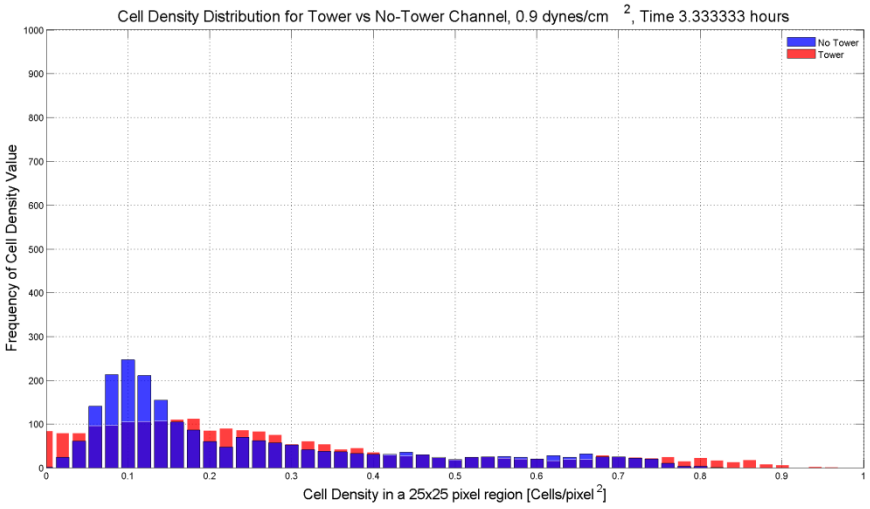
Cell Density Distribution for Tower vs No-Tower Channel, 0.9 dynes/cm 2, Time 3.333333 hours
No Tower
Tower
Frequency of Cell Density Value
Cell Density in a 25x25 pixel region [Cells/pixel 2]

d

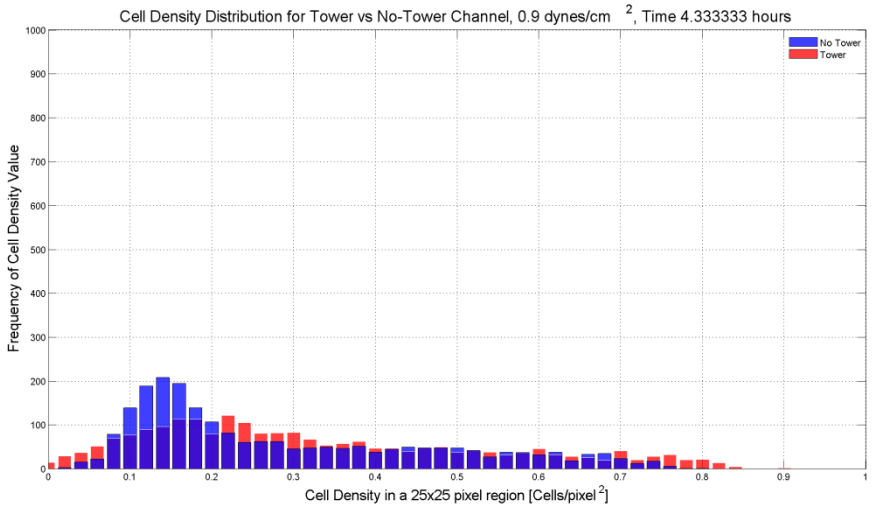
Cell Density Distribution for Tower vs No-Tower Channel, 0.9 dynes/cm 2, Time 4.333333 hours
No Tower
Tower
Frequency of Cell Density Value
Cell Density in a 25x25 pixel region [Cells/pixel 2]

e

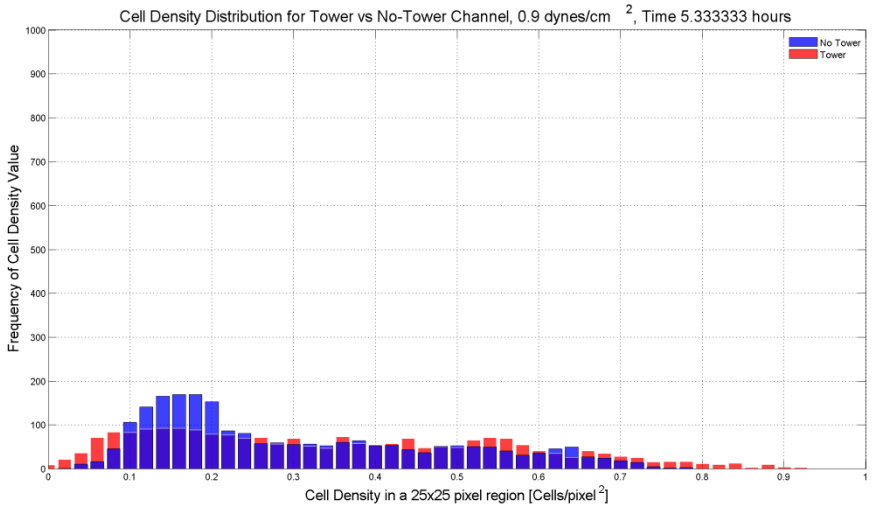
Cell Density Distribution for Tower vs No-Tower Channel, 0.9 dynes/cm 2, Time 5.333333 hours
No Tower
Tower
Frequency of Cell Density Value
Cell Density in a 25x25 pixel region [Cells/pixel 2]

f

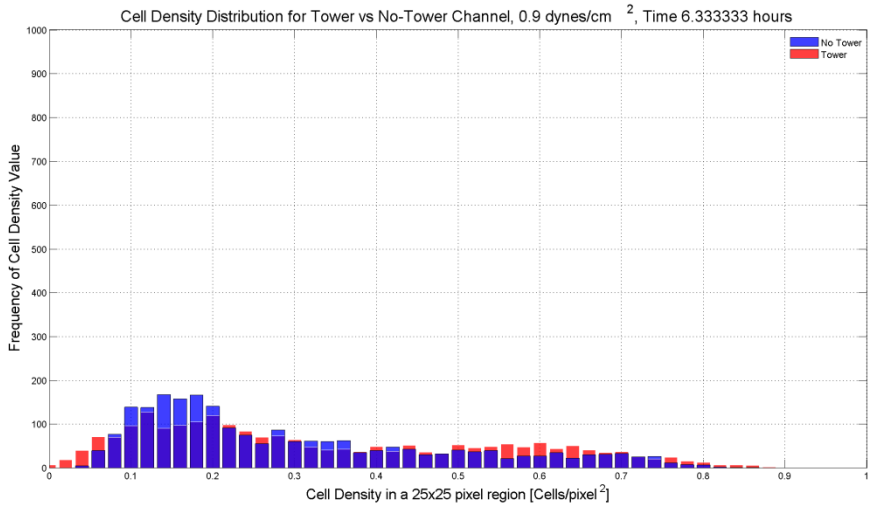
Cell Density Distribution for Tower vs No-Tower Channel, 0.9 dynes/cm 2, Time 6.333333 hours
No Tower
Tower
Frequency of Cell Density Value
Cell Density in a 25x25 pixel region [Cells/pixel 2]

g

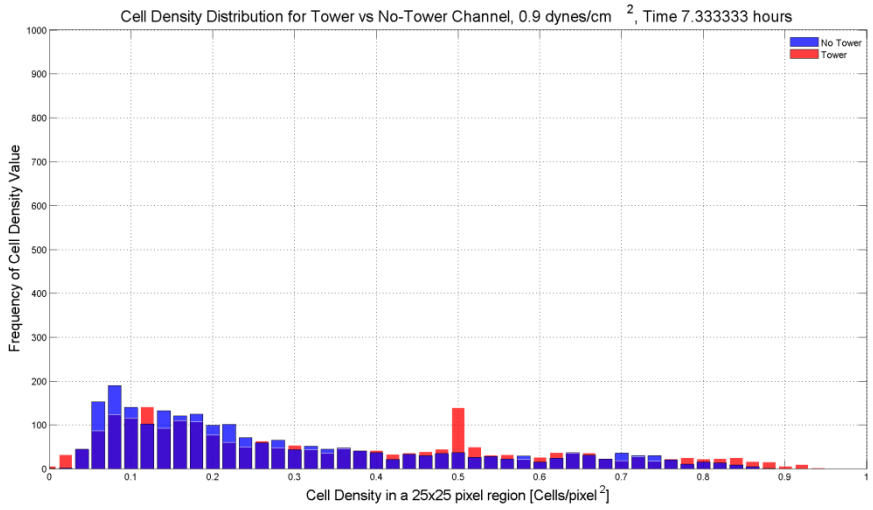
Cell Density Distribution for Tower vs No-Tower Channel, 0.9 dynes/cm 2, Time 7.333333 hours
No Tower
Tower
Frequency of Cell Density Value
Cell Density in a 25x25 pixel region [Cells/pixel 2]

h

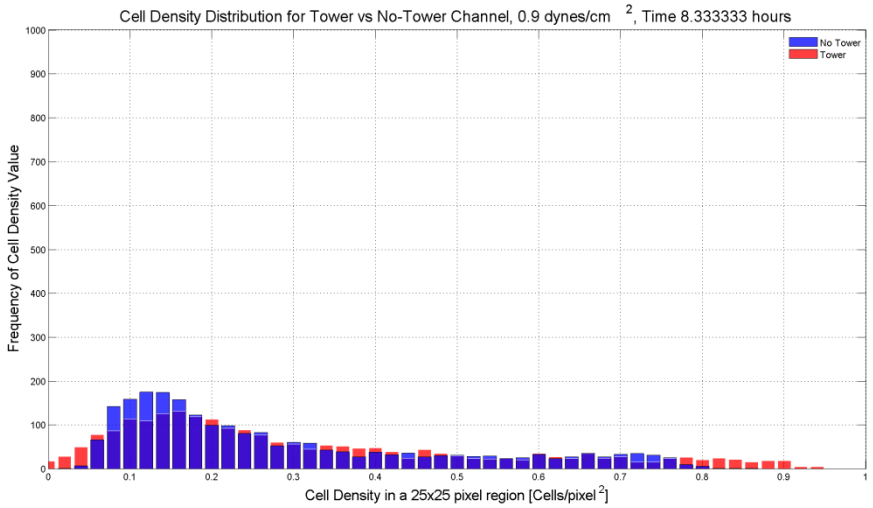
Cell Density Distribution for Tower vs No-Tower Channel, 0.9 dynes/cm 2, Time 8.333333 hours
No Tower
Tower
Frequency of Cell Density Value
Cell Density in a 25x25 pixel region [Cells/pixel 2]

i

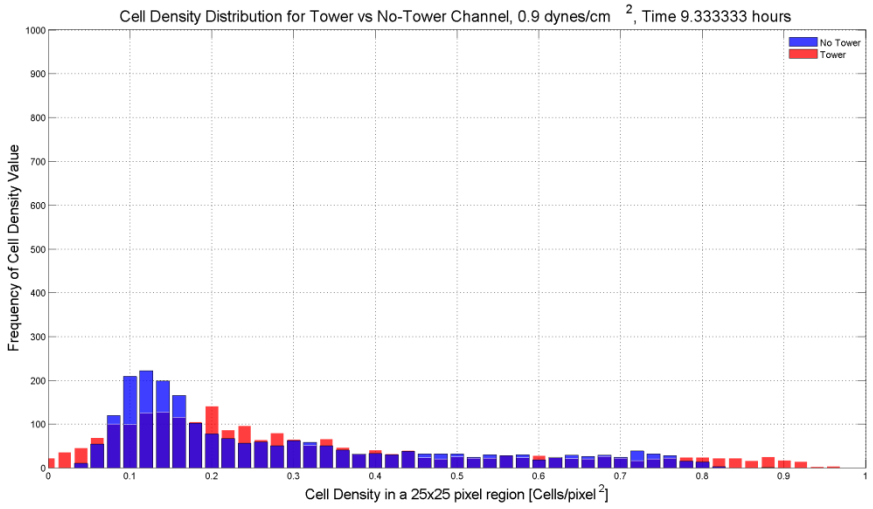
Cell Density Distribution for Tower vs No-Tower Channel, 0.9 dynes/cm 2, Time 9.333333 hours
No Tower
Tower
Frequency of Cell Density Value
Cell Density in a 25x25 pixel region [Cells/pixel 2]

j

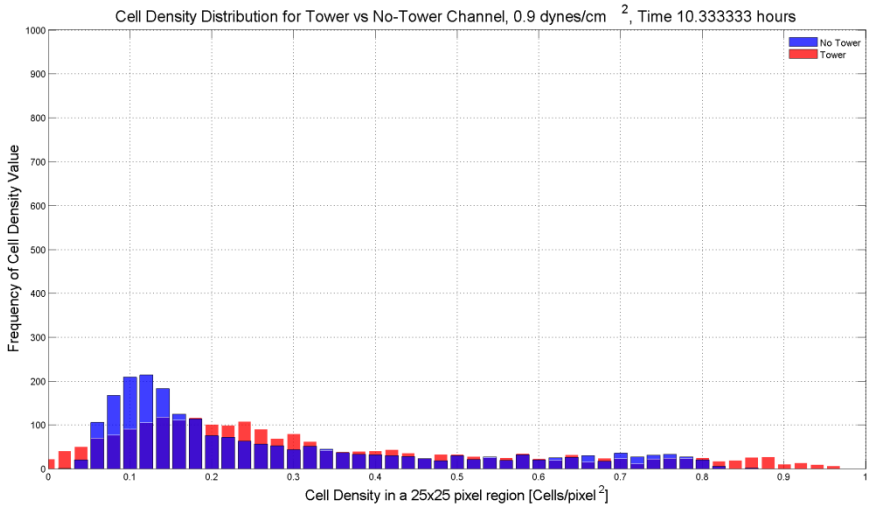
Cell Density Distribution for Tower vs No-Tower Channel, 0.9 dynes/cm 2, Time 10.333333 hours
No Tower
Tower
Frequency of Cell Density Value
Cell Density in a 25x25 pixel region [Cells/pixel 2]

k

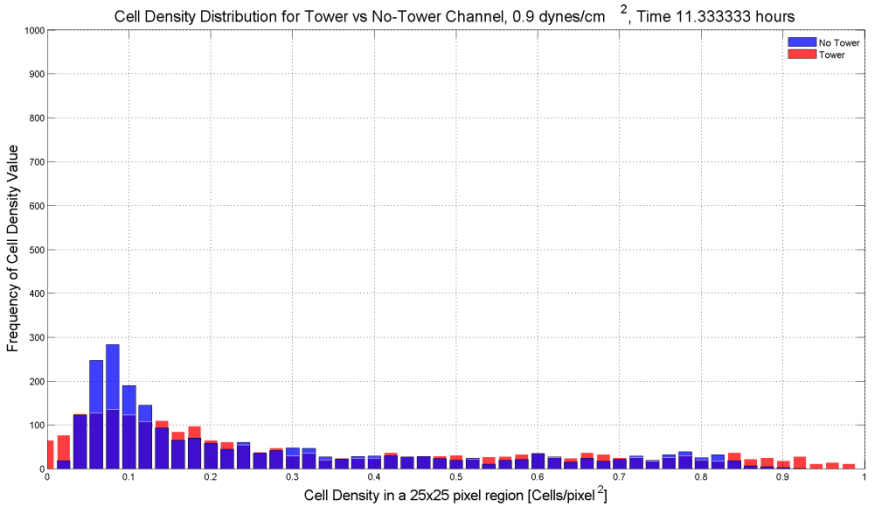
Cell Density Distribution for Tower vs No-Tower Channel, 0.9 dynes/cm 2, Time 11.333333 hours
No Tower
Tower
Frequency of Cell Density Value
Cell Density in a 25x25 pixel region [Cells/pixel 2]

l

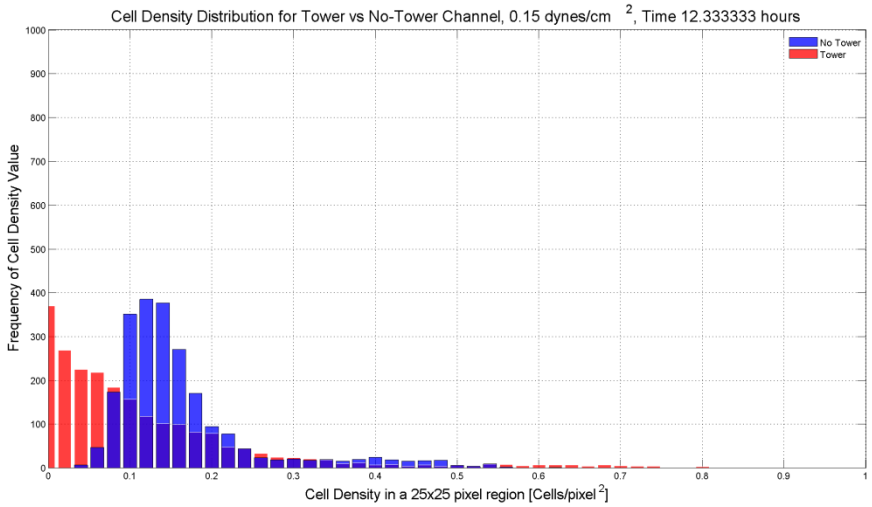
Cell Density Distribution for Tower vs No-Tower Channel, 0.15 dynes/cm 2, Time 12.333333 hours
No Tower
Tower
Frequency of Cell Density Value
Cell Density in a 25x25 pixel region [Cells/pixel 2]

m

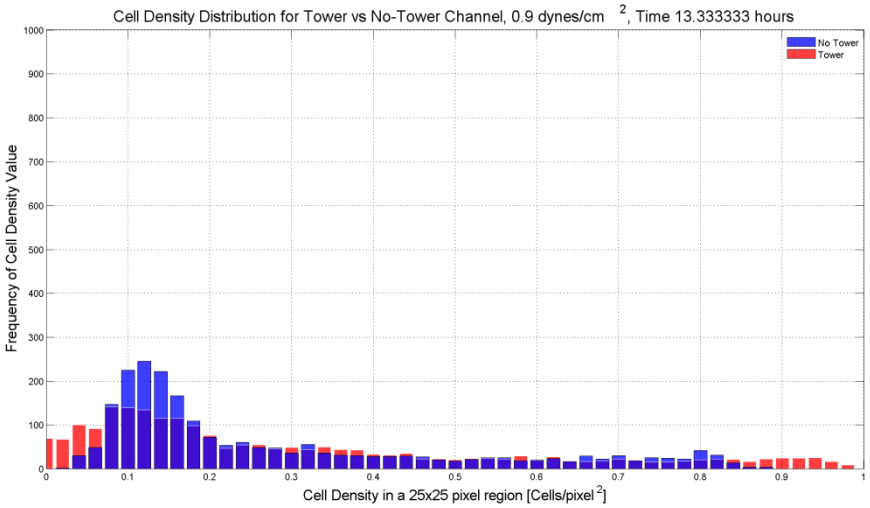
Cell Density Distribution for Tower vs No-Tower Channel, 0.9 dynes/cm 2, Time 13.333333 hours
No Tower
Tower
Frequency of Cell Density Value
Cell Density in a 25x25 pixel region [Cells/pixel 2]

n

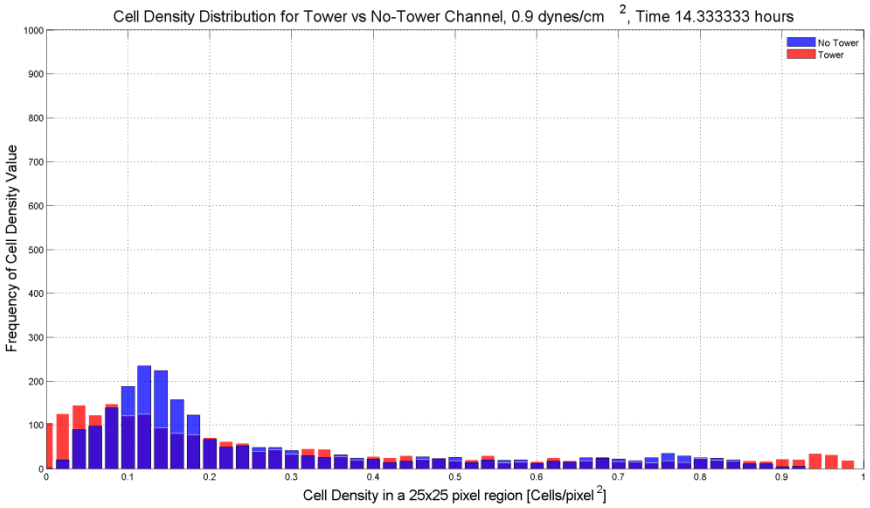
Cell Density Distribution for Tower vs No-Tower Channel, 0.9 dynes/cm 2, Time 14.333333 hours
No Tower
Tower
Frequency of Cell Density Value
Cell Density in a 25x25 pixel region [Cells/pixel 2]

o

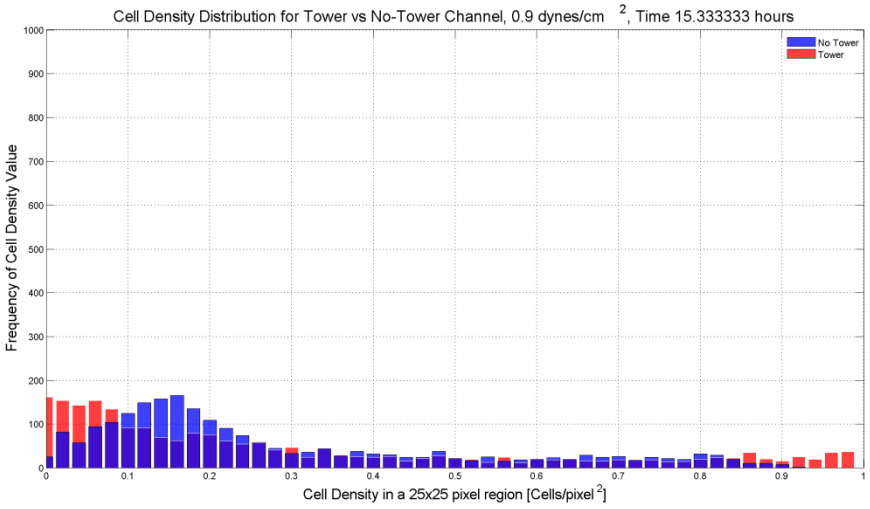
Cell Density Distribution for Tower vs No-Tower Channel, 0.9 dynes/cm 2, Time 15.333333 hours
No Tower
Tower
Frequency of Cell Density Value
Cell Density in a 25x25 pixel region [Cells/pixel 2]

p

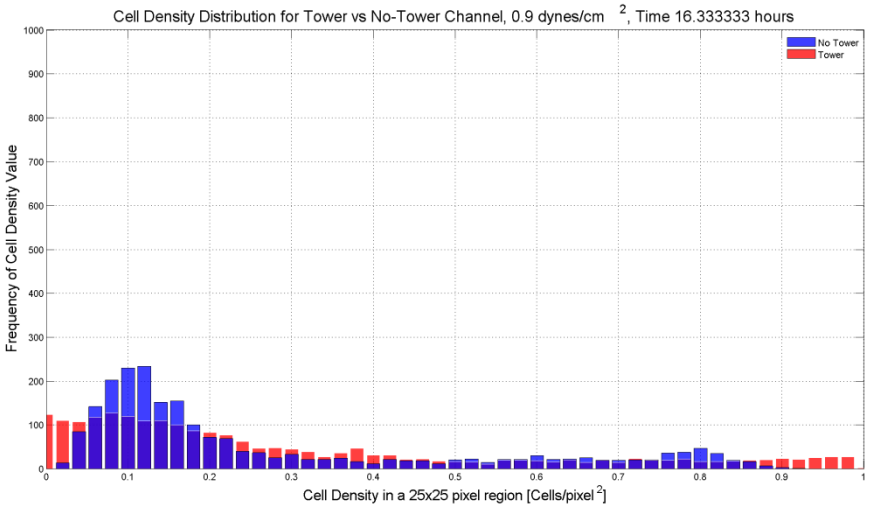

q

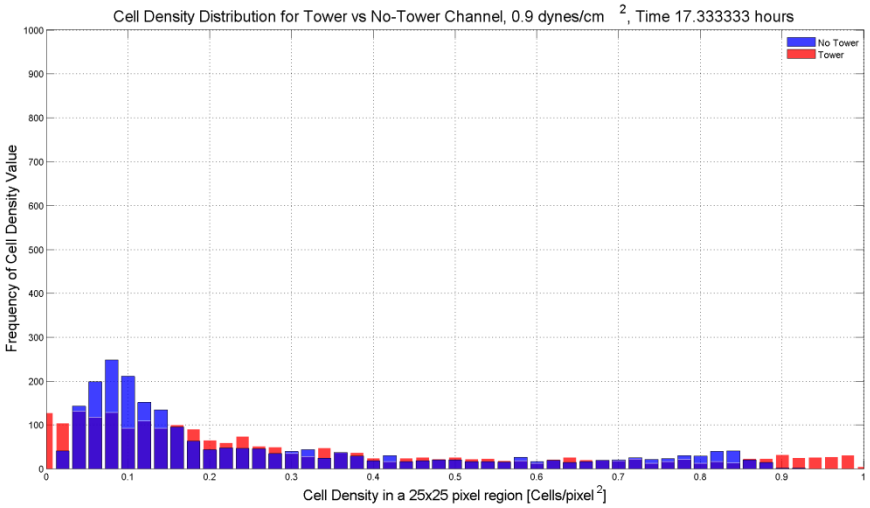

r

Figure 4.4.4 Cell Density Distributions as a function of time for the applied shear stress of 0.9 dynes/cm^2. Tower data is shown in red and non-tower data is shown in blue. Figures a-r show hourly distributions across the experimental timeline.

4.4.5 Cell Density Distribution as a Function of Time: 1.5 dynes/cm^2

Although the applied shear stress of 1.5 dynes/cm^2 does not yield any tower channels, studying the cell density distribution of its non-tower forming channels allows for a comparison of non-tower channels across the range of applied shear stresses studied

and therefore the answer of whether cell density distribution is related to the applied shear stress as well as tower formation frequency.

The distributions of cell density as a function of time for the applied shear stress of 1.5 dynes/cm^2 are shown in Figures 4.4.5a-r, where the cell density distribution for non-tower forming channels is represented in blue. The data are presented at hourly intervals. The vertical axis shows the frequency of cell density values in a 25 x 25 pixel window and the horizontal axis shows the range of cell density values from 0 to 1.

The distribution of cell density as a function of time for the applied shear stress of 1.5 dynes/cm^2 as presented for non-tower forming channels covers a broader range of cell density values at a given time point than the distribution of cell densities for the other applied shear stresses studied except for the applied shear of 0.9 dynes/cm^2. The spatial RMS of cell density for the applied shear stress of 1.5 dynes was found to be similar to that of spatial RMS of cell density for the applied shear stresses of 0.15, 0.3, and 0.9 dynes/cm^2, but only the cell density distribution for the applied shear stress of 0.9 dynes/cm^2 is as broad as that for the applied shear stress of 1.5 dynes/cm^2. These distributions are shown in Figures 4.4.5*a-o*, where the cell density distribution for non-tower forming channels is represented in blue.

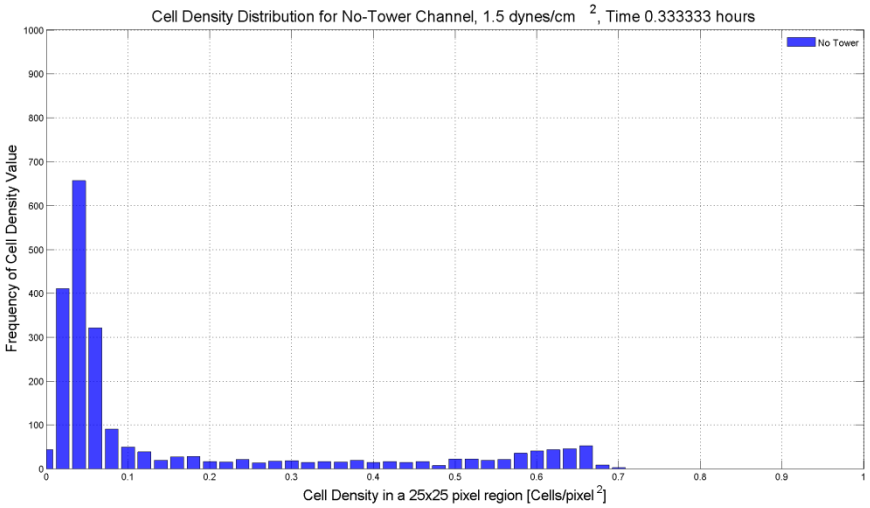
Cell Density Distribution for No-Tower Channel, 1.5 dynes/cm 2, Time 0.333333 hours
No Tower
Frequency of Cell Density Value
Cell Density in a 25x25 pixel region [Cells/pixel 2]

a

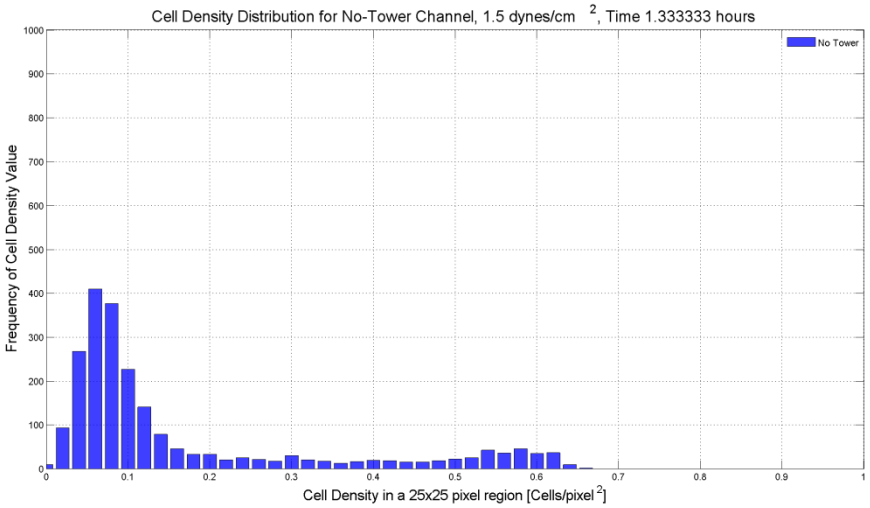
Cell Density Distribution for No-Tower Channel, 1.5 dynes/cm 2, Time 1.333333 hours
No Tower
Frequency of Cell Density Value
Cell Density in a 25x25 pixel region [Cells/pixel 2]

b

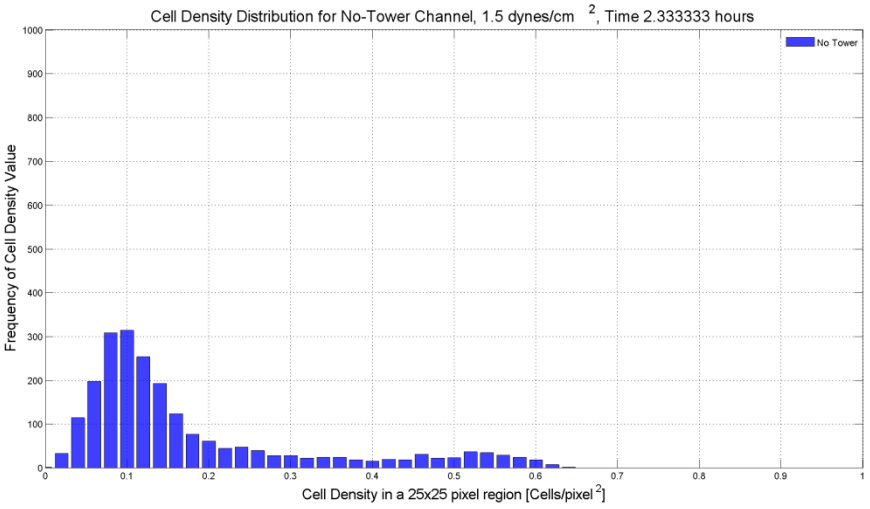
Cell Density Distribution for No-Tower Channel, 1.5 dynes/cm 2, Time 2.333333 hours
No Tower
Frequency of Cell Density Value
Cell Density in a 25x25 pixel region [Cells/pixel 2]

c

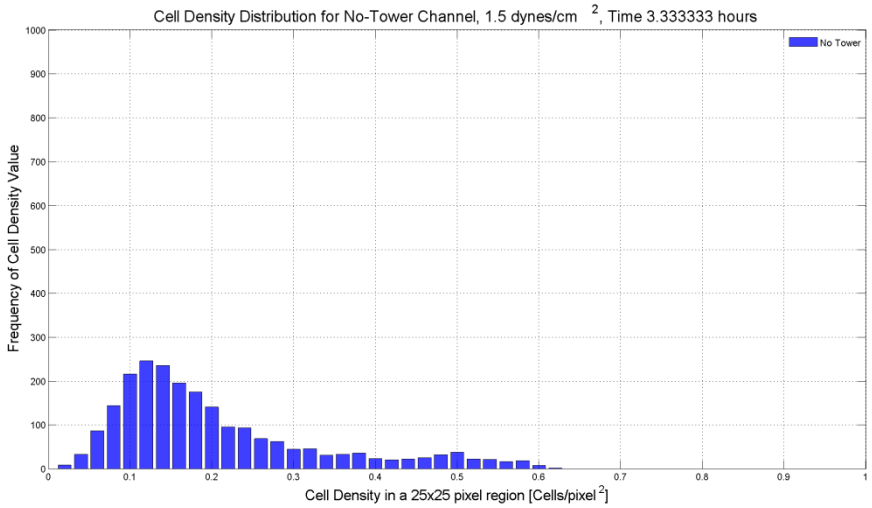
Cell Density Distribution for No-Tower Channel, 1.5 dynes/cm 2, Time 3.333333 hours
No Tower
Frequency of Cell Density Value
Cell Density in a 25x25 pixel region [Cells/pixel 2]

d

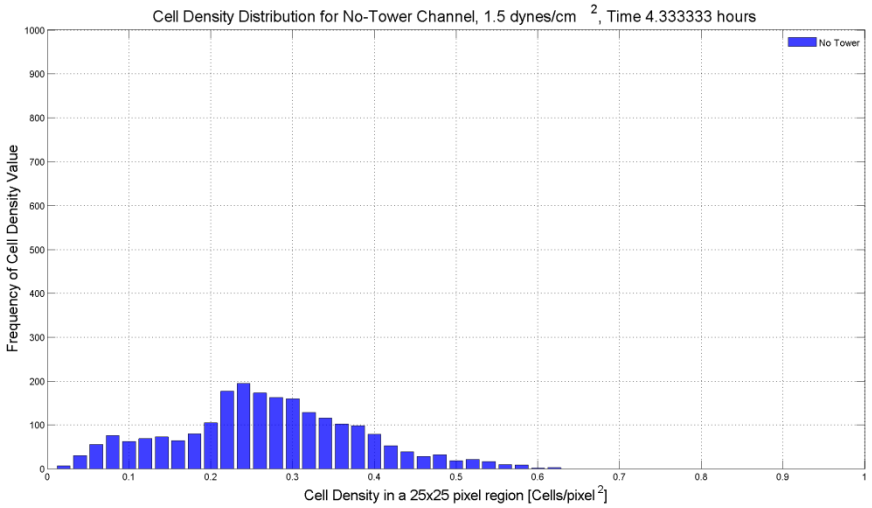
Cell Density Distribution for No-Tower Channel, 1.5 dynes/cm 2, Time 4.333333 hours
No Tower
Frequency of Cell Density Value
Cell Density in a 25x25 pixel region [Cells/pixel 2]

e

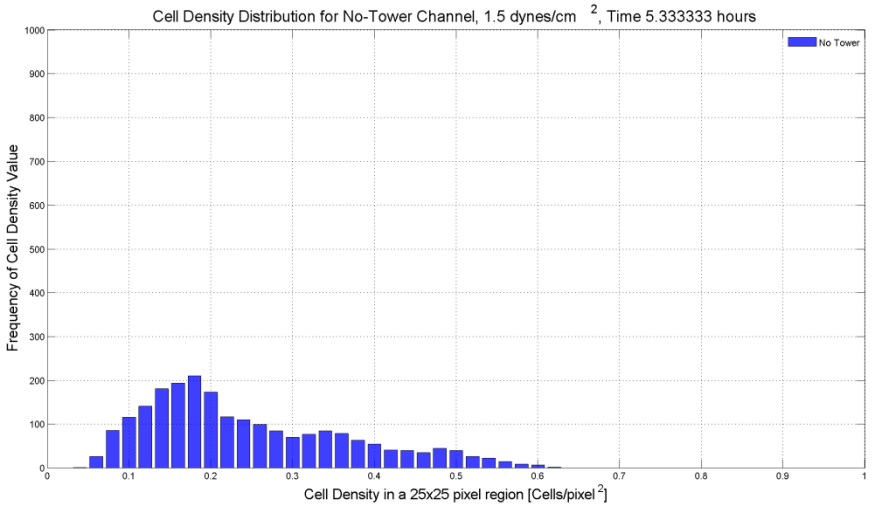
Cell Density Distribution for No-Tower Channel, 1.5 dynes/cm 2, Time 5.333333 hours
No Tower
Frequency of Cell Density Value
Cell Density in a 25x25 pixel region [Cells/pixel 2]

f

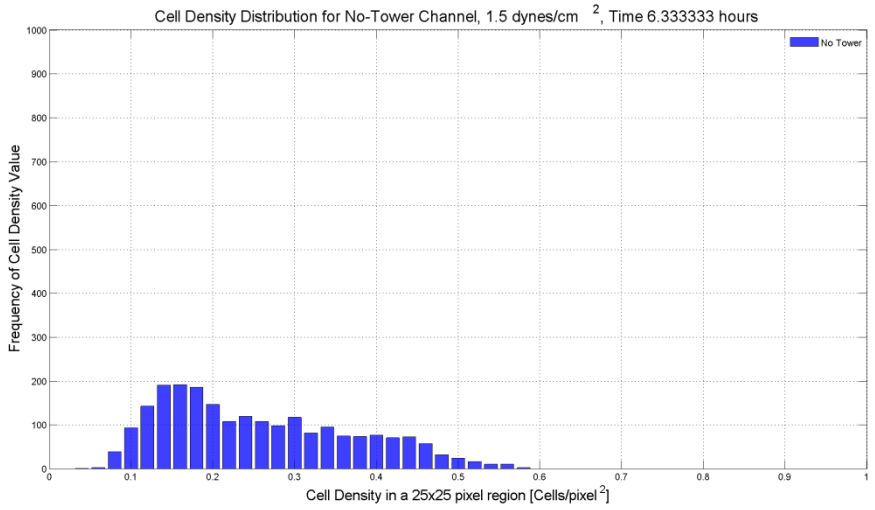
Cell Density Distribution for No-Tower Channel, 1.5 dynes/cm 2, Time 6.333333 hours
No Tower
Frequency of Cell Density Value
Cell Density in a 25x25 pixel region [Cells/pixel 2]

g

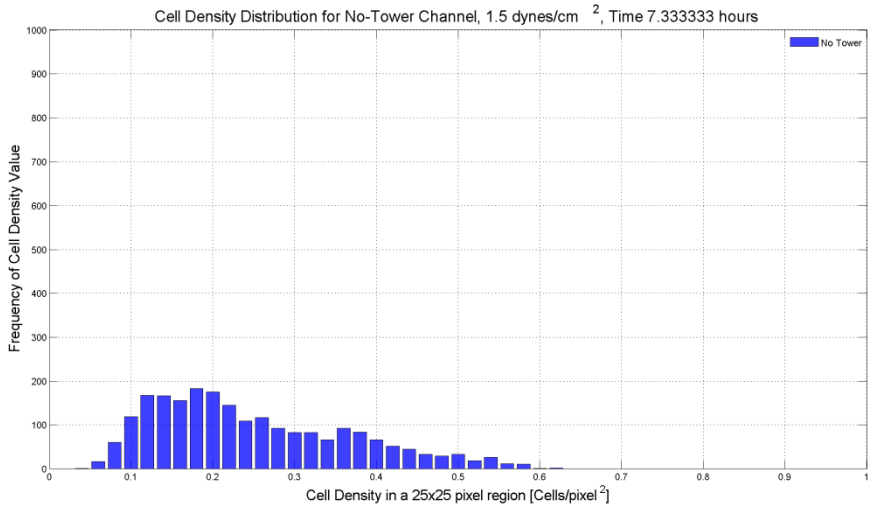
Cell Density Distribution for No-Tower Channel, 1.5 dynes/cm 2, Time 7.333333 hours
No Tower
Frequency of Cell Density Value
Cell Density in a 25x25 pixel region [Cells/pixel 2]

h

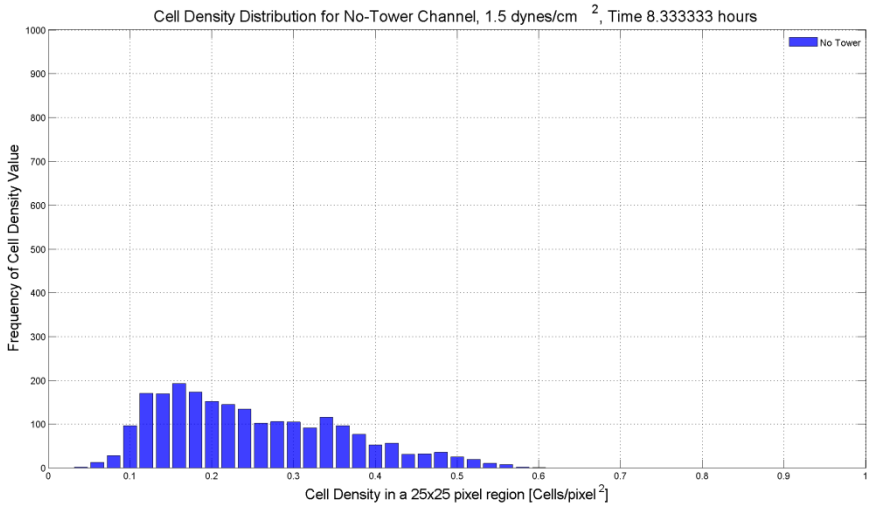
Cell Density Distribution for No-Tower Channel, 1.5 dynes/cm 2, Time 8.333333 hours
No Tower
Frequency of Cell Density Value
Cell Density in a 25x25 pixel region [Cells/pixel 2]

i

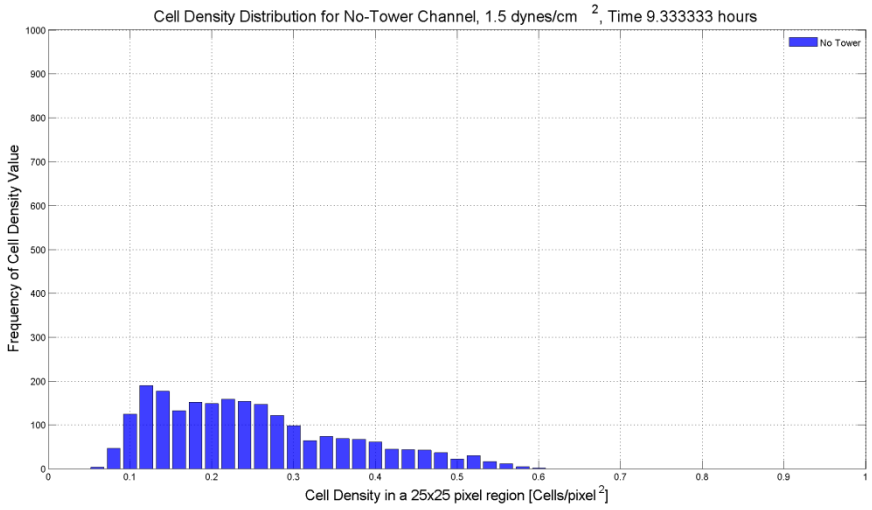
Cell Density Distribution for No-Tower Channel, 1.5 dynes/cm 2, Time 9.333333 hours
No Tower
Frequency of Cell Density Value
Cell Density in a 25x25 pixel region [Cells/pixel 2]

j

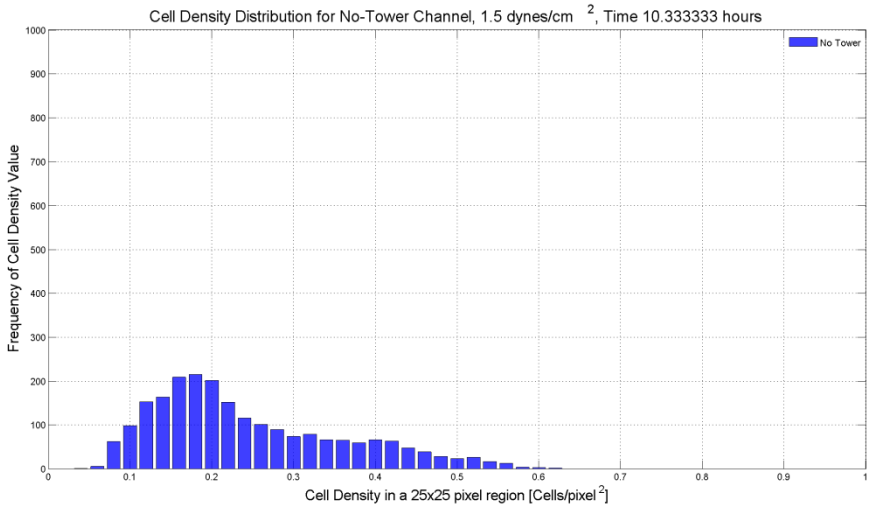
Cell Density Distribution for No-Tower Channel, 1.5 dynes/cm 2, Time 10.333333 hours
No Tower
Frequency of Cell Density Value
Cell Density in a 25x25 pixel region [Cells/pixel 2]

k

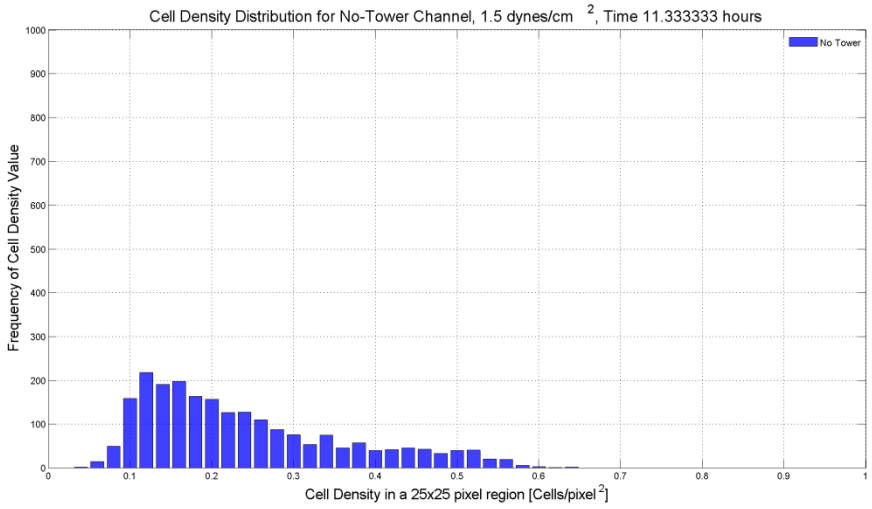
Cell Density Distribution for No-Tower Channel, 1.5 dynes/cm 2, Time 11.333333 hours
No Tower
Frequency of Cell Density Value
Cell Density in a 25x25 pixel region [Cells/pixel 2]

l

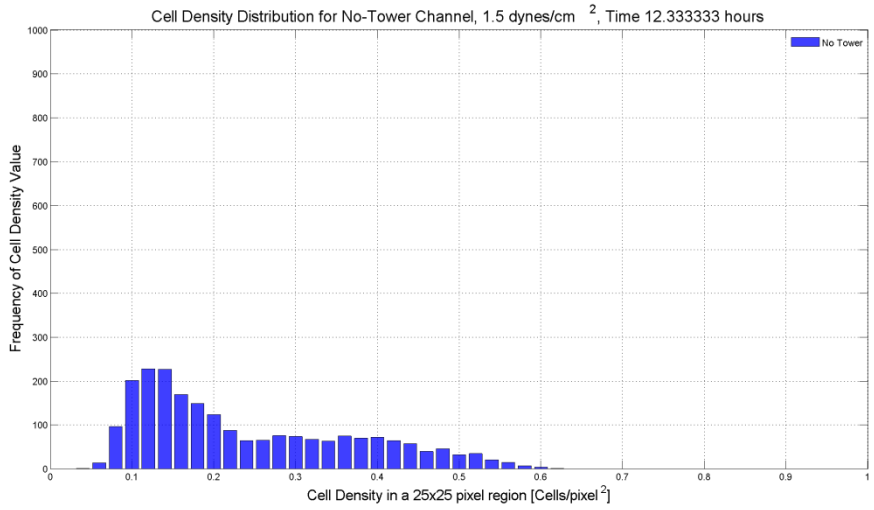
Cell Density Distribution for No-Tower Channel, 1.5 dynes/cm 2, Time 12.333333 hours
No Tower
Frequency of Cell Density Value
Cell Density in a 25x25 pixel region [Cells/pixel 2]

m

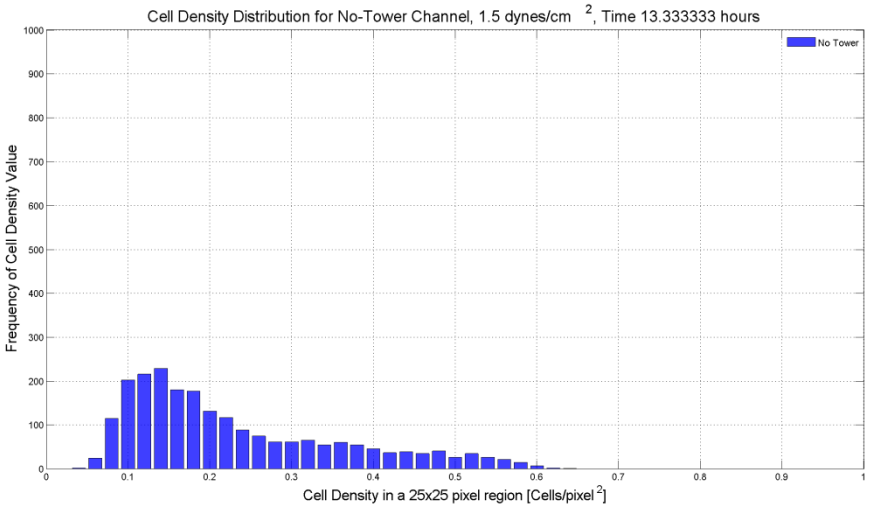
Cell Density Distribution for No-Tower Channel, 1.5 dynes/cm 2, Time 13.333333 hours
No Tower
Frequency of Cell Density Value
Cell Density in a 25x25 pixel region [Cells/pixel 2]

n

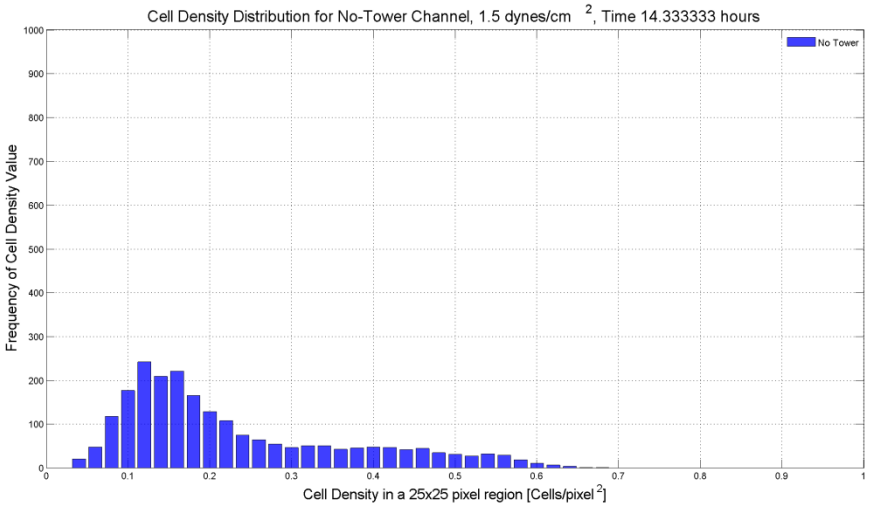
Cell Density Distribution for No-Tower Channel, 1.5 dynes/cm 2, Time 14.333333 hours
No Tower
Frequency of Cell Density Value
Cell Density in a 25x25 pixel region [Cells/pixel 2]

o

Figure 4.4.5 Cell Density Distributions as a function of time for the applied shear stress of 1.5 dynes/cm^2. Tower data is shown in red and non-tower data is shown in blue. Figures a-o show hourly distributions across the experimental timeline.

4.5 Skewness of Cell Density Distributions as a function of time

Calculating the skewness of the cell density distribution provides a metric by which to compare the cell density distributions of channels for the different applied shear stresses. While the cell density distributions for an applied shear stress illustrates non-uniform behavior by depicting the frequency of different cell density values along the channel bottom, the skewness quantifies the uniformity of the cell density distribution to better understand differences among different applied shear stresses and tower and non-tower forming channels. Investigating the skewness at each time point along the development of the biofilm shows whether the skewness of the cell density distribution is a function of time.

The skewness of the cell density within a channel was calculated at each time point as discussed in section 3.5. The skewness measures the asymmetry of the cell density distributions presented in section 4.4. Figure 4.3.1 shows the skewness of cell density results for all of the applied shear stresses studied, broken into the average values for the tower and non-tower forming channels. The tower data are plotted only up until a tower appears. The vertical axis shows the skewness of the cell density and the horizontal axis shows the experimental time in hours.

As the skewness of a normal distribution is zero, the skewness of all cell distributions studied is small, on the order of 10^{-3}, and appears to be positive as a function of time for all applied shear stresses studied except for the non-tower forming channel of

the applied shear stress 0.6 dynes/cm^2. While the value of skewness appears to decrease then increase as a function of applied shear stress, it approaches a near constant value for all applied shear stresses after the first four hours of biofilm development. It is not apparent that there is a clear relationship between applied shear stress, tower formation, and the skewness of cell density distribution.

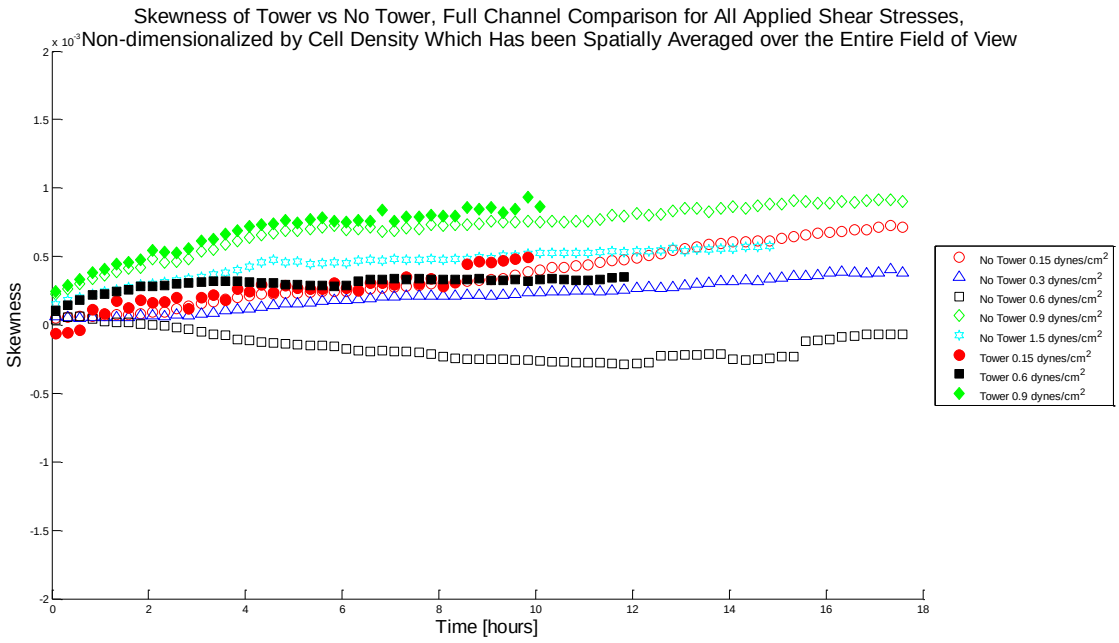

Figure 4.5.1 Skewness of Cell Density Distributions of all applied shears as a function of time: 0.15, 0.3, 0.6, 0.9, 1.5 dynes/cm^2

Studying the skewness of the cell density distribution for another tower forming applied shear stress, 0.15 dynes, may further develop the understanding of what contributes to tower formation, and is it related to the applied shear stress.

The skewness of the cell density for the applied shear stress of 0.15 dynes/cm^2 is presented in Figure 4.5.2. The tower data are plotted only up until a tower appears. The vertical axis shows the skewness of the cell density and the horizontal axis shows the experimental time in hours.

The skewness of the cell density distribution for the tower and non-tower forming channels are very similar, increase in the positive direction with time. This result is similar to the skewness of the cell density distribution for the tower and non-tower forming channels for the applied shear stress of 0.9 dynes/cm^2 and also to the skewness of the cell density of the tower forming channel for the applied shear stress of 0.6 dynes/cm^2.

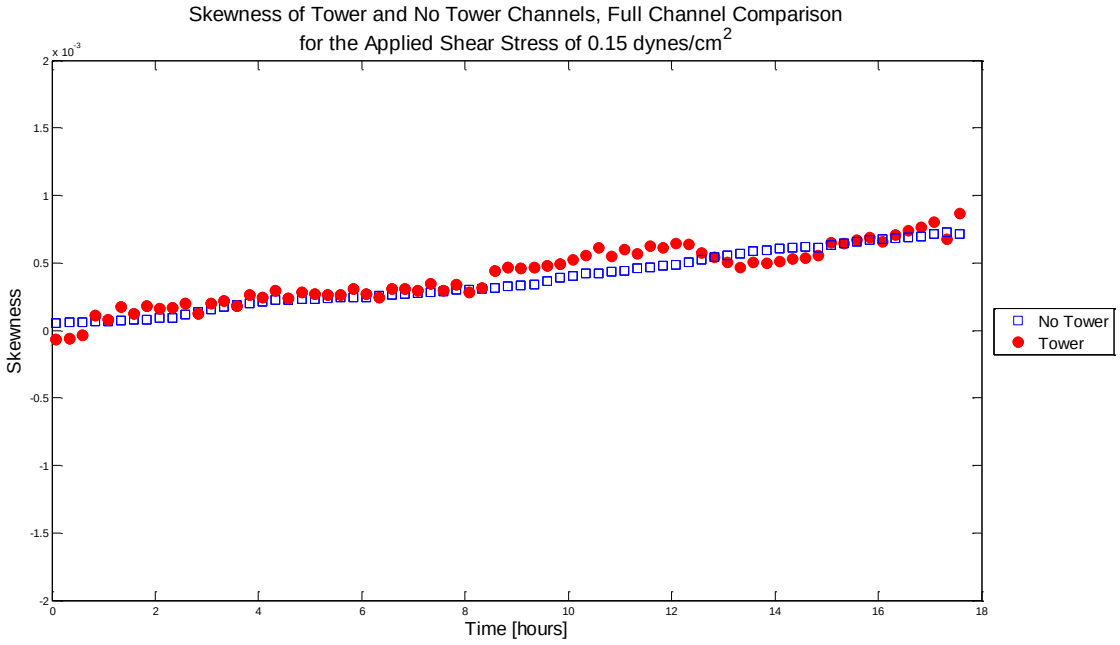

Figure 4.5.2 Skewness of Cell Density Distribution as a function of time: 0.15 dynes/cm^2

While the applied shear stress of 0.3 dynes/cm^2 does not form towers, calculating the skewness of its cell density distribution allows for comparison against the non-tower forming channels of the other shear stresses studied, which helps to answer the question of what effect does the applied shear stress have on biofilm behavior.

The skewness of the cell density for the applied shear stress of 0.3 dynes/cm^2 is presented in Figure 4.5.3. The vertical axis shows the skewness of the cell density and the horizontal axis shows the experimental time in hours.

The skewness of the cell density distribution for the non-tower forming channels becomes positive and increases with time, following a similar trend as the skewness of cell density distribution for all channels for the applied shear stresses of 0.15, 0.9, and 1.5 dynes/cm^2, as well as the skewness of cell density distribution for the tower forming channel of the applied shear stress 0.6 dynes/cm^2.

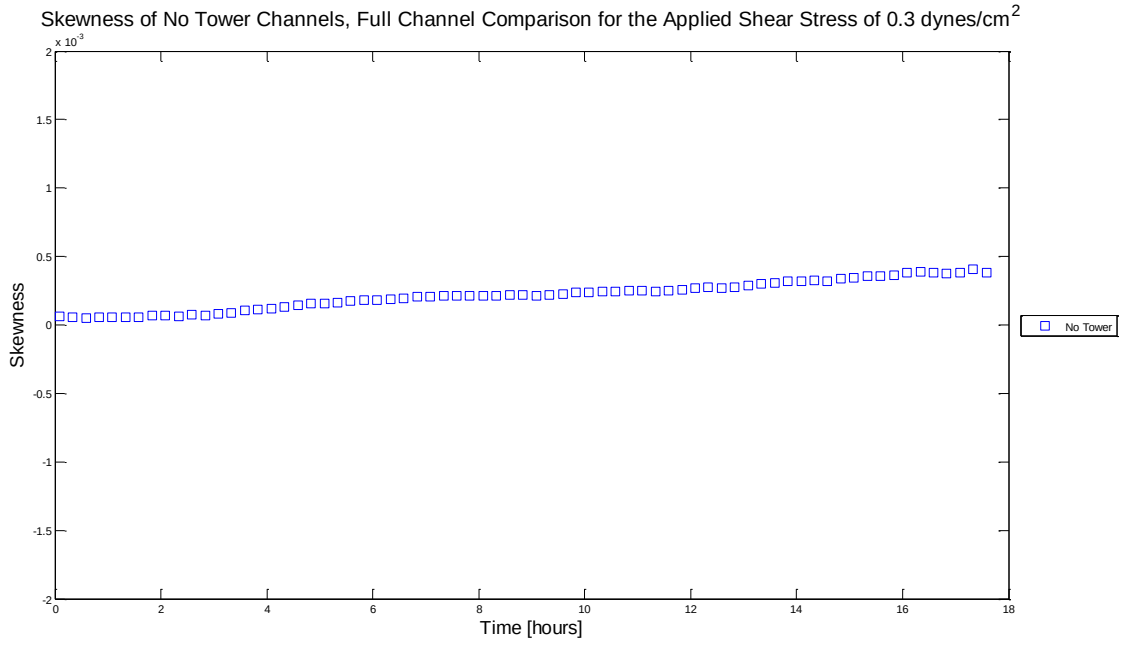

Figure 4.5.3 Skewness of Cell Density Distribution as a function of time: 0.3 dynes/cm^2

Studying the skewness of the cell density distribution for the applied shear stress of 0.6 dynes/cm^2 may help enhance the comparison between tower and non-tower forming channels. As the applied shear stress of 0.6 dynes/cm^2 more frequently yields towers than the other applied shear stresses studied, a better understanding of how the cell density is distributed across the channel bottom may improve our knowledge of what leads to tower formation.

The skewness of the cell density for the tower and non-tower forming channels for the applied shear stress of 0.6 dynes/cm^2 is presented in Figure 4.5.4. The tower data

are plotted only up until a tower appears. The vertical axis shows the skewness of the cell density and the horizontal axis shows the experimental time in hours.

The skewness of the cell density distribution for the tower forming channels becomes and stays positive during the time of the experiment while the skewness of the cell density distribution of the non-tower forming channel becomes negative over time.

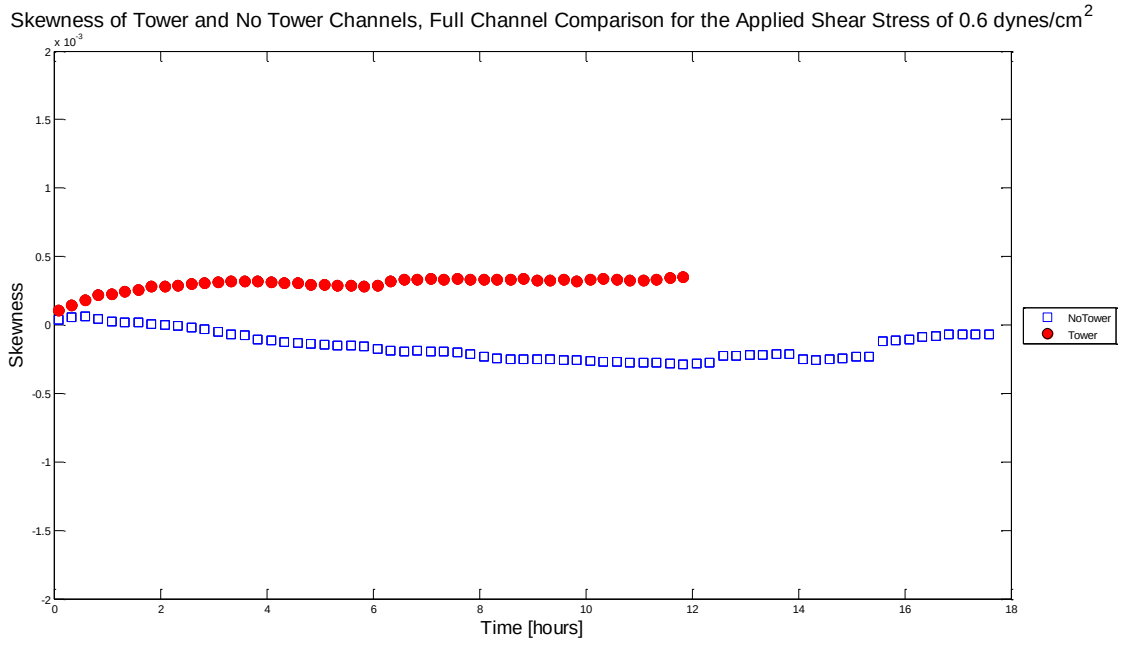

Figure 4.5.4 Skewness of Cell Density Distribution as a function of time: 0.6 dynes/cm^2

Similary to the reason for studying the skewness of cell density distribution of the applied shear stress of 0.15 dynes/cm^2, studying the skewness of the cell density distribution for another tower forming applied shear stress, 0.9 dynes/cm^2 may further develop the understanding of what contributes to tower formation, and is it related to the applied shear stress.

The skewness of the cell density for the applied shear stress of 0.9 dynes/cm^2 is presented in Figure 4.5.5. The tower data are plotted only up until a tower appears. The

vertical axis shows the skewness of the cell density and the horizontal axis shows the experimental time in hours.

The skewness of the cell density distribution for the tower and non-tower forming channels becomes positive and increases with time, following a similar trends as the skewness of cell density distribution for all channels for the applied shear stresses of 0.15, 0.3, and 1.5 dynes/cm^2, as well as the skewness of cell density distribution for the tower forming channel of the applied shear stress 0.6 dynes/cm^2. It is unclear if there is an effect on the skewness of the cell density distribution due to the type of towers that formed in the tower channel as the trend is similar to that of the skewness of the cell density distribution of the tower channel for the applied shear stresses of 0.15 and 0.6 dynes/cm^2.

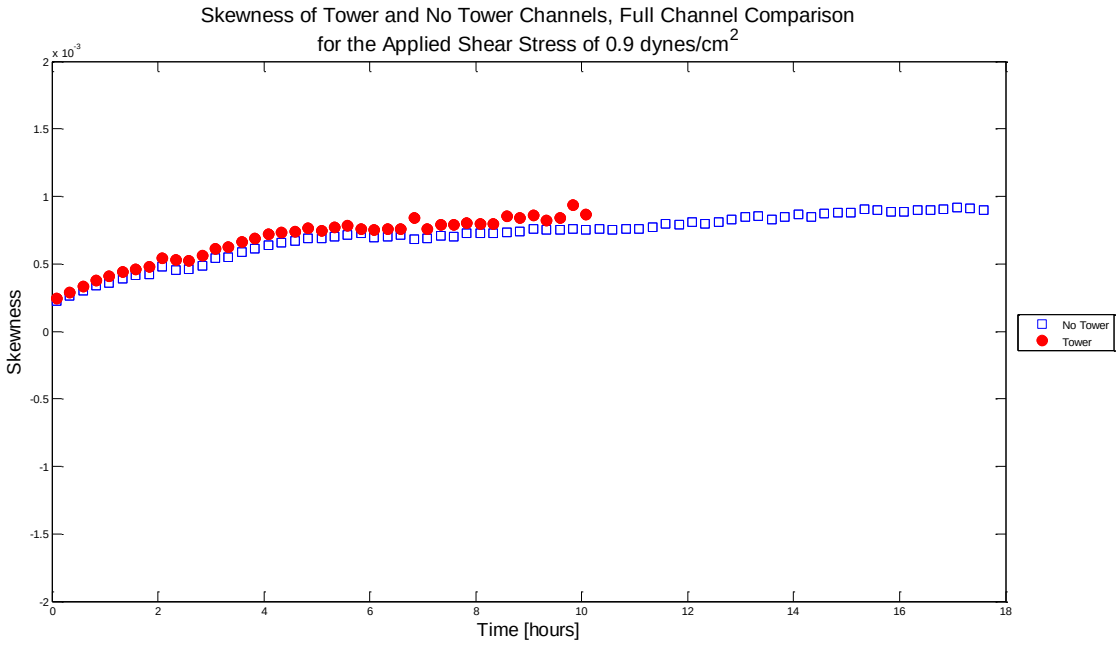

Figure 4.5.5 Skewness of Cell Density Distribution as a function of time: 0.9 dynes/cm^2

As with the presentation of the skewness of cell densifty for the applied shear stress of 0.3 dynes/cm^2, studying the skewness of the cell distribution of the non-tower

forming applied shear stress of 1.5 allows for comparison against the non-tower forming channels of the other shear stresses studied, which helps to answer the question of what effect does the applied shear stress have on biofilm behavior.

The skewness of the cell density for the applied shear stress of 1.5 dynes/cm^2 is presented in Figure 4.5.6. The vertical axis shows the skewness of the cell density and the horizontal axis shows the experimental time in hours.

The skewness of the cell density distribution for the non-tower forming channels becomes positive and increases with time , following a similar trends as the skewness of cell density distribution for all channels for the applied shear stresses of 0.15, 0.3, and 1.5 dynes/cm^2, as well as the skewness of cell density distribution for the tower forming channel of the applied shear stress 0.6 dynes/cm^2. However, the skewness of the cell density distribution for the non-tower forming channels of the applied shear of 1.5 dynes/cm^2 has a slightly higher value in comparison to the skewness for all channels for the applied shear stresses of 0.15, 0.3, 0.9 dynes/cm^2, and the skewness of the cell density of the tower-forming channel for the applied shear stress of 0.6 dynes/cm^2.

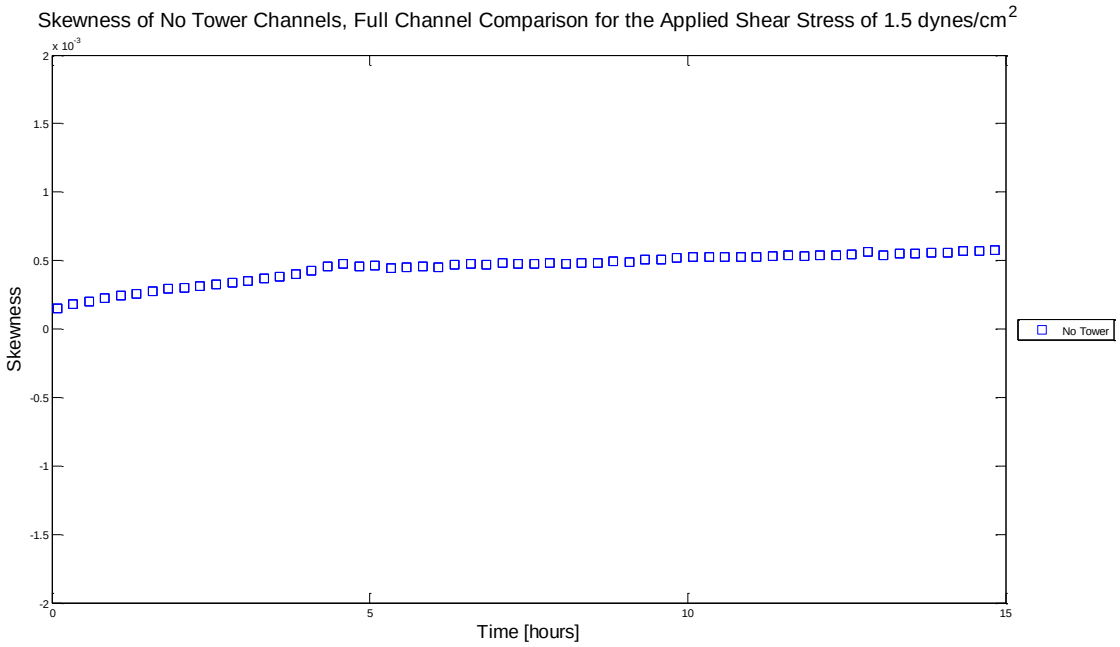

Figure 4.5.6 Skewness of Cell Density Distribution as a function of time: 1.5 dynes/cm^2

4.6 Velocity Field as a function of time

Thus far, there appears to be a relationship between the biofilm cell density and tower formation, and as studies have shown that the *S. aureus* biofilm thrives in specific flow environments and may even respond to flow, it is useful to quantify the flow field as a function of time during biofilm development [3, 9, 12]. Furthermore, a comparison of the flow field as a function of time between channels that do and do not form towers can improve the understanding of if and how the flow environment affects or is affected by tower development. Measurements of the velocity fields of two channels over time are presented below for an applied shear stress of 0.6 dynes/cm^2 as this applied shear has the highest frequency of tower formation. Data for a channel that does form a tower is compared against data for a channel that does not form a tower.

Figure 4.6.1 shows a side by side comparison of the tower and no tower channel region velocity fields for four time points after cell exodus, with the corresponding biofilm background image for each region. Raw data for calculating velocity was processed as described in section 3.5 using micro-Particle Tracking Velocimetry. Flow is from left to right and the contours are colored by streamwise velocity. Due to the changing boundary conditions leading up to the cell exodus event, the velocity fields are presented starting after cell exodus and until tower development, a span of approximately 6 hours.

A change in velocity is observed prior to tower formation in the region in which a tower forms, in comparison to a more steady velocity field in the non-tower forming channel. Specifically, the tower channel region appears to have more areas of larger and smaller velocities in comparison to the non-tower forming region. The velocity in the tower channel region is mostly zero at the 6^{th} hour after cell exodus due to the presence of a tower.

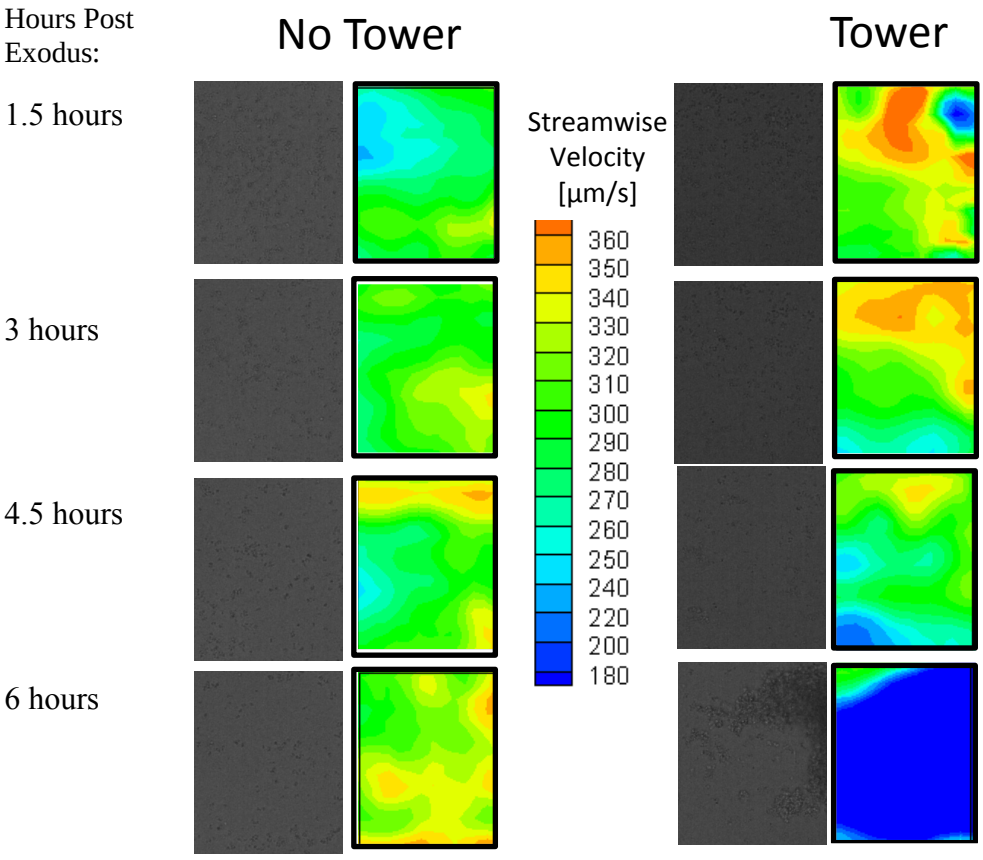

4.6.1 Velocity Contour Field and corresponding biofilm background as a function of time comparing Tower and No-Tower Channels: 0.6 dynes/cm^2. The legend indicates the contour colors. Flow is from left to right.

To more clearly understand the differences in the flow field during biofilm development, the average velocity of the regions shown in Figure 4.6.1 is calculated plotted in Figure 4.6.2. The average velocity may serve as an indicator of whether a specific region may form a tower.

The vertical axis shows the average velocity from each region, non-dimensionalized by the average velocity at the initial post-cell exodus time point of each dataset. The horizontal axis shows the experimental time starting immediately after cell exodus.

The average velocity in the tower channel region decreases 4.5 hours before the tower appears while the average velocity in the region of the non-tower forming channel increases slightly over the first 4.5 hours. It is unclear if the average velocity in a region that will form a tower will always decrease relative to that of region that does not form a tower, but this result shows that there is at least a change with respect to the non-tower forming region.

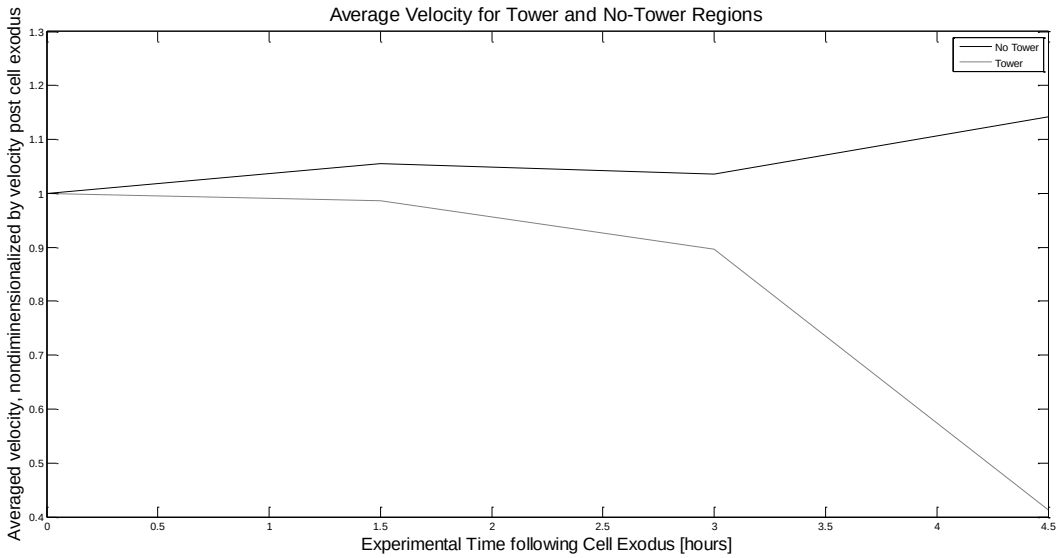

4.6.2 Average region velocity as a function of time comparing Tower and No-Tower Channels: 0.6 dynes/cm^2

While the average velocity may provide a bulk value for the tower and non-tower forming regions, the Spatial RMS of the average region velocity can provide a better description of the range of velocity values within the region.

The Spatial Root Mean Square (RMS) of the average region velocity presented in Figure 4.6.2. The vertical axis shows the Spatial RMS of the region velocity, non-dimensionalized by the initial average velocity each of region. The horizontal axis shows the experimental time starting immediately after cell exodus.

The Spatial RMS for the regions of both the tower and non-tower forming channels is small, on the order of magnitude of 10^{-3}. It appears to be nearly constant for the regions of both tower and non-tower forming channels, prior to the appearance of the tower at 6 hours, with the region of the tower forming channel having a larger value than the region of the non-tower forming channel.

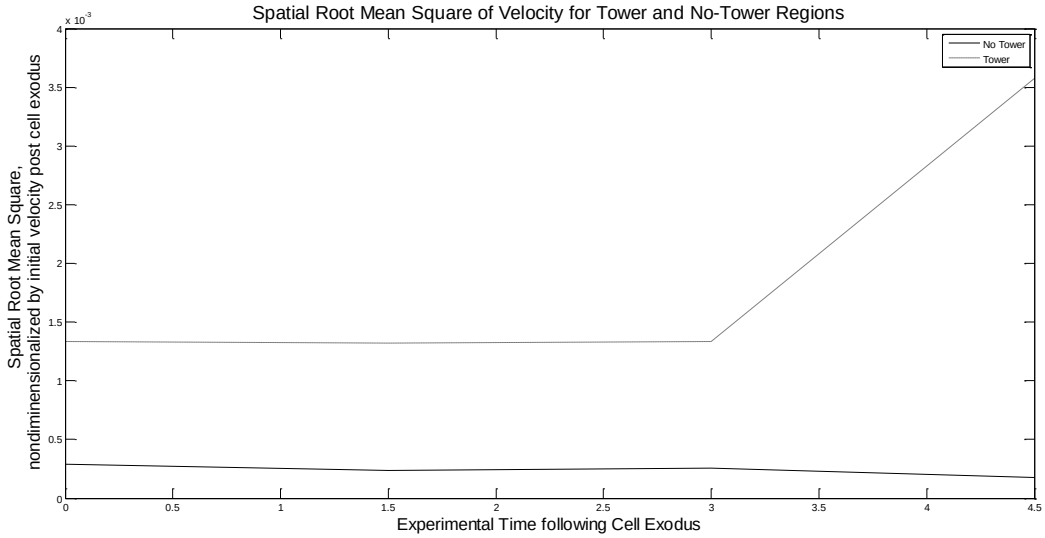

4.6.3 Spatial RMS on Velocity as a function of time comparing Tower and No-Tower Channels: 0.6 dynes/cm^2

CHAPTER 5

DISCUSSION

As stated in the introduction, the working hypothesis is that there are fluid dynamic indicators that precede tower formation and that tower formation is shear stress dependent. The results presented data that explored the relationship between tower formation, applied shear stress, and the structural characteristics of biofilm development in order to address this statement.

5.1 Tower Formation and the Bulk Flow Environment

The frequency at which *S. aureus* biofilms form towers has not been previously studied and is now understood to have a direct relationship with the applied shear stress as shown in Table 4.1. The tower forming frequency has a maximum value at the applied shear stress of 0.6 dynes/cm^2 and drops off significantly as the applied shear stress is increased or decreased. The magnitude and change in the average cell density of a biofilm in a channel, as shown in Figure 4.2.1 and discussed in section 4.2, also appears to be a function of applied shear stress, as the applied shear stress of 0.6 dynes/cm^2 has the highest average cell density and the largest changes during the stages of cell multiplication and exodus, while all other applied shear stresses studied show much smaller average cell densities and less dramatic cell multiplication and exodus stages. This clearly shows a fundamental relationship between the frequency of tower formation, the biofilm cell density, and applied shear stress.

The question remains of how exactly the applied shear stress affects the frequency of tower formation and the biofilm cell density. Research into quorum sensing for *S.*

aureus suggests that the accessory gene regulator (agr)-quorum sensing system affects the biofilm's cell detachment mechanism, and also that quorum sensing itself may be temporally and spatially non-uniform during flow due to advection of autoinducers in comparison to non-flow environments [16, 8]. Could there be a balance between biofilm cell density, applied shear stress (and therefore advection of quorum sensing signals), and production or quantity of such quorum sensing signals that leads to the ideal conditions for tower formation? External control of the levels of autoinducing signals, as shown in Boles *et al*. while studying different applied shear stresses may provide an answer [16].

5.2 Tower formation and the Biofilm Cell Density

It was shown that the applied shear stress has an effect on the average cell density in a channel during biofilm development and that tower formation appears to be highest when the biofilm has a higher cell density over time and follows the clear cell multiplication and exodus pattern observed in the results for the applied shear stress of 0.6 dynes/cm^2. Considering the tower forming channels and non-tower forming channels separately at each applied shear stress provides the opportunity to highlight differences no matter the tower forming frequencies.

As such, there are clear differences between the tower forming and non-tower forming channels across the results for average cell density, spatial RMS of cell density, and the cell density distributions. Tower forming channels tend to have a lower average cell density over time in comparison to their non-tower forming channel counterparts. They also tend to have a higher spatial RMS during the first four hours of biofilm development and after cell exodus. This difference is further expanded by the broader

range of the cell density distribution for tower forming channels relative to non-tower forming channels.

The fact that the cell distributions of tower forming channels and non-tower forming channels are immediately different from the beginning of the experiment indicates that a channel may be predisposed to forming a tower from the onset of the experiment. As described in section 3.1, the cells used in each channel are prepared exactly the same way, across multiple experiments, and rest for an hour at with no flow in the channel to facilitate surface attachment prior to the start of the experiment. Studies have shown that the quorum sensing signal threshold in no flow scenarios is lower than the threshold in flow scenarios, and therefore it may be possible that communication may occur even in this lower cell density time point due to a strong enough signal density that may direct tower formation [18]. Additionally, the activity of the agr-system has been shown to inhibit biofilm growth, but perhaps it may also have a role in directing the type of biofilm (i.e. tower forming) that will develop [11].

Considering both the difference in average cell density and cell density distribution during the early stages of biofilm development between tower and non-tower forming channels raises the question of whether the distribution, not necessarily bulk value, of the cell density across the channel bottom most directly contributes to the formation of towers. Work done by Kim showed that quorum sensing in *S. aureus* was repressed in cells near the inlet of the flow channel but increased further downstream, likely due to the increase of autoinducer concentration along the length of the channel [18]. It is possible that to begin with, cells in specific areas of higher or lower cell density or in the entirety of the tower forming channels are producing autoinducing

signals at a different rate that those in non-tower forming channels. Furthermore, once the experiment begins, the advection role of flow could drive or direct these signals from one subpopulation of cells to others downstream. The fact that non-tower forming channels have a more narrow range of cell densities points to the idea that those specific cell density values that are missing may be responsible for tower formation.

The exception for all these cases was the tower-forming channel results for the applied shear stress of 0.9 dynes/cm^2, but as explained in section 4.2, these towers functioned and developed in a manner that was different from tower development observed at other applied shear stresses. These observations were strengthened by the fact that the average cell density, spatial RMS of cell density, and cell density distribtions of the tower forming channels for the applied shear stress of 0.9 dynes/cm^2 appeared to be very similar to the results for the non-tower forming channel of 0.9 dynes/cm^2 and the non-tower forming channels of other applied shear stresses. This means that different types of towers can be characterized by their cell density, spatial RMS of cell density, and cell density distribution.

Additionally, while the cell density distributions clearly showed differences between tower and non-tower forming channels, the calculation of skewness of cell density did not illustrate a difference within the category of a given applied shear stress between tower and non-tower forming channels.

Studies looking into what specifically causes tower formation have focused on whether it is an environmental or genetic cue that is the cause. However, calculating the average cell density, spatial RMS of cell density, and cell density distributions during an experiment may serve as a tool to predict tower formation. What remains to be

understood is how the differences in the terms described occur. Further study of these terms at different applied shear stresses, in addition to consideration of the quorum sensing agr-system may provide insight into this question.

5.3 Tower formation and the Local Flow Environment

This work has shown that the bulk flow environment plays a measurable role in the frequency of tower formation as well as in structural biofilm development. It is important to understand if and what impact local flow phenomena may have on tower formation. Research into different flow channel geometries have shown that geometry has an impact on biofilm development, for example creating streamers off of corners or between crevices [9,40]. However, the experiments conducted in this study use a channel with a uniform rectangular cross section which has no obstacles to flow. Studying the local flow environment during biofilm and tower formation using this type of flow channel has the potential of revealing how flow affects tower location on a basic level which can be used to better answer the question of what leads to tower formation in the *S. aureus* biofilm and to design future experiments.

The results from this study show that in the region of a channel where a tower forms there are both larger and smaller velocities present prior to tower formation in comparison to the more uniform flow field seen in the region of a non-tower forming channel presented. This is further explained in the lower average velocity and higher spatial RMS for the region where a tower forms.

This lower average velocity and higher spatial RMS of velocity is reminiscent of the lower average cell density and higher spatial RMS of cell density observed in tower

forming channels. Generally, the question is whether the flow phenomena are a response to or a requirement for tower development. The broader distribution of cell density across the channel bottom would create different surface conditions for the flow over the channel bottom, and therefore, developing biofilm. As the cell density distribution was observed to be distinctly different for tower forming channels starting at the beginning of the experiment, it is possible that the broader organization of cell density across the channel bottom preferentially creates areas of more variable flow which in turn leads to tower formation. Work done by Kim shows that flow has a direct effect on the shape of streamer structures that occur during biofilm formation in complex geometries [18]. Perhaps the broader cell density distribution and thus the more uneven surface, leads to more variable velocities across the biofilm, which in turns enables tower development. Therefore, the increase variability in velocity may be both a response to the differentiated cell density distribution of a tower forming channel and a requirement for tower formation itself. However, it is important to recall that the applied shear stresses of 0.9 and 1.5 dynes/cm^2 had the broadest distributions of all tower and non-tower forming channels, yet had minimal or no tower formation. As such, there may be such a thing as too broad of a cell density distribution across the channel bottom.

5.4 Future work

More experiments must be conducted to further describe and quantify these flow phenomena, in addition to evaluating the flow environment within the entire channel. Addressing experimental challenges such as a vertical tilt on the microscope, achieving the precision needed to identify the correct position at which to record images, and

reducing the time interval between recording images will be important parts of understanding the relationship between the local flow environment and tower formation.

Additionally, it is unclear what if any changes in local fluid properties may have on the flow environment. While the viscosity of the media used for experiments is known, the quantity of external DNA and cell-produced enzymes such as nuclease that are released during biofilm development is unknown and their impact on the local flow field is hard to estimate.

Future work should include:

- Expanding and filling out the range of applied shear stresses studied,
- Addressing experimental challenges to examine the flow over the rest of the channel bottom,
- Determining the quantity of extracellular molecules produced from the biofilm development, starting at the cell attachment stage, and identifying their effect on the local fluid environment,
- Conducting gene studies simultaneously with flow and cell density studies to determine how and if cell regulatory activity responds to or changes the local flow environment and biofilm properties to form towers,
- Designing experiments where the local flow environment can be adjusted to determine if flow phenomena are a cause or an effect of tower development,
- Improving the experimental time resolution of the micro-particle imaging velocimetry studies to capture the fluid structure interaction that precedes tower detachment.

CHAPTER 6

CONCLUSION

This work began with the question of whether there is a relationship between the applied shear flow and tower formation in *S. aureus*. Conducting experiments which quantified the fluid environment and biofilm growth characteristics over the course of biofilm development provided the opportunity to answer this question and ask more.

Specifically, we have been able to show that

- There is a relationship between the applied shear flow and the frequency of tower formation
- The magnitude of the applied shear flow has a direct relationship with the biofilm cell density
- The distribution of cell density serves as an indicator of tower development at the onset of an experiment
- The local flow environment is affected by tower development prior to the presence of a tower

Even still questions remain as to what is and how to determine the fundamental cause of tower formation within the *S. aureus* biofilm. Additionally, more information regarding the effect of applied shear stress on the cell density indicators presented could provide a better picture of how the applied shear stress affects biofilm development. Ultimately, as we ask questions, we continue to learn more about the complex physical and biological nature of the *S. aureus* biofilm.

REFERENCES

[1] Klein, E., Smith, D. L., & Laxminarayan, R. (2007). Hospitalizations and Deaths Caused by Methicillin-Resistant *Staphylococcus aureus* , United States, 1999–2005. *Emerging Infectious Diseases, 13*(12), 1840-1846. doi:10.3201/eid1312.070629

[2] Kluytmans, J., A. van Belkum, and H. Verbrugh. 1997. Nasal carriage of *Staphylococcus aureus:* epidemiology, underlying mechanisms, and associated risks. Clin. Microbiol. Rev. 10:505–520.

[3] Donlan, R. M., & Costerton, J. W. (2002). Biofilms: Survival Mechanisms of Clinically Relevant Microorganisms. *Clinical Microbiology Reviews, 15*(2), 167-193. doi:10.1128/cmr.15.2.167-193.2002

[4] SEM image of *Staphylococcus aureus* (2005). Retrieved October 30, 2016, from http://phil.cdc.gov/phil/details.asp?pid=10046

[5] Moormeier, D. E., Bose, J. L., Horswill, A. R., & Bayles, K. W. (2014). Temporal and Stochastic Control of *Staphylococcus aureus* Biofilm Development. *MBio, 5*(5). doi:10.1128/mbio.01341-14

[6] Foster, T. (1996). Chapter 12 *Staphylococcus*. In B. S (Ed.), *Medical Microbiology* (4th ed.). Retrieved October 30, 2016, from https://www.ncbi.nlm.nih.gov/books/NBK8448/

[7] Mann, E. E., Rice, K. C., Boles, B. R., Endres, J. L., Ranjit, D., Chandramohan, L., . . . Bayles, K. W. (2009). Modulation of eDNA Release and Degradation Affects

Staphylococcus aureus Biofilm Maturation. *PLoS ONE, 4*(6). doi:10.1371/journal.pone.0005822

[8] Oliveira, M., Nunes, S., Carneiro, C., Bexiga, R., Bernardo, F., & Vilela, C. (2007). Time course of biofilm formation by *Staphylococcus aureus* and *Staphylococcus epidermidis* mastitis isolates. *Veterinary Microbiology, 124*(1-2), 187-191. doi:10.1016/j.vetmic.2007.04.016

[9] Kim, M. K., Drescher, K., Pak, O. S., Bassler, B. L., & Stone, H. A. (2014). Filaments in curved streamlines: Rapid formation of *Staphylococcus aureus* biofilm streamers. *New Journal of Physics New J. Phys., 16*(6), 065024. doi:10.1088/1367-2630/16/6/065024

[10] Costerton, J. (1995). Overview of microbial biofilms. *Journal of Industrial Microbiology, 15*(3), 137-140. doi:10.1007/bf01569816

[11] Rosenthal, C. B., Mootz, J. M., & Horswill, A. R. (2014). *Staphylococcus aureus* Biofilm Formation and Inhibition. *Springer Series on Biofilms Antibiofilm Agents,* 233-255. doi:10.1007/978-3-642-53833-9_11

[12] Fux, C. A., Wilson, S., & Stoodley, P. (2004). Detachment Characteristics and Oxacillin Resistance of *Staphyloccocus aureus* Biofilm Emboli in an In Vitro Catheter Infection Model. *Journal of Bacteriology, 186*(14), 4486-4491. doi:10.1128/jb.186.14.4486-4491.2004

[13] Stewart, P. S., & Franklin, M. J. (2008). Physiological heterogeneity in biofilms. *Nature Reviews Microbiology, 6*(3), 199-210. doi:10.1038/nrmicro1838

[14] Miller, M. B., & Bassler, B. L. (2001). Quorum Sensing in Bacteria. *Annual Review of Microbiology Annu. Rev. Microbiol., 55*(1), 165-199. doi:10.1146/annurev.micro.55.1.165

[15] Shrout, J. D., Tolker-Nielsen, T., Givskov, M., & Parsek, M. R. (2011). The contribution of cell-cell signaling and motility to bacterial biofilm formation. *MRS Bulletin, 36*(05), 367-373. doi:10.1557/mrs.2011.67

[16] Boles, B. R., & Horswill, A. R. (2008). Agr-Mediated Dispersal of *Staphylococcus aureus* Biofilms. *PLoS Pathogens, 4*(4). doi:10.1371/journal.ppat.1000052

[17] Davies, D. G. (1998). The Involvement of Cell-to-Cell Signals in the Development of a Bacterial Biofilm. *Science, 280*(5361), 295-298. doi:10.1126/science.280.5361.295

[18] Kim, M. K., Ingremeau, F., Zhao, A., Bassler, B. L., & Stone, H. A. (2016). Local and global consequences of flow on bacterial quorum sensing. *Nat. Microbiol Nature Microbiology, 1*(1), 15005. doi:10.1038/nmicrobiol.2015.5

[19] Kirisits, M. J., Margolis, J. J., Purevdorj-Gage, B. L., Vaughan, B., Chopp, D. L., Stoodley, P., & Parsek, M. R. (2007). Influence of the Hydrodynamic Environment on Quorum Sensing in Pseudomonas aeruginosa Biofilms. *Journal of Bacteriology, 189*(22), 8357-8360. doi:10.1128/jb.01040-07

[20**]** Sturges, W. S., and L. F. Rettger **(**1922). *Bacterial autolysis. J. Bacterioogy, 7(*6),551-*577.*

[21] Bayles, K. W. (2007). The biological role of death and lysis in biofilm development. *Nature Reviews Microbiology, 5*(9), 721-726. doi:10.1038/nrmicro1743

[22] Rice, K. C., Mann, E. E., Endres, J. L., Weiss, E. C., Cassat, J. E., Smeltzer, M. S., & Bayles, K. W. (2007). The cidA murein hydrolase regulator contributes to DNA release and biofilm development in *Staphylococcus aureus*. *Proceedings of the National Academy of Sciences, 104*(19), 8113-8118. doi:10.1073/pnas.0610226104

[23] Webb, J. S., Thompson, L. S., James, S., Charlton, T., Tolker-Nielsen, T., Koch, B., . . . Kjelleberg, S. (2003). Cell Death in *Pseudomonas aeruginosa* Biofilm Development. *Journal of Bacteriology, 185*(15), 4585-4592. doi:10.1128/jb.185.15.4585-4592.2003

[24] Hsu, C., Lin, M., Chen, C., Chien, S., Cheng, Y., Su, I., & Shu, J. (2011). Vancomycin promotes the bacterial autolysis, release of extracellular DNA, and biofilm formation in vancomycin-non-susceptible *Staphylococcus aureus*. *FEMS Immunology & Medical Microbiology, 63*(2), 236-247. doi:10.1111/j.1574-695x.2011.00846.x

[25] Rice, K. C., Mann, E. E., Endres, J. L., Weiss, E. C., Cassat, J. E., Smeltzer, M. S., & Bayles, K. W. (2007). The cidA murein hydrolase regulator contributes to DNA release and biofilm development in *Staphylococcus aureus*. *Proceedings of the National Academy of Sciences, 104*(19), 8113-8118. doi:10.1073/pnas.0610226104

[26] Jakubovics, N., Shields, R., Rajarajan, N., & Burgess, J. (2013). Life after death: The critical role of extracellular DNA in microbial biofilms. *Letters in Applied Microbiology*, *57*(6), 467-475. doi:10.1111/lam.12134

[27] Brunskill, E. & Bayles, K. (1996). Identification and Molecular Characterization of a Putative Regulatory Locus that Affects Autolysis in Staphyloccus *aureus*. *Journal of Bacteriology*, 178(3), 611-618. PMCID: PMC177702

[28] Harris LG, Foster SJ. & Richards RG (2009).An introduction to S. *aureus* and techniques for identifying S. *aureus* adhesins in relation to adhesion to biomaterials: A review. *Eur Cell Mater* 4, 39-60. PMID: 14562246

[29] Stoodley, P., Lewandowski, Z., Boyle, J. D., & Lappin-Scott, H. M. (1998). Oscillation characteristics of biofilm streamers in turbulent flowing water as related to drag and pressure drop. *Biotechnology and Bioengineering, 57*(5), 536-544. doi:10.1002/(sici)1097-0290(19980305)57:53.0.co;2-h

[30] Wilking, J. N., Angelini, T. E., Seminara, A., Brenner, M. P., & Weitz, D. A. (2011). Biofilms as complex fluids. *MRS Bulletin, 36*(05), 385-391. doi:10.1557/mrs.2011.71

[31] Wimpenny, J. (1997). A unifying hypothesis for the structure of microbial biofilms based on cellular automaton models. *FEMS Microbiology Ecology, 22*(1), 1-16. doi:10.1016/s0168-6496(96)00078-5

[32] Sternberg, C., Christensen, B. B., Johansen, T., Nielsen, A.T., Anderson, J.B., Givskov, M. & Molin, S. (1999). Distribution of Bacterial growth activity in flow-chamber biofilms. *Applied and Environmental Microbiology*. 65(9), 4108-4117.

[33] Moormeier, D. E., Endres, J. L., Mann, E. E., Sadykov, M. R., Horswill, A. R., Rice, K. C., . . . Bayles, K. W. (2013). Use of Microfluidic Technology To Analyze Gene Expression during *Staphylococcus aureus* Biofilm Formation Reveals Distinct Physiological Niches. *Applied and Environmental Microbiology, 79*(11), 3413-3424. doi:10.1128/aem.00395-13

[34] Yang, X., Beyenal, H., Harkin, G., & Lewandowski, Z. (2000). Quantifying biofilm structure using image analysis. *Journal of Microbiological Methods, 39*(2), 109-119. doi:10.1016/s0167-7012(99)00097-4

[35] Chen, Y., Norde, W., Mei, H. C., & Busscher, H. J. (2012). Bacterial Cell Surface Deformation under External Loading. *MBio, 3*(6). doi:10.1128/mbio.00378-12

[36] Rupp, C. J., Fux, C. A., & Stoodley, P. (2005). Viscoelasticity of *Staphylococcus aureus* Biofilms in Response to Fluid Shear Allows Resistance to Detachment and Facilitates Rolling Migration. *Applied and Environmental Microbiology, 71*(4), 2175-2178. doi:10.1128/aem.71.4.2175-2178.2005

[37] Vo, G. D., Brindle, E., & Heys, J. (2010). An experimentally validated immersed boundary model of fluid–biofilm interaction. *Water Science & Technology, 61*(12), 3033. doi:10.2166/wst.2010.213

[38] Persat, A., Nadell, C., Kim, M., Ingremeau, F., Siryaporn, A., Drescher, K., . . . Stone, H. (2015). The Mechanical World of Bacteria. *Cell, 161*(5), 988-997. doi:10.1016/j.cell.2015.05.005

[39] Kostenko, V., Salek, M. M., Sattari, P., & Martinuzzi, R. J. (2010). *Staphylococcus aureus* biofilm formation and tolerance to antibiotics in response to oscillatory shear stresses of physiological levels. *FEMS Immunology & Medical Microbiology FEMS Immunol Med Microbiol, 59*(3), 421-431. doi:10.1111/j.1574-695x.2010.00694.x

[40] Rusconi, R., Guasto, J. S., & Stocker, R. (2014). Bacterial transport suppressed by fluid shear. *Nature Physics, 10*(3), 212-217. doi:10.1038/nphys2883

[41] Lambert, L.M.(2016). Temporally and spatially resolved quantification of hemodynamic forces and endothelial mechanics. (Doctoral Dissertation). Retrieved from http://
http://digitalcommons.unl.edu/cgi/viewcontent.cgi?article=1097&context=mechengdiss

[42] Fluxion Biosciences (2008). BioFlux System for Cellular Interactions: Microfluidic flow system for live cell assays [White Paper]. Retrieved October 30, 2016 from Fluxion Support Center: support.fluxionbio.com/hc/en-us/article.../**bioflux**_bf200whitepaper-1020.pdf

[43] Depth of Field and Depth of Focus. (n.d.). Retrieved November 30, 2016, from https://www.microscopyu.com/microscopy-basics/depth-of-field-and-depth-of-focus

[44] Fluxion Biosciences (2008). Viscosity: Understanding effects of viscosity in the BioFlux system. [Fact Sheet]. Retrieved October 30, 2016 from Fluxion Supper Center: http://support.fluxionbio.com/hc/en-us/articles/203649638-Viscosity-Understanding-effects-of-viscosity-in-the-BioFlux-system

APPENDIX A

CELL CULTURE AND EQUIPMENT PROTOCOL FOR ALL EXPERIMENTS

A.1 Culturing and inserting *Staphylococcus aureus* UAMS-1 cells.

The first step in preparation for the either µPTV or cell density experiments is to culture the S. aureus UAMS-1 cells.

A.1.1 Materials

- 50% TSB
- 100% TSB
- UAMS-1 culture
- Bioflux^{TM} Plate

A.1.2 Equipment

- Spectrophotometer
- Vacuum System
- Bioflux^{TM} System

A.1.3 Procedure

1. Pick a single colony from a freshly struck plate of UAMS-1 into 3 mL of 100% TSB broth. Incubate at 37C with shaking at 250 rpm for 24 hours.
2. The next day, use a Spectrophotometer to measure the optical density of the overnight culture. Dilute a 50 µL sample of the UAMS-1 culture into 950 µL sterile 100% TSB, using a blank cuvette filled with 1 mL of TSB for comparison.
3. Prepare the UAMS-1 culture to inoculate the channels of the plate. Prepare enough to make sure each well will have 200 µL per well. Use 100% strength TSB to dilute UAMS-1 culture to an optical density of 0.8 and set aside.

4. Open a new Bioflux^{TM} plate and inspect the bottom for cracks. Remove the clear film on top of the plate beneath the cover.
5. Prime channels by pipetting 210 µL of sterile 100% TSB into the output wells. Check TSB for clarity. Replace the lid and place on top of Bioflux^{TM} Stage on the Nikon Ti-S Microscope.
6. Secure the plate with the clamp, remove the lid and attach the pressure interface. Open the Bioflux^{TM} Montage software and enter the serial number on the side of the plate.
7. Switch to manual mode in the control module and choose the 'Fluid' to be TSB at 37C and a maximum shear of 5 dynes/cm2. Select the output wells in order to pump backwards for the columns of the channels being used. The color will change from light green to dark green. Run for 5 minutes.
8. Remove the pressure interface and replace the lid on top of the plate. Check that there is liquid inside the input wells.
9. Use the vacuum system to remove the excess media from the output wells. Measure 200 µL of inoculum and add to the output wells for each channel. Add 300 µL of 100% strength TSB into the input wells of each channel in order to prevent gravity flow. Replace the lid.
10. Secure the plate with the clamp on top of the Nikon Ti-S Microscope, remove the lid, and reattach the pressure interface. Open the Bioflux^{TM} Montage software and set the applied shear to 2 dynes/cm^2. Pump backwards from the output wells for 5 seconds and stop flow.

11. Inspect each channel to see if there are cells in the flow channel. Let the cells sit for 1 hour at 37C to allow the cells to attach to the channel bottom.
12. Remove the pressure interface, replace the lid, and bring plate to the vacuum system in order to remove any media that is left in the output and input wells. Add 1.3 mL of 50% strength TSB to each input well then return the plate to the Nikon Ti-S Microscope.
13. Secure the plate with the clamp, remove the lid, and reattach the pressure interface.

A.2 Camera setup for µPTV data acquisition

A.2.1 Equipment

- Phantom Miro M310 Camera
- Laptop for camera and data acquisition
- Bioflux^{TM} System
- >1 TB Hard Drive for data

A.2.2 Procedure

1. Turn on camera laptop
2. Attach the camera to the Nikon Ti-S Microscope using a C-mount adapter.
3. Connect Ethernet cable between camera and laptop and connect power cord between camera and power source.
4. Turn the camera switch to ‘ON’.
5. Open the PCC 2.22 software on the computer.
6. Click the ‘Live’ tab then select the ‘13130’ camera for use in the drop down window.
7. Set the light intensity on the Nikon Ti-S Microscope to 40% maximum (4th tick mark).
8. Select the 40x objective on the Nikon Ti-S Microscope and use the viewing window to locate the flow channel of interest.
9. Identify the channel bottom based on where adhered cells are brightest. Use the dial controlling z-position to move up through the channel only without changing z-direction to reduce the effect of hysteresis. Save the x-y-z position of this channel

10. Adjust the camera so that the channel walls are horizontal in the image shown on the PCC 2.22 display.
11. Open the ‘Cine Settings’ tab on the right hand side to specify settings.
12. Set the resolution to 1024x768, and use the framing rate and exposure settings described in Table 3.1 for the corresponding shear being studied.
13. Click the button for CSR – Current Session Reference’ to normalize the image.
14. Change the Image Range & Trigger Position by dragging the indicator on the bar all the way to the left so that all images will be recorded after clicking ‘Trigger’.
15. Open the ‘Advanced Settings’ tab and set the sync to ‘internal’, the burst count to 2’, and the burst period to whatever the time period specified in Table 3.1
16. Open the Bioflux^{TM} Montage software and specific the applied shear stress.
17. When recording images, save as a ‘cine’ file.

A.3 Image conversion for µPTV

A.3.1 Equipment

- Laptop for camera and data acquisition
- >1TB Hard Drive for data

A.3.2 Procedure

1. Open PCC 2.22 program
2. Click icon on top left screen ‘Batch Convert Files’
3. Choose the cine file for conversion
4. Change the ‘Save as type’ to ‘TIFF 8,24 images, *.tif’
5. Adjust the range option to ‘User Defined’ to convert the desired amount of images
6. Click on ‘Border data’ on the bottom of the screen. Choose the ‘Standard’ option under ‘Outside image’, and click on the boxes for ‘File Name’, ‘Image Number’, and ‘Exposure’.
7. Click on the drop down window below ‘Time formation’ and choose ‘Absolute time’.
8. Use the naming format of ‘image_+5’ so that the cine video is converted to images with consecutive numbers, showing 5 significant digits.

A.4 Image conversion for Cell Density data

A.4.1 Equipment

- Laptop for camera and data acquisition
- >1TB Hard Drive for data

A.4.2 Procedure

1. Open ImageJ
2. Click the tab labeled ‘Process’, then click ‘Batch’, and then ‘Convert’.
3. Click on the ‘Input’ box and choose the folder containing images to convert.
4. Click on the ‘Output’ box. Create a subfolder within the input folder and use that as the output destination.
5. Change the output format from TIFF to 8-bit TIFF.
6. Keep ‘Interpolation’ as ‘Bilinear’ and ‘Scale factor’ at 1.00.
7. Click ‘convert’.